Electron Phonon Interaction and Strong Correlations in High-Temperature Superconductors: One can not avoid unavoidable

Miodrag L. Kulić

Johann Wolfgang Goethe-University,
Institute for Theoretical Physics,
P.O.Box 111932, 60054 Frankfurt/Main, Germany

Abstract. The important role of the electron-phonon interaction (EPI) in explaining the properties of the normal state and pairing mechanism in high-T_c superconductors (HTSC) is discussed. A number of experimental results are analyzed such as: dynamical conductivity, Raman scattering, neutron scattering, ARPES, tunnelling measurements, isotope effect and etc. They give convincing evidence that the EPI is strong and dominantly contributes to pairing in HTSC oxides. It is argued that strong electronic correlations in conjunction with the pronounced (in relatively weakly screened materials) EPI are unavoidable ingredients for the microscopic theory of pairing in HTSC oxides. I present the well defined and controllable theory of strong correlations and the EPI. It is shown that strong correlations give rise to the pronounced *forward scattering peak* in the EPI - the FSP theory. The FSP theory explains in a consistent way several (crucial) puzzles such as much smaller transport coupling constant than the pairing one ($\lambda_{tr} \ll \lambda$), which are present if one interprets the results in HTSC oxides by the old Migdal-Eliashberg theory for the EPI. The ARPES shift puzzle where the nodal kink at 70 meV is unshifted in the superconducting state, while the anti-nodal one at 40 meV is shifted can be explained at present only by the FSP theory. A number of other interesting predictions of the FSP theory are also discussed.

1. INTRODUCTION

1.1. Importance of strong electronic correlations and EPI

Seventeen years after the discovery of the high-T_c superconductors (HTSC) [1] there is still no consensus about the pairing mechanism in these materials. At present two

possible theories are in the focus, the first one based on the electron-phonon interaction (EPI) and the second one based on spin fluctuation interaction (SFI). In the meantime it was well established that metallic compounds of HTSC oxides are obtained from insulating parent compounds by doping with small number of carriers - usually called holes. It turns out that the parent insulating state is far from being conventional band insulator where usually an even number of electrons (holes) per lattice site fill Bloch bands completely. By counting the electron number one comes (naively) to the conclusion that the parent compounds of copper oxides (for instance La_2CuO_4 and $YBa_2Cu_3O_6$) should be metallic, because in the unit cell there is odd (nine) number of d-electrons per Cu^{2+} ion. The way out from this controversy is in the presence of strong electronic correlations. They are due to the localized d-orbital on the Cu^{2+} ion giving rise to the strong Coulomb repulsion U of two $3d_{x^2-y_2}$ electrons (or holes) at a given lattice site with opposite spins. This repulsion keeps electrons apart making them to be localized on the lattice, but with localized spins ($S = 1/2$). This type of insulating state is called the *Mott-Hubbard insulator*. Speaking in language of electronic bands, for large on-site repulsion $U \gg W$ and for one electron per lattice site the original conduction band (with the width W) is split into the lower Hubbard band with localized spins and the empty upper band separated by U from the lower one - see more in [2] and Section 4.

The relevance of strong correlations is well documented experimentally: (**i**) The electron-energy-loss spectroscopy [24] shows a transfer of intensity (which is a measure of the number of states) from higher to lower energies by doping. Such a property is characteristic for the class of Hubbard models where the number of states in the upper Hubbard band decreases by increasing the hole doping. For comparison, in typical semiconductors the number of states in the valence band is determined by the number of atoms, i.e. it is fixed and doping independent. (**ii**) The self-consistent band-structure calculations and the photoemission experiments gave that the effective Hubbard interaction (U) for the Cu ions is of the order $U \approx 6 - 10\ eV$ [25], which is much larger than the observed band width W ($\sim 2\ eV$) [26]. (**iii**) A rather direct evidence for strong correlations comes from the doping dependence of the dynamic conductivity $\sigma(\omega)$ in $La_{2-x}Sr_xCuO_4$ and $Nd_{2-x}Ce_xCuO_{4-y}$, particularly from the observed shift of the spectral weight from high to low energies with doping [27]. Besides the development of the Drude peak around $\omega = 0$ in the underdoped systems the so called mid-infrared (*MIR*) peak is also developed around $0.4\ eV$.

Regarding the EPI one can put an "old fashioned" question: Does the EPI makes (contributes to) the superconducting pairing in HTSC oxides? Surprisingly, most of researchers in the field believe that the EPI is irrelevant and that the pairing mechanism is due to spin fluctuations and strong correlations alone- see [29]. This belief is mainly based on an incorrect stability criterion (which, if true, would strongly limit T_c in the EPI mechanism), and also on a number of experimental results which give evidence for strong anisotropic ($d - wave$ like) pairing with gapless regions on the Fermi surface [6], etc. Moreover, the phase sensitive *SQUID* measurements of the Josephson effect [30], [31] in the orthorhombic material $YBa_2Cu_3O_{6+x}$ are strongly in favor of an "orthorhombic" $d - wave$ superconducting order parameter, for instance $\Delta(\mathbf{k}) = \Delta_s + \Delta_d(\cos k_x - \cos k_y)$. As experiments of Tsuei et al. [30], [31] show one has $\Delta_s < 0.1\Delta_d$ in optimally doped $YBa_2Cu_3O_{6+x}$, which means that zeros of $\Delta(\mathbf{k})$ are near intersections of the Fermi surface and the lines $k_x \approx \pm k_y$. Recent experiments on the

single-layer crystals $Tl_2Ba_2CuO_{6+x}$ and on $Bi_2Sr_2CaCu_2O_{8+x}$ ($Bi2212$) done by Tsuei group [32], [33], [34], prove the existence of pure $d-wave$ pairing in underdoped, optimally and overdoped systems. The recent interference experiments on $Nd_{2-x}Ce_xCuO_{4-y}$ point also to d-wave pairing in this compound [35]. In that respect, we point out that there is also an widespread (and unfounded) belief that $d-wave$ is incompatible with the EPI pairing mechanism.

Another argument used against the EPI as an origin of superconductivity in HTSC oxides is based on the small value of the oxygen isotope effect α_O ($\alpha = \alpha_O + \alpha_{Cu} + \alpha_Y + \alpha_{Ba}$) in optimally doped materials, such as $YBCO$ with highest critical temperature $T_c \approx 92K$ where $\alpha_O \approx 0.05$ [105], instead of the canonical value $\alpha = 1/2$ which would be in the case of the EPI pairing mechanism alone and in the presence of O-vibrations only.

On the other hand, there is good experimental evidence that the EPI is sufficiently large in order to produce superconductivity in HTSC oxides, i.e. $\lambda > 1$. Let us quote some of them: (**1**) The superconductivity induced *phonon renormalization* [3], [36], [4], [5] is much larger in HTSC oxides than in *LTSC* superconductors. This is partially due to the larger value of Δ/E_F in HTSC than in *LTSC*; (**2**) the *line-shape* in the phonon Raman scattering is very asymmetric (Fano line), which points to a substantial interaction of the lattice with some quasiparticle (electronic liquid) continuum. For instance, the recent phonon Raman measurements [4] on $HgBa_2Ca_3Cu_4O_{10+x}$ at $T < T_c$ give very large softening (self-energy effects) of the A_{1g} phonons with frequencies 240 and 390 cm^{-1} by 6 % and 18 %, respectively. At the same time there is a dramatic increase of the line-width immediately below T_c, while above T_c the line-shape is strongly asymmetric. A substantial phonon renormalization was obtained in $(Cu,C)Ba_2Ca_3Cu_4O_{10+x}$ [5]; (**3**) the *large isotope coefficients* ($\alpha_O > 0.4$) in $YBCO$ away from the optimal doping [105] and $\alpha_O \approx 0.15 - 0.2$ in the optimally doped $La_{1.85}Sr_{0.15}CuO_4$. At the same time one has $\alpha_O \approx \alpha_{Cu}$ making $\alpha \approx 0.25 - 0.3$. This result tell us that other, besides O, ions participate in pairing; (**4**) the most important evidence that the EPI plays an important role in pairing comes from *tunnelling spectra* in HTSC oxides, where the phonon-related features have been clearly seen in the $I-V$ characteristics [37], [38], [39], [40], [41]; (4) the *penetration depth* in the a-b plane of YBCO is increased significantly after the substitution $O^{16} \rightarrow O^{18}$, i.e. $(\Delta\lambda_{ab}/\lambda_{ab}) = (^{18}\lambda_{ab} - ^{16}\lambda_{ab})/^{16}\lambda_{ab} = 2.8$ % at 4 K [42]. Since $\lambda_{ab} \sim m^*$ the latter result, if confirmed, could be due to the nonadiabatic increase of the effective mass m^*.

Recent ARPES measurements on HTSC oxides [43], [109] show a *kink* in the quasiparticle spectrum at characteristic (oxygen) phonon frequencies in the normal and superconducting state. This is clear evidence that the EPI is strong and involved in pairing.

On the *theoretical side* there are self-consistent *LDA* band-structure calculations which (in spite of their shortcomings) give a rather large bare EPI coupling constant $\lambda \sim 1.5$ in $La_{1.85}Sr_{0.15}CuO_4$ [51], [53]. The *nonadiabatic effects* due to poor metallic screening along the c-axis may increase λ additionally [52], [53]. All these facts are in favor of the substantial EPI in HTSC oxides. However, if the properties of the normal and superconducting state in HTSC oxides are interpreted in terms of the standard EPI theory, which holds in *LTSC* systems, some puzzles arise. One of them is related to the normal-state conductivity (resistivity) - in optimally doped systems the width of the Drude peak in $\sigma(\omega)$ and the temperature dependence of the resistivity $\rho(T)$ are not

incompatible with the strong-coupling theory with $\lambda \sim 3$ and $\lambda_{tr} \sim 1$ (if $\omega_{pl} \sim 3\ eV$), where λ_{tr} is the transport EPI coupling constant [50]. On the other side the combined resistivity and low frequency conductivity (Drude part) measurements give $\lambda_{tr} \approx 0.3$ if the plasma frequency takes the value $\omega_{pl} \sim 1\ eV$ - see more below. If one assumes that $\lambda_{tr} \approx \lambda$, which is the case in most low temperature superconductors ($LTSC$), such a small λ can not give large $T_c (\approx 100\ K)$.

In the past there were doubts on the ability of the EPI to explain the linear temperature dependence of the resistivity in the underdoped system [58] $Bi_{2+x}Sr_{2-y}CuO_{6\pm\delta}$, which starts at low $T > 10-20\ K$. Because the asymptotic T^5 behavior of $\rho(T)$ (for $T \ll \Theta_D$) is absent in this sample, then it seems that this experiment is questioning seriously the contribution of the EPI to the resistivity. However, there are other measurements [59] on $Bi_{2+x}Sr_{2-y}CuO_{6\pm\delta}$ where the linear behavior starts at higher temperature, i.e. at $T > 50\ K$. Additionally, the resistivity measurements [14] on Bi_2SrCuO_x samples with low $T_c \simeq 3\ K$ show saturation to finite value at $T = 0\ K$. After subtraction of this constant part one obtains the Bloch-Grüneisen behavior between $T_c \simeq 3\ K$ and $300\ K$, which is due to the EPI.

Concerning the EPI, the above results imply the following possibilities: (**a**) $\lambda_{tr} \ll 1 < \lambda$ and the pairing is due to the *EPI*, or (**b**) $\lambda_{tr} \simeq \lambda \approx 0.4 - 0.6$ and the EPI is ineffective (although present) in pairing; (**c**) $\lambda_{tr} \simeq \lambda$ but the EPI is responsible for pairing on the expense of some peculiarities of equations describing superconductivity. In Section 5. we present a theory of the EPI renormalized by strong electronic correlations, which is in favor of the case (**a**). It is interesting that the similar puzzling situation ($\lambda_{tr} \ll \lambda$) is realized in $Ba_xK_{1-x}BiO_3$ compound (with $T_c \simeq 30\ K$), where optical measurements give $\lambda_{tr} \approx 0.1 - 0.3$ [15], while tunnelling measurements [16] give $\lambda \sim 1$. Note, in $Ba_xK_{1-x}BiO_3$ there are no magnetic fluctuations (or magnetic order) and no signs of strong electronic correlations. Therefore, the EPI is favored as the pairing mechanism in $Ba_xK_{1-x}BiO_3$. It seems that in this compound *long-range forces*, in conjunction with some nesting effects, may be responsible for this discrepancy?

One can summarize, that the EPI theory, which pretends to explain the normal metallic state and superconductivity in HTSC oxides, is confronted with the problem of explaining why the EPI coupling is present in self-energy effects (governed by the coupling constant $\lambda > 1$) but it is suppressed in transport properties (which depend on $\lambda_{tr} < 1$), i.e. why λ_{tr} is (much) smaller than λ. One of the possibilities is that strong electronic correlations, as well as the long-range Madelung forces, affect the EPI significantly. This will be discussed in forthcoming sections. In light of the above discussion it is also important to know the role of the EPI in the formation of $d-wave$ superconducting state in HTSC oxides, i.e. why it is compatible with d-wave pairing?

In this review we discuss theoretical and experimental results in HTSC oxides and mostly those which are related to: (i) strong quasiparticle scattering in the normal state, (ii) the pairing mechanism [17], [18], [19], [20].

The paper is organized as follows. In Section 2. we review important physical properties of HTSC oxides in the normal and superconducting state, whose understanding is a basis for the microscopic theory of superconductivity. Only those experiments (and theoretical interpretations) are discussed here which are in our opinion most important in getting information on the pairing mechanism in HTSC oxides. In Section 3. we discuss

the general theory of the EPI and its low-energy version. The theory of strong electronic correlations is studied in Section 4., where much space is devoted to a systematic, recently elaborated, method for strongly correlated electrons [17], [18], [19], [20] - the X-method. The latter considers strongly interacting quasiparticles as *composite objects*, contrary to the slave-boson method which at some stage assumes spin and charge separation [28]. A systematic theory of the renormalization of the EPI coupling by strong electronic correlations [17], [18] is exposed in Section 5. It is shown there, that the *forward scattering peak* develops in the EPI by lowering doping, while the coupling at large transfer momenta (the backward scattering) is suppressed .

In Section 6. we summarize the basic predictions of the theory based on the existence of the forward scattering peak in the EPI, impurity and Coulomb scattering, and possible relation between the forward scattering peak in the EPI and pseudogap. The comparison between the EPI and SFI prediction is given in Section 7. The (im)possibility of superconductivity in the Hubbard and t-J mode is studied in Section 8., while the obtained results are summarized in Section 9.

1.2. Prejudices on the EPI

In spite of the reach experimental evidence in favor of the strong EPI in HTSC oxides there was a disproportion in the research (especially theoretical) activity, since the investigation of the spin fluctuations mechanism of pairing prevailed in the literature. This was partly due to a theoretically unfounded statement - given in [10], on the upper limit of T_c in the phonon mechanism of pairing. It is well known that in an electron-ion system besides the EPI there is also the repulsive Coulomb interaction and these are not independent. In the case of an isotropic and homogeneous system with a weak (quasi)particle interaction the effective potential $V_{eff}(\mathbf{k}, \omega)$ in the leading approximation looks like as for two external charges (*e*) embedded in the medium with the *total macroscopic longitudinal dielectric function* $\varepsilon_{tot}(\mathbf{k}, \omega)$ (**k** is the momentum and ω is the frequency) [12], i.e.

$$V_{eff}(\mathbf{k}, \omega) = \frac{V_{ext}(\mathbf{k})}{\varepsilon_{tot}(\mathbf{k}, \omega)} = \frac{4\pi e^2}{k^2 \varepsilon_{tot}(\mathbf{k}, \omega)}. \tag{1}$$

In the case when the interaction between quasiparticles is strong, the state of embedded quasiparticles changes substantially due to the interaction with other quasiparticles, giving rise to $V_{eff}(\mathbf{k}, \omega) \neq 4\pi e^2/k^2 \varepsilon_{tot}(\mathbf{k}, \omega)$. In that case V_{eff} depends on other (than $\varepsilon_{tot}(\mathbf{k}, \omega)$) response functions. However, in the case when Eq.(1) holds the weak-coupling limit is realized where T_c is given by $T_c = \bar{\omega} \exp(-1/(\lambda - \mu^*)$ [9], [12]). Here, λ is the EPI coupling constant, $\bar{\omega}$ is the average phonon frequency and μ^* is the Coulomb pseudo-potential, $\mu^* = \mu/(1 + \mu \ln E_F/\bar{\omega})$ (E_F is the Fermi energy). λ and μ are expressed by $\varepsilon_{tot}(\mathbf{k}, \omega = 0)$

$$\langle N(0) V_{eff}(\mathbf{k}, \omega = 0) \rangle \equiv \mu - \lambda = N(0) \int_0^{2k_F} \frac{k dk}{2k_F^2} \frac{4\pi e^2}{k^2 \varepsilon_{tot}(\mathbf{k}, \omega = 0)}, \tag{2}$$

where $N(0)$ is the density of states at the Fermi surface and k_F is the Fermi momentum - see more in [11]. In [10] it was claimed that the lattice stability of the system with respect to the charge density wave formation implies that the condition $\varepsilon_{tot}(\mathbf{k}, \omega = 0) > 1$ must be fulfilled for all $\mathbf{k}$. If this were correct then from Eq.(2) follows that $\mu > \lambda$, which limits the maximal value of T_c to the value $T_c^{\max} \approx E_F \exp(-4 - 3/\lambda)$. In typical metals $E_F < (1 - 10)\ eV$ and if one accepts this (unfounded) statement that $\lambda \leq \mu \leq 0.5$ one obtains $T_c \sim (1 - 10)\ K$. The latter result, of course if it would be true, means mean that the EPI is ineffective in producing high-T_c superconductivity, let say not higher than 20 K? However, this result is apparently in conflict with a number of experimental results in low-T_c superconductors (LTS), where $\mu \leq \lambda$ and $\lambda > 1$. For instance, $\lambda \approx 2.5$ is realized in *PbBi* alloy, which is definitely much higher than $\mu(< 1)$ thus contradicting the statement made in Ref.[10].

The statement in [10] that $\varepsilon_{tot}(\mathbf{k}, \omega = 0) > 1$ must be fulfilled for all $\mathbf{k}$ is in an apparent conflict with the basic theory [12], which tells us that $\varepsilon_{tot}(\mathbf{k}, \omega)$ is not the response function. If a small external potential $\delta V_{ext}(\mathbf{k}, \omega)$ is applied to the system it induces screening by charges of the medium and the total potential is given by $\delta V_{tot}(\mathbf{k}, \omega) = \delta V_{ext}(\mathbf{k}, \omega) / \varepsilon_{tot}(\mathbf{k}, \omega)$ which means that $1/\varepsilon_{tot}(\mathbf{k}, \omega)$ is the response function. The latter obeys the Kramers-Kronig dispersion relation which implies the following stability condition: $1/\varepsilon_{tot}(\mathbf{k}, \omega = 0) < 1$ for $\mathbf{k} \neq 0$, i.e. either $\varepsilon_{tot}(\mathbf{k} \neq 0, \omega = 0) > 1$ or $\varepsilon_{tot}(\mathbf{k} \neq 0, \omega = 0) < 0$. This important theorem has been first proved in the seminal article by David Abramovich Kirzhnits [12] and it invalidates the formula for $T_c^{\max}$ by setting aside the above restriction on the maximal value of T_c.

Is $\varepsilon_{tot}(\mathbf{k} \neq 0, \omega = 0) < 0$ realized in real systems? This question was thoroughly studied in Ref. [13] and in the context of HTSC in [11], while here we enumerate the main results. In the inhomogeneous system, such as a crystal, the total longitudinal dielectric function is matrix in the space of reciprocal lattice vectors ($\mathbf{Q}$), i.e. $\hat{\varepsilon}_{tot}(\mathbf{k} + \mathbf{Q}, \mathbf{k} + \mathbf{Q}', \omega)$, and $\varepsilon_{tot}(\mathbf{k}, \omega)$ is defined by $\varepsilon_{tot}^{-1}(\mathbf{k}, \omega) = \hat{\varepsilon}_{tot}^{-1}(\mathbf{k} + \mathbf{0}, \mathbf{k} + \mathbf{0}, \omega)$. For instance in the dense metallic systems with one ion per cell (such as the metallic hydrogen) and with the electronic dielectric function $\varepsilon_{el}(\mathbf{k}, 0)$ one has [13]

$$\varepsilon_{tot}(\mathbf{k}, 0) = \frac{\varepsilon_{el}(\mathbf{k}, 0)}{1 - \frac{1}{\varepsilon_{el}(\mathbf{k}, 0) G_{EP}(\mathbf{k})}}. \tag{3}$$

At the same time the frequency of the longitudinal phonon $\omega_l(\mathbf{k})$ is given by

$$\omega_l^2(\mathbf{k}) = \frac{\Omega_{pl}^2}{\varepsilon_{el}(\mathbf{k}, 0)} [1 - \varepsilon_{el}(\mathbf{k}, 0) G_{EP}(\mathbf{k})], \tag{4}$$

where G_{EP} is the local field correction G_{EP} - see Ref. [13]. The right condition for the lattice stability requires that the phonon frequency must be positive, $\omega_l^2(\mathbf{k}) > 0$, which implies that for $\varepsilon_{el}(\mathbf{k}, 0) > 0$ one has $\varepsilon_{el}(\mathbf{k}, 0) G_{EP}(\mathbf{k}) < 1$. The latter gives $\varepsilon_{tot}(\mathbf{k}, 0) < 0$. The calculations [13] show that in the metallic hydrogen crystal $\varepsilon_{tot}(\mathbf{k}, 0) < 0$ for all $\mathbf{k} \neq \mathbf{0}$. The sign of $\varepsilon_{tot}(\mathbf{k}, 0)$ for a number of crystals with more ions per unit cell is thoroughly analyzed in [13], where it is shown that $\varepsilon_{tot}(\mathbf{k} \neq \mathbf{0}, 0) < 0$ is *more a rule than an exception*. The physical reason for $\varepsilon_{tot}(\mathbf{k} \neq \mathbf{0}, 0) < 0$ is due to local field effects described by $G_{EP}(\mathbf{k})$. Whenever the local electric field $\mathbf{E}_{loc}$ acting on electrons (and

ions) is different from the average electric field $\mathbf{E}$, i.e. $\mathbf{E}_{loc} \neq \mathbf{E}$ there are corrections to $\varepsilon_{tot}(\mathbf{k},0)$ (or in the case of the electronic subsystem to $\varepsilon_e(\mathbf{k},0)$) which may lead to $\varepsilon_{tot}(\mathbf{k},0) < 0$.

The above analysis tells us that in real crystals $\varepsilon_{tot}(\mathbf{k},0)$ can be negative in the large portion of the Brillouin zone giving rise to $\lambda - \mu > 0$, due to local field effects. This means that the dielectric function ε_{tot} *does not limit T_c in the phonon mechanism of pairing*. The latter does not mean that there is no limit on T_c at all. We mention in advance that the local field effects play important role in HTSC oxides, due to their layered structure with ionic-metallic binding, thus giving rise to large *EPI* - see more subsequent sections.

In concluding we point out, that there are no theoretical and experimental arguments for ignoring the EPI in HTSC oxides. However, it is necessary to answer several important questions which are also related to experimental findings in HTSC oxides: (**1**) If the EPI is responsible for pairing in HTSC oxides and if superconductivity is of $d-wave$ type, how these two facts are compatible? (**2**) Why is the transport EPI coupling constant λ_{tr} (entering the resistivity formula) much smaller than the pairing EPI coupling constant $\lambda (> 1)$ (entering the formula for T_c), i.e. why one has $\lambda_{tr}(\approx 0.4 - 0.9) \ll \lambda (\sim 2)$? (**3**) Is the high T_c value possible for a moderate EPI coupling constant, let say for $\lambda \leq 1$? (**4**) Finally, if the EPI interaction is ineffective for pairing in HTSC oxides why it is so?

2. EXPERIMENTS RELATED TO PAIRING MECHANISM

A much more extensive discussion (than here) of the experimental situation in HTSC oxides is given in a number of papers - see reviews [2], [11]. In the following we discuss briefly experimental results, by including the most recent ones, which can give us a clue for the pairing mechanism in the HTSC oxides.

2.1. Magnetic neutron scattering

2.1.1. Normal state

The cross-section for the *inelastic neutron magnetic scattering* is expressed via the Fourier transform of the spin-correlation function (the spin structure factor) $S^{\alpha\alpha}(\mathbf{k},\omega)$ which is proportional to the imaginary part of the susceptibility $Im\chi(\mathbf{k},k_z,\omega)$. In the (normal) metallic state of doped HTSC oxides without magnetic order the inelastic scattering (in absence of the AF magnetic order) is of interest and in most systems $Im\chi(\mathbf{k},k_z,\omega)$ is peaked around the *AF* wave-vector $\mathbf{Q} = (\pi,\pi)$. The pronounced magnetic fluctuations in the underdoped metallic state is contrary to usual metals (described by the Landau-Fermi liquid) where the magnetic fluctuations are much weaker. In HTSC oxides $Im\chi(\mathbf{k},\omega)$ depends on hole doping, and for instance, in the bilayer (two layers per the unit cell) compound $YBa_2Cu_3O_{6+x}$ the low energy spectra is peaked at $\mathbf{Q}$, whose width δ_m broadens by increasing doping concentration - see review [66]. Around the optimal doping the magnetic correlation length $\xi_m = (2/\delta_m) \sim (1-2)a$ is almost tem-

perature independent. This fact contradicts the assumption of the theory of spin fluctuation mechanism by the Pines group [29], where ξ_m is strongly T-dependent. We stress that in the SFI theory $Im\chi(\mathbf{k},\omega)$ is important quantity since the effective pairing potential $V_{eff}(\mathbf{k},\omega)$ and the self-energy $\Sigma_{sf}(\mathbf{k},\omega)$ are approximately given by (on the real frequency axis - see [2])

$$\Sigma_{sf}(\mathbf{k},\omega) \approx \sum_{\mathbf{q}} \int \frac{d\Omega}{\pi} G(\mathbf{q},\Omega) V_{eff}(\mathbf{k}+\mathbf{q},\omega+\Omega),$$

$$V_{SF}(\mathbf{q},\omega+i0^+) = g_{SF}^2 \int_{-\infty}^{\infty} \frac{d\Omega}{\pi} \frac{Im\chi(\mathbf{q},\Omega+i0^+)}{\Omega-\omega} \tag{5}$$

where $G(\mathbf{q},\Omega)$ is the electron Green's function. This approach can be theoretically justified in the weak coupling limit ($U \ll W$) only . Although the HTSC oxides are far from this limit this expression is frequently used in the SFI theories of pairing, where larger $Im\chi(\mathbf{k},\omega)$ should give larger T_c.

What is the experimental situation? The antibonding (odd) spectral function $Im\chi^{(odd)}(\mathbf{k},\omega)$ of $YBa_2Cu_3O_{6+x}$ is strongly doping dependent as it is seen in Fig. 1. By comparing the magnetic neutron scattering (normal state) spectra in $YBa_2Cu_3O_{6.92}$ and $YBa_2Cu_3O_{6.97}$ in Fig. 1a the difference is reflected in their spectral functions $Im\chi^{(odd)}(\mathbf{k},\omega)$. Namely, in the frequency interval which is important for superconducting pairing $Im\chi^{(odd)}(\mathbf{Q},\omega)$ of

$YBa_2Cu_3O_{6.92}$ is much larger than that in $YBa_2Cu_3O_{6.97}$ although the differences in their critical temperatures T_c is very small, i.e. $T_c = 91$ K for $YBa_2Cu_3O_{6.92}$ and $T_c = 92.5$ K for $YBa_2Cu_3O_{6.97}$. This result, in conjunction with the anti-correlation between the NMR spectral function $I_\mathbf{Q} = \lim_{\omega \to 0} Im\chi(\mathbf{Q},\omega)/\omega$ and T_c - shown in Fig. 1a, is apparently against the SFI theoretical models for pairing mechanism [29], [65].

2.1.2. Superconducting state

In the superconducting state the magnetic fluctuations are drastically changed, what is in fact expected for the singlet pairing state which induces spin gap in the magnetic excitation spectrum of s-wave superconductors. However, the spectrum in the superconducting state of HTSC oxides is more complex due to d-wave pairing and specificity of the band structure. For instance, at $T < T_c$ the sharp peak in $Im\chi^{(odd)}(\mathbf{k},\omega)$ is seen at $\omega_{reson} = 41$ meV and at $\mathbf{k}_{2D} = (\pi/a, \pi/a)$ of the fully oxygenated (optimally doped) $YBa_2Cu_3O_{6+x}$ ($x \sim 1$, $T_c \approx 92$ K) [71], [72]. The doping dependence of the peak position and its width [66] is shown in Fig. 1c, where it is seen that by increasing doping the peak in the superconducting state becomes sharper and moves to higher frequencies (scaling with T_c), while its height is decreasing. This can be qualitatively explained by using the *RPA* susceptibility

$$\chi(\mathbf{k},\omega) = \frac{\chi_0(\mathbf{k},\omega)}{1 - U_{eff}(\mathbf{q})\chi_0(\mathbf{k},\omega)}, \tag{6}$$
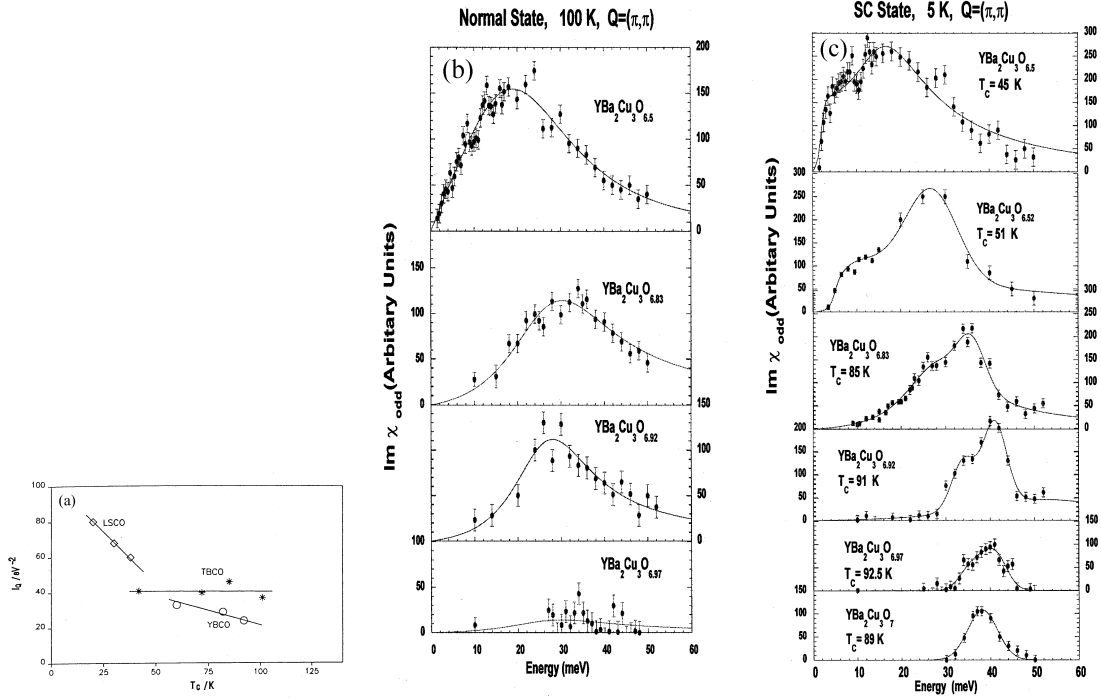
FIGURE 1. Magnetic spectral function $Im\chi^{(-)}(\mathbf{k}, \omega)$: (a) $I_Q(T_c)$ values at $T = 200\ K$ for various HTSC oxides: $LSCO$ - $La_{2x}Sr_xCuO_4$; $TBCO$ - $Tl_2Ba_2CuO_{6+x}$ and $Tl_2Ba_2CaCu_2O_8$; $YBCO$ - and $YBa_2Cu_4O_8$ - from [67]; (b) for $YBa_2Cu_3O_{6+x}$ in the normal state at $T = 100\ K$ and at $Q = (\pi, \pi)$. 100 counts in the vertical scale corresponds to $\chi_{max}^{(-)} \approx 350\mu_B^2/eV$ - from [66]; (c) for $YBa_2Cu_3O_{6+x}$ in the superconducting state at $T = 5\ K$ and at $Q = (\pi, \pi)$ - from [66].

where the bare susceptibility $\chi_0(\mathbf{k}, \omega)$ contains the coherence factor $[1 - (\xi_{\mathbf{k+q}}\xi_{\mathbf{q}} + \Delta_{\mathbf{k+q}}\Delta_{\mathbf{q}})/E_{\mathbf{k+q}}E_{\mathbf{q}}]$ - see [2]. This (type II) coherence factor reflects the (well known) fact that the magnetic scattering is not the time reversal symmetry. In the case when $\mathbf{k}$ and $\mathbf{k} + \mathbf{q}$ are near the Fermi surface and when $\Delta_{\mathbf{k+q}} \approx -\Delta_{\mathbf{q}}$ at $\mathbf{k} = \mathbf{Q} = (\pi/a, \pi/a)$ the coherence factor is of the order of one at or near the Fermi surface (note $\xi_{\mathbf{k+q}}\xi_{\mathbf{q}} \leq 0$) and therefore contributes significantly to $\chi_0(\mathbf{k} = \mathbf{Q}, \omega)$. The case $\Delta_{\mathbf{q}}\Delta_{\mathbf{k+q}} < 0$ is realized when the $d - wave$ order parameter, for instance $\Delta_{\mathbf{k}} = (\Delta_0/2)[\cos k_x - \cos k_y]$. So, the mechanism of the peak formation (below T_c) is the consequence of the electron-pair creation with an electron in the $(+)$ lobe and a hole in the $(-)$ lobe of the superconducting order parameter. Note, that the $(\pm)$ lobes of $\Delta_{\mathbf{k}}$ are separated approximately by the wavevector $\mathbf{Q} = (\pi/a, \pi/a)$. Due to the large density of states near the lobes a large peak in $Im\chi(\mathbf{k} = \mathbf{Q}, k_z, \omega)$ is expected to be realized, i.e. $\omega_{reson} \geq 2\Delta_0$. Of course the better (than RPA) calculations of $\chi(\mathbf{k} = \mathbf{Q}, k_z, \omega)$ is needed for a full quantitative analysis, where a possible resonance in $\chi(\mathbf{k}, \omega)$ with $\omega_{reson} \leq 2\Delta_0$ can also contribute. It is important to stress, that the magnetic resonance in the superconducting state is *consequence of superconductivity* but not its cause as it was stated in some papers. It can not be the cause for superconductivity simply because its intensity at T around T_c is vanishing small and not affecting T_c at all. If the magnetic resonance would be the origin for

superconductivity (and high T_c) the phase transition at T_c must be first order, contrary to experiments where it is second order.

The next very serious argument against the SFI pairing mechanism is the *smallness of the coupling constant g_{sf}*. Namely, the real spin-fluctuation coupling constant is rather small $g_{sf} \leq 0.2$ eV, what is in contrast to the large value ($g_{sf}^{(MMP)} \sim 0.6$ eV) assumed in the SFI theory by the Pines group - see the MMP model in Section 7.1. The upper limit of $g_{sf} (\leq 0.2$ $eV)$ is extracted from : (**i**) the width of the resonance peak [68], and (**ii**) the small magnetic moment ($\mu < 0.1$ μ_B) in the antiferromagnetic state of LASCO and YBCO [69]. Note, that the pairing coupling in the SFI theory is $\lambda_{sf} \sim g_{sf}^2$, and for the realistic value of $g_{sf} \leq 0.2$ eV it would produce $\lambda_{sf} \sim 0.2$ and very small $T_c \sim 1$ K. The *SFI* model roots on its basic $t - J$ Hamiltonian. However, recently it was shown in [70] that *there is no superconductivity in the t-J model* at temperatures characteristic for HTSC oxides - see Fig. 27 below. If it exists T_c must be very low.

In conclusion, the inelastic magnetic neutron scattering give evidence that the spin fluctuations interaction (SFI), although pronounced in underdoped systems, is *ineffective* in the pairing mechanism of HTSC oxide. However, the SFI in conjunction with the residual Coulomb repulsion *triggers* superconductivity from s-wave to d-wave, whose strength is predominantly due to the EPI - see discussion in Sections 5.-7..

2.2. Dynamical conductivity and resistivity $\rho(T)$

Since $\sigma(\omega)$ and $\rho(T)$ give important information on the dominant scattering mechanism, in the following we analyze their properties in more details.

2.2.1. Dynamical conductivity $\sigma(\omega)$

$\sigma(\omega)$ is in fact *derived quantity* since it is extracted from the *measured* optic reflectivity $R(\omega)$ and absorption $A(\omega)$. By measuring the normal-incident (of light) reflectivity $R(\omega)$ in the whole frequency region ($0 \leq \omega < \infty$) one can determine the phase $\phi(\omega)$ of the complex reflectivity

$$r(\omega) = \sqrt{R(\omega)} e^{i\phi(\omega)} = \frac{\sqrt{\varepsilon(\omega)} - 1]}{\sqrt{\varepsilon(\omega)} + 1} \tag{7}$$

by the Kramers-Kronig relation, and accordingly to determine in principle the complex dielectric function

$$\varepsilon(\omega) = \varepsilon_\infty + \varepsilon_{latt}(\omega) + \frac{4\pi i \sigma(\omega)}{\omega}, \tag{8}$$

where ε_∞ and $\sigma(\omega)$ are electronic contributions and ε_{latt} is the lattice contribution. However, $R(\omega)$ is usually measured in a finite ω region and extrapolations is needed, especially at very low frequencies. This extrapolation of $R(\omega)$ also contains some model assumptions on the scattering processes in the system (on $\sigma(\omega)$), i.e. $1 - R(\omega) \sim \sqrt{\omega}$ - the Hagen-Rubens relation for the standard (with elastic scattering only) Drude metal,

or $1 - R(\omega) \sim \omega$ for strong EPI (or for marginal Fermi liquid). So, one should be always cautious not to overinterpret the meaning of $\sigma(\omega)$ obtained in such a way.

In HTSC oxides $R(\omega)$, $A(\omega)$ are usually measured in a broad frequency region - up to several eV. At such high frequencies the interband transitions take place and in order to calculate $\sigma(\omega)$ the knowledge of the band structure is needed. This problem was analyzed in the framework of the LDA band structure calculations [73] by taking into account the interband transitions, where a rather good agreement with experiments for $\omega > 1$ eV was found. This is surprising since the *LDA*-method does not contain the Hubbard bands, and according to [73] there is no sign of transitions between Hubbard sub-bands in the high energy region of $\sigma(\omega)$. This very interesting result deserves to be further analyzed since it contradicts the physics of the Hubbard models.

Here we discuss briefly the normal state $\sigma(\omega)$ in the low frequency region $\omega < 1$ eV where the *intraband* effects dominate the quasiparticle scattering. In the low ω regime the processing of the data in the metallic state of HTSC oxides is usually done by using the generalized Drude formula for the inplane conductivity $\sigma(\omega) = \sigma_1 + i\sigma_2$ [86], [87], [88]

$$\sigma_{ii}(\omega) = \frac{\omega_{p,ii}^2}{4\pi} \frac{1}{\Gamma_{tr}(\omega, T) - i\omega m_{tr}(\omega)/m_\infty}. \tag{9}$$

$i = a, b$ enumerates the plane axis, $\Gamma_{tr}(\omega, T)$ and $m_{tr}(\omega)$ are the transport scattering rate and optic mass, respectively. Sometimes in the analysis of experimental data the effective transport scattering rate $\Gamma_{tr}^*(\omega, T)$ and the effective plasma frequency $\omega_p^*(\omega)$ are used, which are defined by

$$\Gamma_{tr}^*(\omega, T) = \frac{m}{m_{tr}(\omega)}\Gamma_{tr}(\omega, T) = \frac{\omega\sigma_1(\omega)}{\sigma_2(\omega)}, \tag{10}$$

and

$$\omega_p^{*2}(\omega) = \frac{m}{m_{tr}(\omega)}\omega_p^2. \tag{11}$$

For best optimally doped HTSC systems the best fit for $\Gamma_{tr}^*(\omega, T)$ is given by $\Gamma_{tr}^*(\omega, T) \approx \max\{\alpha T, \beta\omega\}$ in the temperature and frequency range from very low (~ 100 K) up to 2000 K, where α, β are of the order one - see Fig. 2. These results tell us that the quasiparticle liquid, which is responsible for transport properties in HTSC, is not a simple (weakly interacting) Fermi liquid. We remind the reader that in the usual (canonical) normal Fermi liquid with the Coulomb interaction on has $\Gamma_{tr}(\omega, T) \sim \Gamma_{tr}^*(\omega, T) \sim \Gamma(\omega, T) \sim \max\{T^2, \omega^2\}$ at low T and ω, which means that quasiparticles are well defined objects near (and at) the Fermi surface since $\omega \gg \Gamma(\omega, T)$. In case of HTSC oxides with $\Gamma(\omega, T) \sim \max(\omega, T)$ in the broad regions and the quasiparticles decay rapidly and therefore are not well defined objects. At these temperatures and frequencies the simple canonical Landau quasiparticle concept fails. The latter behavior can be due to the strong electron-electron inelastic scattering, or due to the quasiparticle scattering on phonons (or on other bosonic excitations). It is important to stress, that quasiparticles interacting with phonons at finite T are not described with the standard Fermi liquid, in particular at $T > \Theta_D/5$, since the scattering rate is larger than the quasiparticle energy, i.e. one has $\Gamma \sim \max(\omega, T)$. Such a system is well described by the *Migdal-Eliashberg theory* whenever $\omega_D \ll E_F$ is fulfilled, which in fact treats quasiparticles
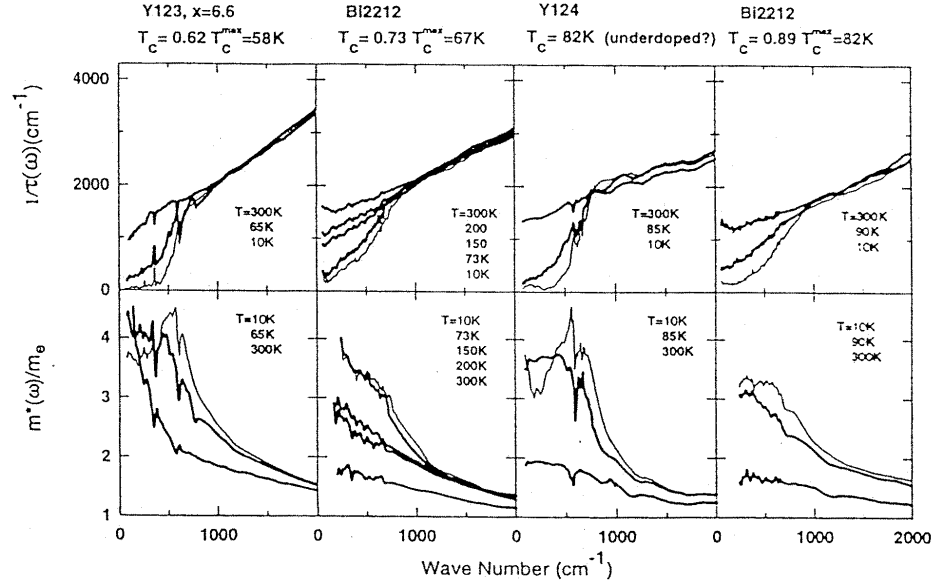
FIGURE 2. The transport scattering rate $1/\tau(\omega)$ (in the text $\Gamma_{tr}(\omega)$) and the transport effective mass $m^*(\omega)/m_e$ (in the text $m_{tr}(\omega)/m_\infty$) for series of underdoped HTSC oxides. $\Gamma_{tr}(\omega)$ is temperature independent above $1000\ cm^{-1}$ but it is depressed at low T and low ω- from [62].

beyond the original Landau quasiparticle concept. Note, that even when the original Landau quasiparticle concept fails the transport properties may be described by the Boltzmann equation, which is a wider definition of the Landau-Fermi liquid.

We point out, that in a number of articles it was *incorrectly* assumed that $\Gamma(\omega,T) \approx \Gamma_{tr}(\omega,T) \approx \Gamma_{tr}^*(\omega,T)$ holds in HTSC oxides . The above discussed experiments (see Fig. 2) give that $\Gamma_{tr}^*(\omega,T)$ is linear in the broad region of ω and T up to $2500\ K$ - see in Fig. 2. However, if $\Gamma(\omega,T)$ is due to the EPI it saturates at the maximum phonon frequencies $\omega_{max}^{ph}(\leq 1000\ K)$. By assuming also that $\Gamma^{EPI}(\omega,T) \approx \Gamma_{tr}^{EPI}(\omega,T)$ holds for all ω, in a number of papers it was concluded, that the EPI does not contribute to the inelastic scattering of quasiparticles and to the Cooper pairing in HTSC oxides. Does it hold $\Gamma^{EPI}(\omega,T) \approx \Gamma_{tr}^{EPI}(\omega,T)$ in HTSC oxides? The answer is NO.

$\sigma(\omega)$ of HTSC oxides was theoretically analyzed [87], [88] in terms of the EPI, where it was found that $\Gamma_{tr}(\omega,T)$ and $m_{tr}(\omega,T)$ depend on the transport spectral function $\alpha_{tr,EP}^2 F(\omega)$ - see more in [2]. Their analysis is based on: (i) the assumption that $\alpha_{tr,EP}^2 F(\omega) \approx \alpha_{EP}^2 F(\omega)$ - the Eliashberg spectral function: (ii) the shape of $\alpha_{EP}^2 F(\omega)$ is extracted from various tunnelling conductivity measurements, [38], [39], [40], [41], which makes a rather large EPI coupling constant and the critical temperature $\lambda = 2\int_0^\infty d\omega \alpha^2(\omega)F(\omega)/\omega \approx 2$ and $T_c \approx 90\ K$, respectively; (iii) the plasma frequency is taken to be $\omega_{pl} = 3\ eV$. It was obtained that $\Gamma_{tr}^{EP}(\omega,T) \sim \omega$ in a very broad ω-interval (up to $250\ meV$), which is much larger than the maximum phonon frequency $\omega_{max}^{ph} \approx 80\ mev$. This is illustrated in Fig. 3. Moreover, $\Gamma_{tr}^{EP}(\omega,T)$ *differs significantly* from the
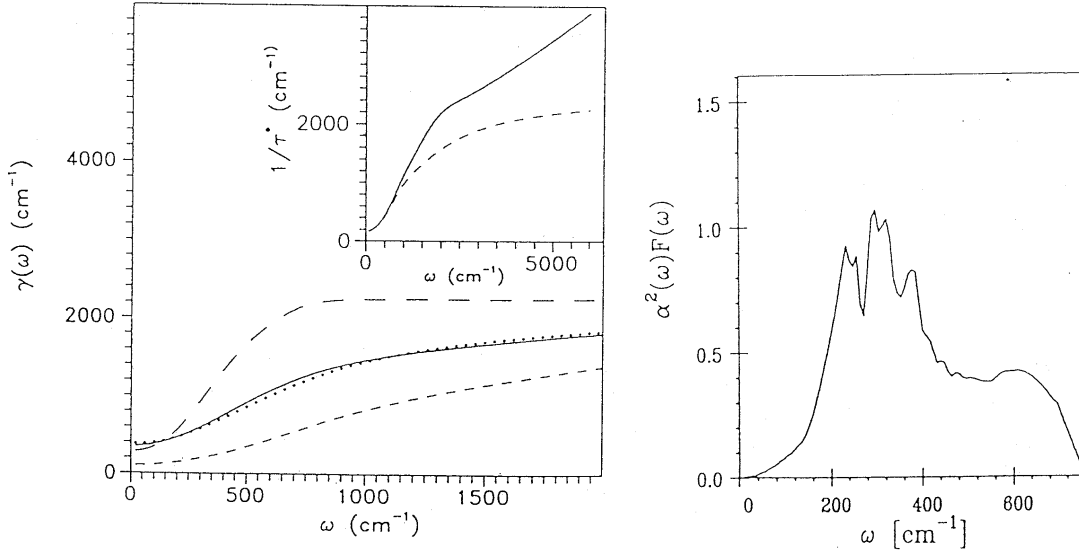
FIGURE 3. The theoretical predictions for the frequency dependence of the various relaxation rates $\gamma(=\Gamma)$ with $\alpha^2 F(\omega)$ - right: the generalized Drude fit for $\Gamma_{tr}(\omega)$ - solid line; $\Gamma_{tr}^*(\omega)$ - short-dashed line; $\Gamma(\omega)$ - long dashed line; $\Gamma_{tr}(\omega)$ calculated - dotted line. In the inset the calculated $\Gamma_{tr}^*(\omega)(= 1/\tau^*(\omega))$ with (solid line) and without (dashed line) the interband contributions with $\alpha^2 F(\omega)$ from right and at $T = 100\,K$ - from [88].

quasiparticle scattering rate $\Gamma^{EP}(\omega,T) = -2Im\Sigma(\omega)$ [87], [88]. We see from Fig. 3 that $\Gamma^{EP}(\omega,T)$ is much steeper function than $\Gamma_{tr}^{EP}(\omega,T)$ and the former saturates at much lower frequency - of the order of the maximum phonon frequency ω_{max}^{ph}.

Note, that $\Gamma_{tr}^{*,EP}(\omega,T) = (m/m_{tr}(\omega))\Gamma_{tr}^{EP}(\omega,T)$ is also quasi-linear function in a very broad region $150\,K < \omega < 3000\,K$ - see Fig. 3. The slope of $\Gamma_{tr}^{*,EP}(\omega,T)$ is of the order of one, in accordance with experiments results [87], [88], and it (and $\Gamma_{tr}^{EP}(\omega,T)$) saturates at $\omega_{sat} \simeq -Im\Sigma_{tr}(\omega_{sat}) \gg \omega_{max}^{ph}$ only. The transport spectral function $\alpha_{tr}^2(\omega)F(\omega)$ can be also extracted from the transport scattering rate $\Gamma_{tr}(\omega,T=0)$ - see [2], [11], since the theory gives that

$$\Gamma_{tr}(\omega,T=0) = \frac{2\pi}{\omega}\int_0^\omega d\Omega(\omega-\Omega)\alpha_{tr}^2(\Omega)F(\Omega). \qquad (12)$$

However, real measurements are performed at finite $T(> T_c)$ where $\alpha_{tr}^2(\omega)F(\omega)$ is the solution of the Fredholm integral equation (of the first kind) . Such an inverse problem at finite temperatures in HTSC oxides is studied first in [87] (see also [88]), where the smeared structure of $\alpha_{tr}^2(\omega)F(\omega)$ in $YBa_2Cu_3O_{7-x}$ was obtained, which is in qualitative agreement with the shape of the phonon density of states $F(\omega)$. At finite T the problem is more complex because the fine structure of $\alpha_{tr}^2(\omega)F(\omega)$ gets blurred as the calculations in [74] show. The latter gave that $\alpha_{tr}^2(\omega)F(\omega)$ ends up at $\omega_{max} \approx 70-80\,meV$, which is the maximal phonon frequency in HTSC oxides. This result indicates strongly that the EPI in HTSC oxides is dominant in the IR optics. We point out, that if $R(\omega)$ (and $\sigma(\omega)$) are due to some bosonic process with large frequency cutoff ω_c in the spectrum, as it is

the case with the spin-fluctuation (SFI) scattering where $\omega_c \approx 400 \ meV$, the extracted $\alpha_{tr}^2(\omega)F(\omega)$ should end up at this high ω_c. The latter is *not seen* in optic measurements at $T > T_c$, which tells us that the SFI scattering, with $\alpha_{tr}^2(\omega)F(\omega) \sim g_{sf}^2 Im\chi_s(\omega)$ and with the cutoff $\omega_c \geq 400 \ meV$, is rather weak and ineffective in optics of HTSC oxides..

We stress that the extraction of Γ_{tr} from $R(\omega)$ is subtle procedure, because it depends also on the assumed value of ε_∞. For instance, if one takes $\varepsilon_\infty = 1$ then Γ_{tr}^{EP} is linear up to very high ω, while for $\varepsilon_\infty > 1$ the linearity of Γ_{tr}^{EP} saturates at lower ω. Since $\Gamma_{tr}^{EP}(\omega, T)$, extracted in [62], and recently also in [63], is linear up to very high ω it may be that the ion background and interband transitions (contained in ε_∞) are not properly taken into account in these papers. As a curiosity in a number of papers, even in the very cited ones such as [62], [63], there is no information which value for ε_∞ they take. We stress again, that the behavior of $\Gamma_{tr}(\omega)$ is linear up to much higher frequencies for $\varepsilon_\infty = 1$ than for $\varepsilon_\infty \approx 4 - 5$ - the characteristic value for HTSC, giving a lot of room for inadequate interpretations of results. In that respect, the recent elipsometric optic measurements on YBCO [75] confirm the results of the previous ones [76] that $\varepsilon_\infty \geq 4$ and that Γ_{tr}^{EP} saturates at lower frequency than it was the case in Ref. [62]. We stress again that the reliable estimation of the value and ω, T dependence of $\Gamma_{tr}(\omega)$ and $m(\omega)$ can be done, not from the reflectivity measurements [62], [63], but from elipsometric ones only [76], [75].

In concluding this part we stress two facts: (**1**) The large difference in the ω, T behavior of $\Gamma_{tr}^{EP}(\omega, T)$ and $\Gamma^{EP}(\omega, T)$ is not a specificity of HTSC oxides but it is realized also in a number of *LTSC* materials. In fact this is a common behavior even in simple metals, such as Al, Pb, as shown in [118], where $\Gamma^{EP}(\omega, T)$ saturates at much lower (Debay) frequency than $\Gamma_{tr}^{EP}(\omega, T)$ and $\Gamma_{tr}^{*,EP}(\omega, T)$ do. In that respect the difference between simple metals and HTSC oxides is in the scale of phonon frequencies, i.e. $\omega_{\max}^{ph} \sim 100 \ K$ in simple metals, while $\omega_{\max}^{ph} \sim 1000 \ K$ in HTSC oxides. Having in mind these well established and well understood facts, it is very surprising that even nowadays, 18 years after the discovery of HTSC oxides, the principal and quantitative difference between Γ and Γ_{tr} is neglected in the analysis of experimental data. For instance, by neglecting the pronounced (qualitative and quantitative) difference between $\Gamma_{tr}(\omega, T)$ and $\Gamma(\omega, T)$, in the recent papers [63], [64] were made far reaching, but unjustified, conclusions that the magnetic pairing mechanism prevails; (**2**) It is worth of mentioning, that quite similar (to HTSC oxides) properties, of $\sigma(\omega)$, $R(\omega)$ and $\rho(T)$ were observed in experiments [92] on isotropic metallic oxides $La_{0.5}Sr_{0.5}CoO_3$ and $Ca_{0.5}Sr_{0.5}RuO_3$ - see Fig. 4. We stress that in these compounds there are no signs of antiferromagnetic fluctuations (which are present in HTSC oxides) and the peculiar behavior is probably due to the EPI.

It is worth of mentioning that after the discovery of HTSC in 1986 a number of controversial results related to $\sigma(\omega)$ were published, followed by a broad spectrum of results and interpretations, from standard approaches up to highly exotic ones. For example, the reported experimental values for ω_{pl} were in the surprisingly large range $(0.06 - 25) \ eV$, causing a number of exotic (and confusing) theoretical models for electronic dynamics - see more in [76]. (The similar situation was with ARPES measurements - see below.) So, one should be very cautious in interpreting experimental and theoretical results. In that respect, recent experiments related to the *optical sum-rule* is an additional example
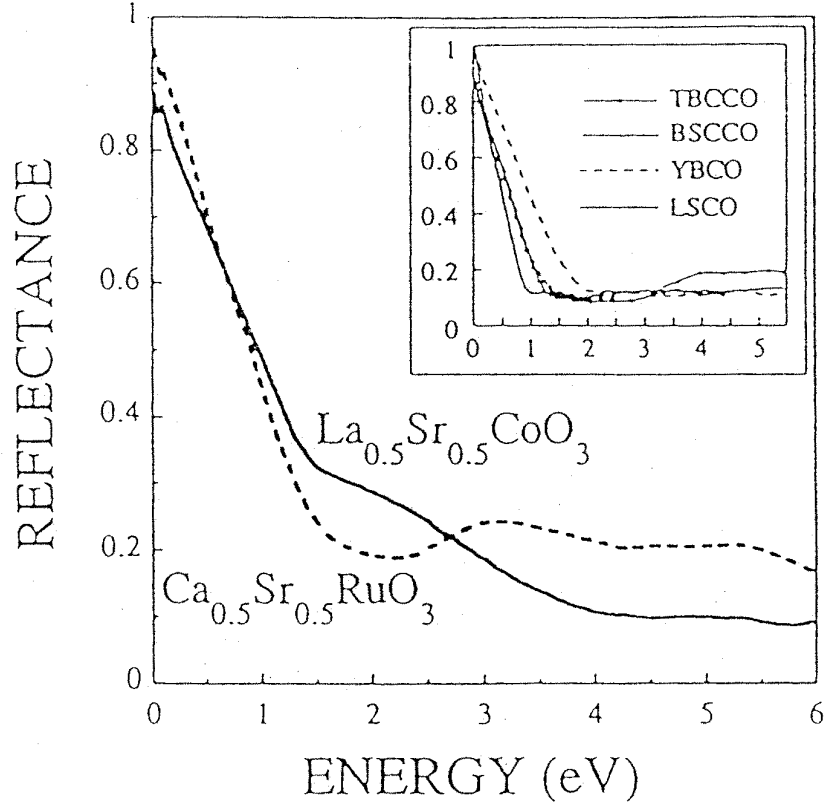
FIGURE 4. Broad range specular reflectance spectra of $Ca_{0.5}Sr_{0.5}RuO_3$ (broken line) and $La_{0.5}Sr_{0.5}CoO_3$ (solid line). Inset spectra of $Tl_2Ba_2Ca_2Cu_3O_{10}$, $Bi_2Sr_2CaCu_2O_8$, $YBa_2Cu_3O_7$ and $La_{1.85}Sr_{0.15}CuO_4$. From [92].

for controversies in this field coming from inadequate interpretations of results. This is the reason why we devote more space to the problem of "violation" of partial sum-rule.

There are two kinds of sum rules which are used in interpreting results on $\sigma(\omega)$. The first one is the *total sum rule* and in the normal state it reads

$$\int_0^\infty \sigma_1^N(\omega)d\omega = \frac{\omega_{pl}^2}{8} = \frac{\pi n e^2}{2m}, \tag{13}$$

while in the *superconducting state* [77] it is given by the Tinkham-Ferrell-Glover (TFG) sum-rule

$$\frac{c^2}{8\lambda_L^2} + \int_{+0}^\infty \sigma_1^S(\omega)d\omega = \frac{\omega_{pl}^2}{8}. \tag{14}$$

Here, n - is the total electron density, e - the electron charge, m - the bare electron mass, λ_L - the London penetration depth. The first term $c^2/8\lambda_L^2$ is due to the appearance of the superconducting condensate (ideal conductivity) which contributes $\sigma_{1,cond}^S(\omega) =$

$(c^2/4\lambda_L^2)\delta(\omega)$. The total sum rule represents the fundamental property of matter - the conservation of the electron number. To calculate it one should use the total Hamiltonian $\hat{H}_{tot} = \hat{T}_e + \hat{H}_{int}$ by taking into account all electrons, bands and their interactions $\hat{H}_{int}$ (Coulomb, EPI, with impurities,etc.). Here T_e is the kinetic energy of bare electrons

$$\hat{T}_e = \sum_{\sigma} \int d^3x \psi_{\sigma}^{\dagger}(x) \frac{\hat{\mathbf{p}}^2}{2m} \psi_{\sigma}(x) = \sum_{\mathbf{p},\sigma} \frac{\mathbf{p}^2}{2m_e} c_{\mathbf{p}\sigma}^{\dagger} c_{\mathbf{p}\sigma}. \tag{15}$$

The *partial sum rule* is related to the energetics in the conduction (valence) band. Usually it is derived by using the Hamiltonian of the valence electrons

$$\hat{H}_v = \hat{T}_v + \hat{V}_{v,Coul} = \sum_{\mathbf{p},\sigma} \varepsilon_{\mathbf{p}} c_{v,\mathbf{p}\sigma}^{\dagger} c_{v,\mathbf{p}\sigma} + \hat{V}_{v,Coul}, \tag{16}$$

which contains the band-energy (with dispersion $\varepsilon_{\mathbf{p}}$) and the Coulomb interaction of valence electrons $\hat{V}_{v,Coul}$. In the normal state the *partial sum-rule* reads [78] (for general form of $\varepsilon_{\mathbf{p}}$)

$$\int_0^{\infty} \sigma_{1,v}^N(\omega) d\omega = \frac{\pi e^2}{2V} \sum_{\mathbf{p}} \frac{\langle n_{v,\mathbf{p}} \rangle_{H_v}}{m_{\mathbf{p}}} \equiv \frac{\omega_{pl,v}^2(T)}{8} \tag{17}$$

where $n_{v,\mathbf{p}} = c_{\mathbf{p}\sigma}^{\dagger} c_{\mathbf{p}\sigma}$ and the reciprocal mass is given by $1/m_{\mathbf{p}} = \partial^2 \varepsilon_{\mathbf{p}}/\partial p_x^2$. To simplify further discussion we assume for $\varepsilon_{\mathbf{p}} = -2t(\cos p_x a + \cos p_y a)$ the *tight-binding model with nearest neighbors* (n.n.) where $1/m_{\mathbf{p}} = -2ta^2 \cos p_x a$. In practice measurements are performed up to finite ω and the integration over ω goes up to some cutoff frequency ω_c (of the order of band plasma frequency). It is straightforward to show that one has (for the n.n. tight-binding model)

$$\int_0^{\omega_c} \sigma_{1,v}^N(\omega) d\omega = \frac{\pi e^2 a^2}{2} \langle -T_v \rangle \equiv \frac{\omega_{pl,v}^2(T)}{8} \tag{18}$$

where $\langle -T_v \rangle_{H_v} = -\sum_{\mathbf{p}} \varepsilon_{\mathbf{p}} \langle n_v \rangle_{H_v}$ and by $\omega_{pl,v}^2$ is defined the band plasma frequency.

In that case the *partial sum-rule in the superconducting state* reads

$$\frac{c^2}{8\lambda_L^2} + \int_{+0}^{\omega_c} \sigma_{1,v}^S(\omega) d\omega = \frac{\pi e^2 a^2}{2} \langle -T_v \rangle. \tag{19}$$

The sum-rule was studied intensively in optimally and underdoped $Bi_2Sr_2CaCu_2O_{8-x}$ and in $YBa_2Cu_3O_{7-x}$ for the *intraplane conductivity*, where the whole frequency region is separated into the low ("intraband")- and high ("interband")-frequency parts A_L and $(A_H + A_{VH})$, respectively

$$\bar{A}_L(0,\omega_c) + A_H(\omega_c, \alpha\omega_c) + A_{VH}(\alpha\omega_c, \infty) = \omega_{pl}^2/8 \tag{20}$$

with $\bar{A}_L(0,\omega_c) = A_L(0,\omega_c) + \delta_{SN}\omega_{pl,S}^2$ where $\delta_{SN} = 1$ in superconducting state and $A(\omega_1,\omega_2) = \int_{\omega_1}^{\omega_2} \sigma_1(\omega) d\omega$. The temperature dependence of A_L and A_H in the above
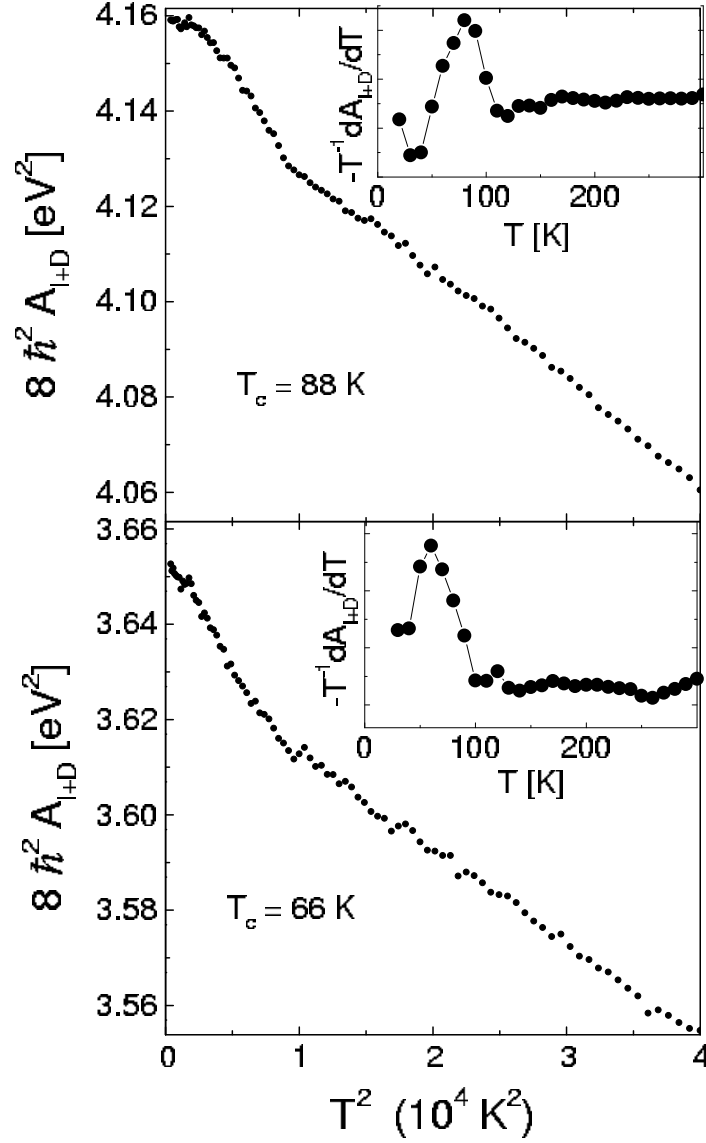
FIGURE 5. Measured T-dependence of $\bar{A}_L(0, \omega_c)$ and $\bar{A}_H(\omega_c, 2\omega_c)$ for $\omega_c \approx 1.25 eV$ of *Bi2212* ($T_c = 88$ *K*). The data from [79]

HTSC oxides was studied in [79] and [75], by assuming that "intraband" effects are exhausted for $\omega_c \approx 1.25$ *eV* and the main temperature dependence of the high-frequency region comes for $\alpha = 2$ in Eq.(22), i.e. for 1.25 *eV* $< \omega < 2.5$ *eV*, while the temperature dependence of the very high energy part A_{VH} is negligible. It was found that $\bar{A}_L(0, \omega_c)$ grows (quadratically with T) about 6% between 300 and 4 K, while $A_H(\omega_c, \alpha\omega_c)$ decreases with decreasing T^2. In the superconducting state there is a small extra increase of $\bar{A}_L(0, \omega_c)$. The results are shown in Fig. 5.

In connection with this experiment let us stress that in the BCS superconductor the

TFG sum-rule is practically satisfied if the integration goes up to $\omega_s \approx (4-6)\Delta$, where Δ is the superconducting gap. This means that in the BCS superconductors the spectral weight appearing in the condensate (at $\omega = 0$) is transferred from the region $0^+ - \omega_s$. However, the experiment in [79] shows a transfer of the spectral-weight from the high ($\omega > 1$ eV) to low energies - see below. This fact was interpreted by some researchers [80], [81] as a "violation" of the TFG sum-rule, i.e. that there is more spectral weight in the condensate (at $\omega = 0$) than it is expected from the TFG sum-rule and effectively means the decrease of the kinetic energy in the superconducting state. This is in contrast to the increase of the kinetic energy in the BCS superconducting state. We are going to discuss this problem in details and to demonstrate that the analysis in terms of the kinetic energy only, is untenable.

What is the origin of the spectral-weight transfer, especially in the superconducting state of HTSC oxides? Here, we shall study the *inplane* $\sigma_{a-b}(\omega)$ only, since the origin of the quasiparticle dynamics along the c-axis is still unclear.

The *first theoretical interpretation* of the spectral-weight transfer was based on the partial sum-rule in which the temperature dependence is related to the temperature change of the kinetic energy $\langle -T_v \rangle$ (or for more realistic spectrum of $\omega_{pl,v}^2(T)$) - see Eq.(17-19). In this framework the extra increase of $\bar{A}_L(0, \omega_c)$ is related to the lowering of the band kinetic energy in the superconducting state [80], [81]. If this would be true, then the lowering of the band kinetic energy (per particle) is approximately $(\langle T_v \rangle_{N,T>T_c} - \langle T_v \rangle_{S,T<T_c})/N \sim 1$ meV, what is approximately by factor ten larger than the superconducting condensation energy. Note, that in the weak coupling BCS theory of superconductivity the kinetic energy is increased in the superconducting state. So, the alleged large lowering of the kinetic energy in the superconducting state is interpreted as a result of some exotic pairing mechanism in which the kinetic energy (or $\omega_{pl,v}^2(T)$ for more general spectrum) is significantly lowered but the potential energy is increased in the superconducting state, contrary to the case of BCS approach. However, this interpretation misses a very important contribution to the partial sum rule, which is due to the large and strongly T, ω dependent transport scattering rate $\Gamma_{tr}(T, \omega)$.

Before discussing the partial sum rule more adequately, let us mention that the separation of the valence-band kinetic energy from the potential one in strongly correlated systems is *not well defined procedure*. For instance, in the Hubbard model with $U >> t$ and nearest neighbor hoping t one has (see below and also in [2]) the low-energy (valence) Hamiltonian H_v is given

$$H_v = -t \sum_{i,\delta,\sigma} X_i^{\sigma 0} X_{i+\delta}^{0\sigma}, \tag{21}$$

where the Hubbard operators X_i describe the motion of composite quasiparticles with excluded doubly occupancy - see more in Section 4. They have complicated non-canonical (anti)commutation rules, which means that Eq.(21) mixes the kinetic energy with the (kinematical) potential energy of band (valence) quasiparticles.

The *second theoretical approach is* proposed recently [82], which is in principle exact, is based on the fact that in HTSC oxides there is strong electron scattering - direct or via phonons, on impurities, etc. So, the presence of an inelastic (and elastic) scattering prevents the interpretation of the partial sum rule in terms of the band kinetic energy

only. As an illustrative example for this assertion may serve the scattering of electrons on impurities, where the intraband contribution to $\sigma_{1,v}(\omega)$ is given by

$$\sigma_{1,v}(\omega) = \frac{\omega_{pl,v}^2}{4\pi} \frac{\Gamma_{i,tr}}{\omega^2 + \Gamma_{i,tr}^2}. \tag{22}$$

Here, $\Gamma_{i,tr}/2 = 1/\tau_{i,tr}$ is the quasiparticle transport relaxation rate due to impurities. In this case the partial sum-rule reads

$$\int_0^{\omega_c} \sigma_{1,v}^N(\omega) d\omega = \frac{\omega_{pl,v}^2}{8}(1 - \frac{2\Gamma_{i,tr}}{\omega_c}). \tag{23}$$

This result means that the intraband sum-rule can be satisfied in the presence of impurities only for $\omega_c \to \infty$. The similar conclusion holds in the case of inelastic scattering via phonons although in that case Γ_{tr} is ω- and T-dependent. The similar reasoning holds for interband transitions which in the presence of scattering have also the low-frequency tail. Since in HTSC oxides $\Gamma_{tr}(\omega)$ is dominantly due to the EPI and reaches values up to 100 *meV*, there is no other way to study the partial sum-rule (the value of $\int_0^{\omega_c} \sigma_{1,v}(\omega)d\omega$) than to calculate $\sigma_{1,v}(\omega)$ directly from a microscopic model. The latter must incorporate relevant scattering mechanisms and bands. Such calculations were done in [82] by taking into account the large EPI interaction. By using the EPI spectral function $\alpha^2(\omega)F(\omega)$ from tunnelling measurements and by assuming $\alpha_{tr}^2(\omega)F(\omega) \approx \alpha^2(\omega)F(\omega)$ the authors have calculated $A_H(\omega_c, 2\omega_c)$ (and $A_L(0, \omega_c)$) in the normal state and found a good agreement with experiments [79] - see Fig. 6. We stress that the recent elipsometric measurements of the dielectric function $\varepsilon(\omega)$ [75] confirms this theoretical prediction [82].

From the above analysis we conclude that: (i) the interpretation of the partial sum-rule in HTSC oxides only in terms of the kinetic energy (or $\omega_{pl,v}^2(T)$) is physically unjustified; (ii) *the EPI interaction is strong and dominating scattering mechanism in the optical properties of the normal state*. Reliable calculations of the partial sum-rule in the superconducting state are still missing, since in that case one should know much more details on the superconducting order $\Delta(\mathbf{k}, \omega)$ and $\Gamma_{tr}(\mathbf{k}, \omega)$, which are at present too ambitious task.

2.2.2. Resistivity $\rho(T)$

A lot of experimental and theoretical works were devoted to the temperature dependence of resistivity $\rho(T)$ in HTSC oxides. General properties of the resistivity in HTSC oxides are the following: (**1**) The resistivity is very anisotropic in single crystals where one has $r_c \equiv (\rho_c(T)/\rho_{a-b}(T)) \gg 1$ at T above T_c - see [90], i.e. $r_c \approx 300$ in $La_{1.85}Sr_{0.15}CuO_4$ and $Nd_{1.85}Ce_{0.15}CuO_4$, $r_c \approx 20 - 150$ in $YBa_2Cu_3O_{7-x}$, $r_c \approx 10^5$ in $Bi_2Sr_2CaCu_2O_8$ depending also on the sample preparation, temperature etc. The anisotropy of the in-plane resistivity is much less, i.e. $r_a \equiv (\rho_{aa}(T)/\rho_{bb}(T)) \sim 1-2$, depending also on the sample preparation, temperature etc.; (**2**) The in-plane resistivity $\rho_{a-b}(T)$ at room temperature is more than two orders of magnitude higher than that of the metallic Cu (where $\rho_{Cu}(T_{room}) \approx 1.5 \ \mu\Omega cm$), i.e. $\rho_{a-b}(T)$ of HTSC oxides lies more
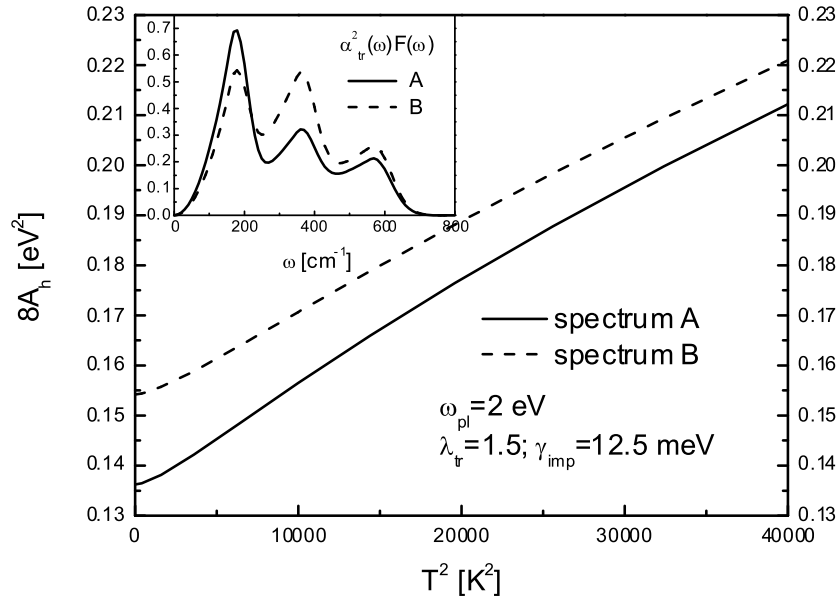
FIGURE 6. Calculated theoretical T-dependence of high-energy part of the sum rule $\bar{A}_H(\omega_c = 1.25eV, 2\omega_c = 2.5eV)$ by taking into account the electron-phonon interaction. The data from [82]

in the semiconductor range and $\rho_{a-b}(T) \gg \rho_{Cu}(T)$; (**3**) $\rho_{a-b}(T) \sim T$ for $T > T_c$, which deviates at $T > (800 - 1000) \; K$ and saturates at even higher temperatures, depending on samples etc.; (**4**) ρ_{a-b} varies from $\rho_{a-b}(T) \sim T$ (with small residual resistivity) in optimally doped systems being $\rho_{a-b}(T) \sim T^{3/2}$ in overdoped systems, as experiments on $La_{2-x}Sr_xCuO_4$ show [89]; (**5**) In most samples of HTSC oxides the c-axis resistivity $\rho_c(T)$ shows a non-metallic behavior especially in samples with huge anisotropy along the c-axis, growing by decreasing temperature, i.e. $(d\rho_c(T)/dT) < 0$, being supercon-ducting below T_c.

We discuss briefly the *in-plane resistivity* $\rho_{a-b}(T)$ only, because its temperature behavior is a direct consequence of the quasi-2D motion of quasiparticles and of the inelastic scattering which they suffer. At present there is no consensus on the origin of the linear temperature dependence of the inplane resistivity $\rho_{a-b}(T)$ in the normal state. As it is stressed several times many researchers are (erroneously) believing that such a behavior can not be due to the EPI? The inadequacy of this claim was already demonstrated by analyzing the dynamical conductivity $\sigma(\omega)$. The inplane resistivity in HTSC oxides is usually analyzed by the Kubo approach, or by the Boltzmann equation. In the latter case $\rho(T)$ is given by

$$\rho(T) = \frac{4\pi}{\omega_p^2}\Gamma_{tr}(T) \tag{24}$$

$$\Gamma_{tr}(T) = \frac{\pi}{T}\int_0^\infty d\omega \frac{\omega}{\sin^2(\omega/2T)}\alpha_{tr}^2(\omega)F(\omega), \tag{25}$$

where $\alpha_{tr}^2(\omega)F(\omega)$ is the EPI transport spectral function. It is well-known that at $T > \Theta_D/5$ and for the Debay spectrum one has

$$\rho(T) \simeq 8\pi^2 \lambda_{tr}^{EP} \frac{k_B T}{\hbar \omega_p^2} = \rho' T. \tag{26}$$

In HTSC oxides the reach and broad spectrum of $\alpha_{tr}^2(\omega)F(\omega)$ is favorable for such a linear behavior. The measured transport coupling constant λ_{tr} contains in principle all scattering mechanisms, although usually some of them dominate. For instance, the proponents of the spin-fluctuations mechanism assume that λ_{tr} is entirely due to the scattering on spin fluctuations. However, by taking into account specificities of HTSC oxides the experimental results for the inplane resistivity $\rho_{a-b}(T)$ can be satisfactory explained by the *EPI* mechanism. From tunnelling experiments [37], [38], [39], [40], [41] one obtains that $\lambda \approx 2-3$ and if one assumes that $\lambda_{tr} \approx \lambda$ and $\omega_{pl} \geq (3-4)$ *eV* (the value obtained from the band-structure calculations) then Eq.(26) describes the experimental situation rather well. The plasma frequency ω_{pl} which enters Eq.(26) can be extracted from optic measurements ($\omega_{pl,ex}$), i.e. from the width of the Drude peak at small frequencies. However, since $\lambda_{tr} \approx 0.25\omega_{pl}^2(eV)\rho'(\mu\Omega cm/K)$ there is an experimental constraint on λ_{tr}. The experiments [76] give that $\omega_{pl} \approx (2-2.5)$ *eV* and $\rho' \approx 0.6$ in oriented YBCO films, and $\rho' \approx 0.3$ in single crystals of BISCO. These results makes a limit on $\lambda_{tr} \approx 0.9 - 0.4$.

So, in order to explain $\rho(T)$ with small λ_{tr} and high T_c (which needs large λ) by the EPI it is necessary to have $\lambda_{tr} \leq (\lambda/3)$. This means that in HTSC oxides the *EPI* is reduced in transport properties where $\lambda_{tr} \ll \lambda$. This reduction of ω_p^2 and λ_{tr} means that the*y* contain renormalization (with respect to the *LDA* results) due to various quasiparticle scattering processes and interactions, which do not enter in the *LDA* theory. In subsequent chapters we shall argue that the strong suppression of λ_{tr} may have its origin in strong electronic correlations [17], [18], [19].

In conclusion, optic and resistivity measurements in normal state of HTSC oxides are much more in favor of the EPI than against it. However, some intriguing questions still remains to be answered: (**i**) which are the values of λ_{tr} and ω_{pl}: (ii) why one has $\lambda_{tr} \ll \lambda$: (iii) what is the role of the Coulomb scattering in $\sigma(\omega)$ and $\rho(T)$. The ARPES measurements (see discussion below) give evidence for the appreciable Coulomb scattering at higher frequencies, where $\Gamma(\omega) \approx \Gamma_0 + \lambda_c \omega$ for $\omega > \omega_{max}^{ph}$ with $\lambda_c \approx 0.4$. So, in spite of the fact that the EPI is suppressed in transport properties it is sufficiently strong in order to dominate in some temperature regime. It may happen that at higher temperatures the Coulomb scattering dominates in $\rho(T)$, which certainly does not disqualify the EPI as the pairing mechanism in HTSC oxides. For better understanding of $\rho(T)$ we need a controllable theory for the Coulomb scattering in strongly correlated systems, which is at present lacking.

2.3. Raman scattering in HTSC oxides

If the elementary excitation involved in the Raman scattering are electronic we deal with the *electronic Raman effect*, while if an optical phonon is involved we deal with the

phonon Raman effect. The Raman scattering in the normal and superconducting state of HTSC oxides is an important spectroscopic tool which gives additional information on quasiparticle properties - the electronic Raman scattering, as well as on phonons and their renormalization by electrons - the phonon Raman scattering.

2.3.1. Electronic Raman scattering

The Raman measurements on various HTSC oxides show a remarkable correlation between the Raman cross-section $\tilde{S}_{exp}(\omega)$ and the optical conductivity $\sigma_{a-b}(\omega)$, i.e.

$$\tilde{S}_{exp}(\omega) \sim [1 + n_B(\omega)]\langle | \gamma_{sc}(\mathbf{q}) |^2 \rangle_F \omega \sigma_{a-b}(\omega), \tag{27}$$

where $n_B(\omega)$ is the Bose function and $\gamma_{sc}(\mathbf{q})$ screened Raman vertex - see more in [2]. Previously it was demonstrated that $\sigma_{a-b}(\omega)$ depends on the transport scattering rate $\Gamma_{tr}(\omega, T)$ where $\Gamma_{tr}(\omega, T) \sim T$ and $n_B(\omega) \sim T/\omega$ for $\omega < T$, thus giving $\tilde{S}(\mathbf{q}, \omega) \approx Const_1$ in that range. For $\omega > T$ one has $\omega \sigma_{a-b}(\omega) \approx Const$ giving also $\tilde{S}(\mathbf{q}, \omega) \approx Const_2$. We have also demonstrated that the *EPI* with the very broad spectral function $\alpha^2 F(\omega)$ (see Fig. 11 below) explains in a natural way ω, T dependence of $\sigma_{a-b}(\omega)$ and $\Gamma_{tr}(\omega, T)$. So, the Raman spectra in HTSC oxides can be explained by the EPI in conjunction with strong correlations. This conclusion is supported by calculations of the Raman cross-section [91] which take into account the EPI with $\alpha^2 F(\omega)$ extracted from the tunnelling measurements on $YBa_2Cu_3O_{6+x}$ and $Bi_2Sr_2CaCu_2O_{8+x}$ [37]. They are in a good qualitative agreement with experimental results - see more in [2].

We stress again, that quite similar (to HTSC oxides) properties of the electronic Raman scattering (besides $\sigma(\omega)$, $R(\omega)$ and $\rho(T)$) were observed in experiments [92] on isotropic metallic oxides $La_{0.5}Sr_{0.5}CoO_3$ and $Ca_{0.5}Sr_{0.5}RuO_3$ - see Fig. 7. To repeat again, in these compounds there are no signs of antiferromagnetic fluctuations (which are present in HTSC oxides) and the peculiar behavior is probably due to the EPI.

2.3.2. Phonon Raman scattering

Normal state. - The effect of the EPI on the Raman scattering is characterized by the *Fano asymmetry parameter* $q(\omega)$ - see more in [2]. If it is finite the line shape is *asymmetric* - the *Fano effect (resonance)*. By decreasing $q(\omega)$ the phonon line shape becomes more asymmetric, which means stronger EPI (in case when continuum states are due to conduction carriers). The Fano resonance is experimentally found in HTSC oxide $YBa_2Cu_3O_{7-\delta}$ [94], where the line asymmetry is clearly seen in optimally doped ($\delta \ll 1$) systems, while it is absent in the insulating state ($\delta = 1$). The existence of the Fano (asymmetric) line shape in HTSC oxides is a direct proof that the discrete phonon level interacts with continuum of states, which are conduction electrons in the metallic state - see Fig. 8.
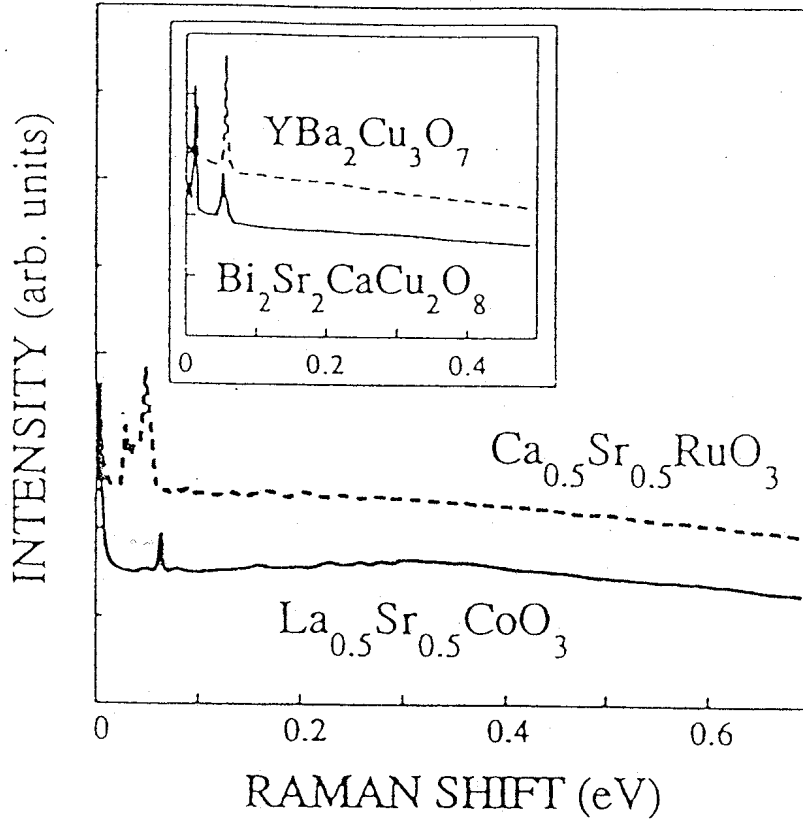
FIGURE 7. Broad range Raman scattering spectra of $Ca_{0.5}Sr_{0.5}RuO_3$ (broken line) and $La_{0.5}Sr_{0.5}CoO_3$ (solid line). Inset spectra of $Tl_2Ba_2Ca_2Cu_3O_{10}$, $Bi_2Sr_2CaCu_2O_8$, $YBa_2Cu_3O_7$ and $La_{1.85}Sr_{0.15}CuO_4$. From [92].

Superconducting state. - It is well known that the renormalization of phonon frequencies and their life-times by superconductivity in *LTSC* materials is rather small - around one percent. The smallness of the effect is characterized by the parameter Δ/E_F which is very small in low temperature superconductors. However, Δ/E_F is much larger in HTSC oxides and already from that point of view one expects much stronger renormalization effects. At the very beginning several Raman active phonon modes, with frequencies $128, 153, 333, 437$ and 501 cm^{-1}, were detected in $YBa_2Cu_3O_7$ and these modes are totally symmetric modes (with respect to the orthorhombic point group D_{2h}). ($1cm^{-1} = 29.98GHz = 0.123985meV = 1.44K$) However, by using the approximate tetragonal symmetry (with the point group D_{4h}) the mode at $\omega_{B_{1g}} = 333$ cm^{-1} transforms according to the B_{1g} representation, while the other modes according to the A_{1g} one - see Fig. 9. The *Fano resonance* (asymmetric line shape) of the B_{1g} mode indicates an appreciable coupling of the lattice to the continuum, which in fact corresponds to the charge carries. It is interesting to note that the A_{1g} modes in *YBCO* are weakly affected in the presence of superconductivity, while the B_{1g} mode *softens* by 9 cm^{-1} (by approximately 3 %) [93]. It is well established also that this softening is due to super-
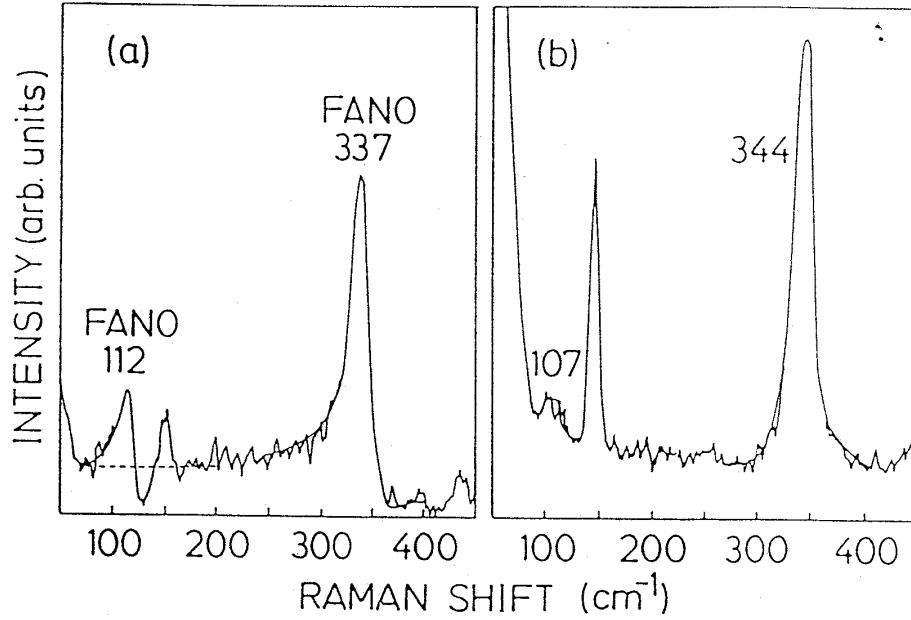
FIGURE 8. Fano resonance in $YBa_2Cu_3O_{7-x}$. The asymmetry is seen for 112 and 337 cm^{-1} phonons in the superconductor ($x = 0$). The semiconductor ($x = 1$) has Lorenzian line shapes. From [94].

conductivity and not due to, for instance, structural changes, because it disappears in magnetic fields higher than H_{c2} .

The frequency shift $\delta\omega_\lambda$ and the phonon line width Γ_λ in the superconducting state have been studied numerically in [97] for the case of the isotropic $s - wave$ superconducting gap ($\Delta(\mathbf{k}) = \Delta = const$) and for strong coupling superconductivity. They have predicted the *phonon-softening* and line-width *narrowing* for $\omega_0 < 2\Delta$, while for $\omega_0 > 2\Delta$ there is a *phonon-hardening* and line-width broadening. These predictions are surprisingly in agreement with experiments [93], in spite of the assumed isotropic $s - wave$ pairing what is contrary to the experimentally well established $d - wave$ pairing in $YBCO$. Later calculations of the renormalization of the B_{1g} Raman phonon mode in the presence of the weak coupling $d - wave$ superconductivity [100] show that if one assumes that $\omega_{B_{1g}} < 2\Delta_{max}$ there is phonon softening accompanied with the line broadening below T_c. The latter is possible because of the gapless character (on a part of the Fermi surface) of $d - wave$ pairing. In that respect the calculations of the phonon renormalization based on the strong coupling $d - wave$ superconductivity are of significant interest and still awaiting.

Recent report [4] on the superconductivity-induced strong phonon renormalization of the A_{1g} phonons at 240 and 390 cm^{-1} (by 6 and 18 % respectively) in $HgBa_2Ca_3Cu_4O_{10+x}$ ($T_c = 123$ K) - the so called $Hg - 1234$) compound, renders an additional evidence for the strong EPI in HTSC oxides. In [4] the EPI coupling constant is estimated to be rather large for the A_{1g} phonons ($\lambda_{A_{1g}} \approx 0.08$). Since there are 60 phonon modes in $HgBa_2Ca_3Cu_4O_{10+x}$ they are capable to produce large EPI coupling
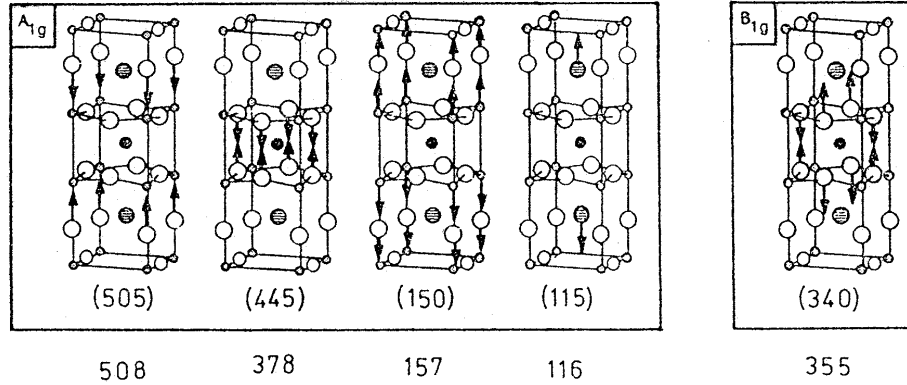
FIGURE 9. Assignation of A_g modes according to calculations in [95]. In brackets are experimental phonon frequencies in cm^{-1}. $115\ cm^{-1}$ is the Ba mode, $150\ cm^{-1}$ is the $Cu2$ mode, $340\ cm^{-1}$ (B_{1g} mode) and $445\ cm^{-1}$ modes are due to vibration of $O(2,3)$ ions in the CuO_2, while $505\ cm^{-1}$ mode is due to $O4$ ions. From [96].

constant $\lambda = \sum_{\nu=1}^{60} \lambda_\nu > 1$ - see Fig. 10(a-b). A conservative estimation of the upper limit of $\lambda_{\max}$ gives $\lambda_{\max} \approx 60 \times 0.08 = 4.8$ which is, of course, far from the realistic value of $\lambda \leq 2$. In any case this analysis confirm that the EPI of some Raman modes in HTSC oxides is strong. To this point, very recent Raman scattering measurements on the $(Cu,C) - 1234$ compound with $T_c = 117\ K$ reveal strong superconductivity induced phonon self-energy effects [5]. The A_{1g} phonons at 235 cm^{-1} and 360 cm^{-1} (note $\omega_{pl} < 2\Delta_0$), which involve vibrations of the plane oxygen with some admixture of Ca displacements, exhibit pronounced Fano line shape (in the normal and superconducting state) with the following interesting properties in the superconducting state: *(i)* the phonon intensity is increased substantially; *(ii)* both phonons soften; *(iii)* the phonon line width (of both phonons) increases dramatically below T_c passing through a maximum slightly below T_c, and decreases again at low T but remaining broader than immediately below T_c. This line broadening is difficult to explain by $s-wave$ pairing, where the line narrowing is expected, but it can be explained by superconducting pairing with nodes in the quasiparticle spectrum, for instance by $d-wave$ pairing [98]. The large EPI coupling constants for these two modes are estimated from the asymmetric Fano line shape, which gives $\lambda_{235} = 0.05$ and $\lambda_{360} = 0.07$ (note in $YBCO$ $\lambda_{A_{1g}} = 0.01$ for $\omega_{A_{1g}} = 440\ cm^{-1}$ and $\lambda_{B_{1g}} = 0.02$ for $\omega_{B_{1g}} = 340\ cm^{-1}$, rather small values) giving the upper value for the total coupling constant $\lambda_{\max} = 4$. This result gives additional important evidence for the strong *EPI* in HTSC oxides.

2.3.3. Electron-phonon coupling in Raman scattering

We would like to stress the importance of the (phonon) Raman scattering measurements for the theory of the EPI in HTSC oxides. The *covalent part* of the EPI is due to
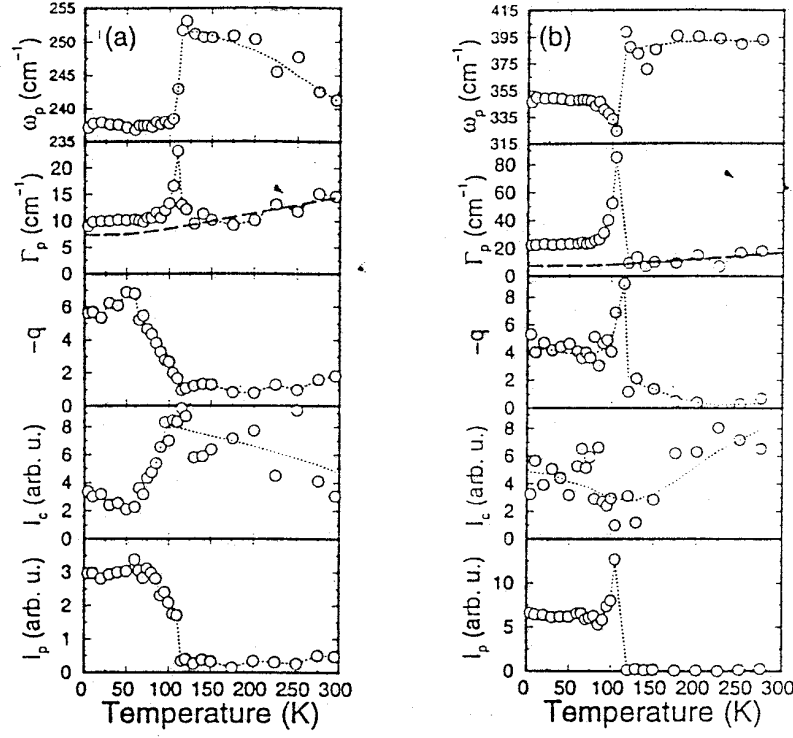
FIGURE 10. The fitted frequency ω_p, line-width Γ_p, asymmetry parameter q, and the phonon intensity I_p of the $Hg-1234$ Raman spectra in the A_{1g} mode measured in $x/x/$ polarization with 647.1 nm laser line: (a) at 240 cm^{-1}; (b) at 390 cm^{-1} - from [4].

the strong *covalency* of the Cu and O orbitals in the CuO_2 planes. In that case the EPI coupling constant is characterized by the parameter ("field") $E^{cov} \sim \partial t_{p-d}/\partial R \sim q_0 t_{p-d}$, where t_{p-d} is the hopping integral between $Cu(d_{x^2-y^2})$ and $O(p_{x,y})$ orbitals and the length q_0^{-1} characterizes the spacial exponential fall-off of the hopping integral t_{p-d}. The covalent EPI is unable to explain the strong phonon renormalization (the self-energy features) in the B_{1g} mode in $YBa_2Cu_3O_7$ by superconductivity, since in this mode the O-ions move along the $c-axis$ in opposite directions, while for this mode $\partial t_{p-d}/\partial R$ is zero in the first order in the phonon displacement. Therefore the EPI in this mode must be due to the *ionic contribution* to the *EP* interaction which comes from the change in the Madelung energy as it was first proposed in [47], [48]. Namely, the Madelung interaction creates an electric field perpendicular to the CuO_2 planes, which is due to the surrounding ions which form an asymmetric environment. In that case the site energies ε_i^0 contain the matrix element $\varepsilon^{ion} = \langle \psi_i \mid \phi(\mathbf{r}) \mid \psi_i \rangle$, where $\mid \psi_i \rangle$ is the atomic wave function at the i-th site, while the potential $\phi(\mathbf{r})$ steams from surrounding ions. In simple and transition metals the surrounding ions are well screened and therefore the change of ε^{ion} in the presence of phonons is negligible, contrary to HTSC oxides which are almost *ionic compounds* (along the c-axis) where the change of ε^{ion} is appreciable

and characterized by the field strength $E^{ion} = V/a_n$. Here, V is the characteristic potential due to surrounding ions and a_n is the distance of the neighboring ions. Immediately after the discovery of HTSC oxides in many papers [114], [60], [99] it was (incorrectly) assumed that the covalent part dominates the EPI in these materials. The calculation of T_c by considering only covalent effects [114], [60] gave rather small T_c ($\sim 10 - 20$ K in $YBCO$, and $20 - 30$ K in $La_{1.85}Sr_{0.15}CuO_4$). It turns out that in HTSC oxides the opposite inequality $E^{ion} \gg E^{cov}$ is realized for most c-axis phonon modes, on which basis the renormalization of the Raman B_{1g} mode can be explained - see more in [2]. This is supported by detailed theoretical studies in for the $YBCO$ compound [48], [49], where it is calculated the change in the *ionic Madelung energy* due to the out of plane oxygen vibration in the B_{1g} mode. Similarly as in $YBCO$, the large superconductivity-induced phonon self-energy effects in $HgBa_2Ca_3Cu_4O_{10+x}$ and in $(Cu,C)Ba_2Ca_3Cu_4O_{10+x}$ for the A_{1g} modes are also due to the ionic (Madelung) coupling. In these modes oxygen ions move also along the $c - axis$ and the ionicity of the structure is involved in the EPI. This type of the (*long-range*) EPI is absent in usual isotropic metals (*LTSC* superconductors), where the large Coulomb screening makes it to be local. Similar ideas are recently incorporated into the Eliashberg equations in [133], [132]. The weak screening along the c-axis, which is due to the very small hopping integral for carrier motion, is reflected in the very small plasma frequency $\omega_p^{(c)}$ along this axis. Since for some optical phonon modes one has $\omega_{ph} > \omega_p^{(c)}$ then nonadiabatic effects in the screening are important. The latter can give rise to much larger EPI coupling constant for this modes [52], [53].

In conclusion, the electron and phonon Raman scattering measurements in the normal and superconducting state of HTSC oxides give the following important results: (a) phonons interact strongly with the electronic continuum, i.e. the EPI is substantial; (b) the ionic contribution (the Madelung energy) to the EPI interaction for c-axis phonon modes gives substantional contribution to the (large) EPI coupling constant ($\lambda > 1$).

2.4. Tunnelling spectroscopy in HTSC oxides

Tunnelling methods are important tools in studying the electronic density of states $N(\omega)$ in superconductors and in the past they have played very important role in investigating of low T_c-superconductors. By measuring the current-voltage ($I - V$) characteristic in typical tunnelling junctions (with large tunnelling barrier) it was possible from the tunnelling conductance $G(V)(= dI/dV)$ to determine $N(\omega)$ and the superconducting gap as a function of temperature, magnetic field etc. Moreover, by measuring of $G(V)$ at voltages $eV > \Delta$ in the *NIS* (normal metal - isolator - superconductor) junctions it was possible to determine the Eliashberg spectral function $\alpha^2 F(\omega)$ (which is due to some bosonic mechanism of quasiparticle scattering) and finally to confirm (definitely) the phonon mechanism of pairing in *LTSC* materials, except maybe heavy fermions [101]. We shall discuss here only the results for $\alpha^2 F(\omega)$ obtained from $I - V$ measurements, while a more extensive discussion of other aspects is given in [2].

2.4.1. $I - V$ characteristic and $\alpha^2 F(\omega)$

If one considers a *NIS* contact where the left (*L*) and right (*R*) banks of the contact can be normal (*N*) metal or superconductor (*S*), respectively, with very small transparency then tunnelling effects are studied in the framework of the tunnelling Hamiltonian $\hat{H}_T = \sum_{\mathbf{k},\mathbf{p}} (T_{\mathbf{k},\mathbf{p}} c^{\dagger}_{\mathbf{k}L} c_{\mathbf{q}R} + h.c)$. In that case the single-particle tunnelling current is given by the formula [102]

$$I_{qp}(V) = 2e \sum_{\mathbf{k},\mathbf{p}} |T_{\mathbf{k},\mathbf{p}}|^2 \times$$

$$\times \int_{-\infty}^{\infty} d\omega A_N(\mathbf{k},\omega) A_S(\mathbf{p},\omega+eV)[n_F(\omega) - n_F(\omega+eV)]. \tag{28}$$

The single-particle spectral function $A_{N(S)}(\mathbf{k},\omega)$ is related to the imaginary part of the retarded single particle Green's function, i.e. $A(\mathbf{k},\omega) = -ImG^{ret}(\mathbf{k},\omega)/\pi$, while the tunnelling matrix element $|T_{\mathbf{k},\mathbf{p}}|^2$ is derived in the quantum-mechanical theory of tunnelling through the barrier - see [2]. Note, in the superconducting state $A(\mathbf{k},\omega)$ depends on the superconducting gap function $\Delta(\mathbf{k},\omega)$, which is on the other hand a functional of the spectral function $\alpha^2 F(\omega)$. The fine structure in the second derivative $d^2 I/dV^2$ at voltages above the superconducting gap is related to the spectral function $\alpha^2 F(\omega)$. For instance, plenty of break-junctions made from $Bi - 2212$ single crystals [37] show that negative peaks in $d^2 I/dV^2$, although broadened, coincide with the peaks in the generalized phonon density of states $G_{ph}(\omega)$ measured by neutron scattering - see more in [2]. Note, the reported broadening of these peaks might be partly due to $d - wave$ pairing in HTSC oxides. The tunnelling density of states $N_T(V) \sim dI/dV$ shows a gap structure and it was found that $2\bar{\Delta}/T_c = 6.2 - 6.5$, where $T_c = 74 - 85\ K$ and $\bar{\Delta}$ is some average value of the gap. By assuming $s - wave$ superconductivity [37] and by solving the *MR* problem (inversion of Eliashberg equations), the spectral function $\alpha^2 F(\omega)$ is obtained which gives $\lambda \approx 2.3$. Note, in extracting λ [37] the standard value of the effective Coulomb parameter $\mu^* \approx 0.1$ is assumed. Although this analysis [37] was done by assuming $s - wave$ pairing it is qualitatively valuable procedure also in the case of $d - wave$ pairing, because one expects that $d - wave$ pairing does not spoil significantly the global structure of $d^2 I/dV^2$ at $eV > \Delta$, but introducing mainly a broadening of peaks. The latter effect can be partly due to an inhomogeneity of the gap. The results obtained in [37] were *reproducible* on more than 30 junctions, while in $Bi(2212) - GaAs$ and $Bi(2212) - Au$ planar tunnelling junctions similar results were. Several groups [39], [40], [41] have obtained similar results for the shape of the spectral function $\alpha^2 F(\omega)$ from the $I - V$ measurements on various HTSC oxides as shown in Fig. 11. The results shown in Fig. 11 leave no much doubts on the effectiveness of the EPI in pairing mechanism of HTSC oxides. In that respect recent tunnelling measurements on $Bi_2 Sr_2 CaCu_2 O_8$ [103] are impressive, since the Eliashberg spectral function $\alpha^2 F(\omega)$ was extracted from the measurements of $d^2 I/dV^2$. The obtained $\alpha^2 F(\omega)$ has several peaks in the broad frequency region up to $80\ meV$ - see Fig. 11 (curve Shimada et al.), which coincide rather well with the peaks in the phonon density of states $F(\omega)$. Moreover, the authors of [103] were able to extract the coupling constant for modes laying in (and around) these peaks and their contribution to T_c. They managed to extract the EPI coupling constant, which is unexpectedly very large, i.e. $\lambda (= 2 \int d\omega \alpha^2 F(\omega)/\omega) = \sum \lambda_i \approx 3.5$. Since almost all
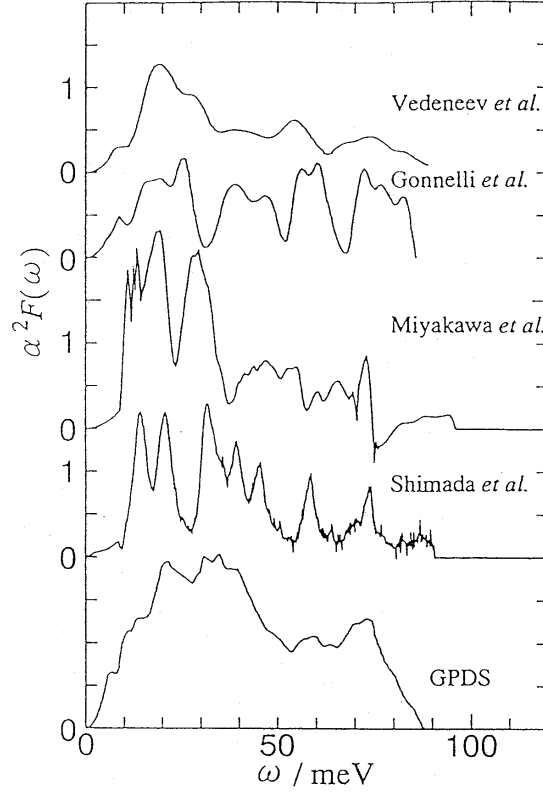
FIGURE 11. The spectral function $\alpha^2 F(\omega)$ obtained from measurements of $G(V)$ by various groups on various junctions: Vedeneev et al. [37], Gonnelli et al. [41], Miyakawa et al. [39], Shimada et al.[38]. The generalized density of states GPDS for $Bi2212$ is plotted at the bottom - from [38].

phonon mode contributes to λ, this means that on the average each particular phonon mode is moderately coupled to electrons thus keeping the lattice stable. Additionally, they have found that some low-frequency phonon modes corresponding to Cu, Sr and Ca vibrations are rather strongly coupled to electrons, similarly as the high frequency oxygen vibrations along the c-axis do. These results confirm the importance of the axial modes in which the change of the Madelung energy is involved, thus supporting the idea conveyed through this article of the importance of the ionic Madelung energy in the EPI interaction of HTSC oxides.

In conclusion, the common results for all reliable tunnelling measurements in HTSC oxides, including $Ba_{1-x}K_xBiO_3$ too [104], [16], is that no particular mode can be singled out in the spectral function $\alpha^2 F(\omega)$ as being the only one which dominates in pairing mechanism. This important result means that the high T_c is not attributable to a particular phonon mode in the EPI mechanism, since all phonon modes contribute to λ. Having in mind that the phonon spectrum in HTSC oxides is very broad (up to 80 meV), then the large *EPI* coupling constant ($\lambda \approx 2$) in HTSC oxides is not surprising at all. We stress,

that compared to neutron scattering experiments the tunnelling experiments are superior in determining the EPI spectral function $\alpha^2 F(\omega)$.

2.5. Isotope effect in HTSC oxides

The isotope effect has played an important role in elucidating the pairing mechanism in *LTSC* materials. Note, the standard BCS theory predicts that for the pure phonon-mediated mechanism of pairing the isotope coefficient $\alpha = -d \ln T_c / d \ln M$, where M is the ionic mass, takes its canonical value $\alpha = 1/2$. However, later on it was clear that α can take values less (even negative) then its canonical value in the phonon-mediated mechanism of pairing if there is pronounced Coulomb pseudopotential $\mu*$ - see more in [2].

2.5.1. Experiments on the isotope coefficient α

A lot of measurements of α_O and α_{Cu} were performed on various hole-doped and electron-doped HTSC oxides and we give a brief summary of the main results [105]: (**1**) The *O* isotope coefficient α_O strongly depends on the hole concentration in the hole-doped materials where in each group of HTSC oxides ($YBa_2Cu_3O_{7-x}$, or $La_{2-x}Sr_xCuO_4$ etc.) a small oxygen isotope effect is observed in the optimally doped (maximal T_c) samples. For instance $\alpha_O \approx 0.02 - 0.05$ in $YBa_2Cu_3O_7$ with $T_{c,\max} \approx 91\ K$, $\alpha_O \approx 0.1 - 0.2$ in $La_{1.85}Sr_{0.15}CuO_4$ with $T_{c,\max} \approx 35\ K$; $\alpha_O \approx 0.03 - 0.05$ in $Bi_2Sr_2CaCu_2O_8$ with $T_{c,\max} \approx 76\ K$; $\alpha_O \approx 0.03$ and even negative (-0.013) in $Bi_2Sr_2Ca_2Cu_2O_{10}$ with $T_{c,\max} \approx 110\ K$; the experiments on $Tl_2Ca_{n-1}BaCu_nO_{2n+4}$ $(n = 2, 3)$ with $T_{c,\max} \approx 121\ K$ are still unreliable and α_O is unknown; $\alpha_O < 0.05$ in the electron-doped $(Nd_{1-x}Ce_x)_2CuO_4$ with $T_{c,\max} \approx 24\ K$. (**2**) For hole concentrations away from the optimal one, T_c decreases while α_O increases and in some cases reaches large value $\alpha_O \approx 0.5$ - see Fig. 12 for *La* compounds. This holds not only for parent compounds but also for systems with substitutions, like $(Y_{1-x-y}Pr_xCa_y)Ba_2Cu_3O_7$, $Y_{1-y}Ca_yBa_2Cu_4O_4$ and $Bi_2Sr_2Ca_{1-x}Y_xCu_2O_8$. Note, the decrease of T_c is not a prerequisite for the increase of α_O. This became clear from the *Cu* substituted experiments $YBa_2(Cu_{1-x}Zn_x)_3O_7$ where the decrease of T_c (by increasing of the *Zn* concentration) is followed by only small increase of α_O [106]. Only in the case of very low $T_c < 20\ K$ then α_O becomes large, i.e. $\alpha_O > 0.1$. (**3**) The largest α_O is obtained even in the optimally doped compounds like in systems with substitution, such as $La_{1.85}Sr_{0.15}Cu_{1-x}M_xO_4$, $M = Fe, Co$, where $\alpha_O \approx 1.3$ for $x \approx 0.4\ \%$. (**4**) In $La_{2-x}M_xCuO_4$ there is a *Cu* isotope effect which is of the order of the oxygen one, i.e. $\alpha_{Cu} \approx \alpha_O$ giving $\alpha_{Cu} + \alpha_O \approx 0.25 - 0.35$ for optimally doped systems ($x = 0.15$). In the case when $x = 0.125$ with $T_c \ll T_{c,\max}$ one has $\alpha_{Cu} \approx 0.8 - 1$ with $\alpha_{Cu} + \alpha_O \approx 1.8$. The appreciate copper isotope effect in $La_{2-x}M_xCuO_4$ tells us that vibrations of other than oxygen ions could be important in giving high T_c. The latter property is more obvious from tunnelling measurements, which are discussed above. (**5**) There is *negative* Cu isotope effect in the oxygen-deficient system $YBa_2Cu_3O_{7-x}$ where α_{Cu} is between -0.14 and -0.34 if T_c lies in the $60\ K$ plateau. (**6**) There are reports on *small negative* α_O in
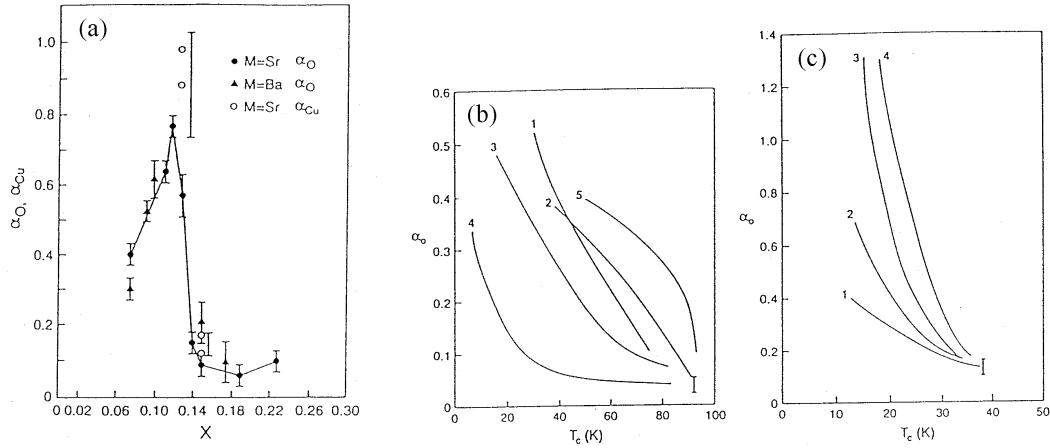
FIGURE 12. The oxygen isotope exponent α_O for: (a) $La_{2-x}Sr_xCuO_4$ as a function of Sr concentration - from [105]. The oxygen isotope exponent α_O as a function of T_c for: (b) $YBa_2Cu_3O_7$. 1: $(Y_{1-x}Pr_x)Ba_2Cu_3O_7$; 2: $YBa_{2-x}La_xCu_3O_7$; 3: $YBa_2(Cu_{1-x}Co_x)_3O_7$; 4: $YBa_2(Cu_{1-x}Zn_x)_3O_7$; 5: $YBa_2(Cu_{1-x}Fe_x)_3O_7$. (c) $La_{1.85}Sr_{0.15}CuO_4$. 1: $La_{1.85}Sr_{0.15}(Cu_{1-x}Ni_x)O_4$; 2: $La_{1.85}Sr_{0.15}(Cu_{1-x}Zn_x)O_4$; 3: $La_{1.85}Sr_{0.15}(Cu_{1-x}Co_x)O_4$; 4: $La_{1.85}Sr_{0.15}(Cu_{1-x}Fe_x)O_4$ - from [105].

some systems like $YSr_2Cu_3O_7$ with $\alpha_O \approx -0.02$ and in $BISCO - 2223$ ($T_c = 110\ K$) where $\alpha_O \approx -0.013$ etc. However, the systems with negative α_O present considerable experimental difficulties, as it is pointed out in [105].

The above enumerated results, despite experimental difficulties, are more in favor than against of the hypothesis that the EPI interaction is strongly involved in the pairing mechanism of HTSC oxides. By assuming that the experimental results on the isotope effect reflect an intrinsic property of HTSC oxides one can rise a question: which theory can explain these results? Since at present there is no consensus on the pairing mechanism in HTSC materials there is also no definite theory for the isotope effect. Besides the calculation of the coupling constant λ any microscopic theory of pairing is confronted also with the following questions: (**a**) why is the isotope effect small in optimally doped systems and (**b**) why α increases rapidly by further under(over)doping of the system?

It should be stressed, that at present all theoretical approaches are semi-microscopic, but what is interesting most of them indicate that in order to explain the rather unusual isotope effect in HTSC materials one should invoke the *forward scattering peak* in the EPI [2].

In conclusion, experimental investigations of the isotope effect in HTSC oxides have shown the importance of the EPI interaction in the pairing mechanism.

2.6. ARPES experiments in HTSC oxides

2.6.1. Spectral function $A(\vec{k}, \omega)$ from ARPES

The *angle-resolved photoemission spectroscopy* (ARPES) is nowadays a leading spectroscopy method in the solid state physics. The method consists in shining light (photons) with energies between $20 - 1000 \ eV$ on the sample and by detecting momentum ($\mathbf{k}$)- and energy(ω)-distribution of the outgoing electrons. The resolution of ARPES is drastically increased in the last decade with the energy resolution of $\Delta E \approx 2 \ meV$ (for photon energies $\sim 20 \ eV$) and angular resolution of $\Delta\theta \approx 0.2°$. The ARPES method is surface sensitive technique, since the average escape depth (l_{esc}) of the outgoing electrons is of the order of $l_{esc} \sim 10$ Å. Therefore, one needs very good surfaces in order that the results be representative for the bulk sample. In that respect the most reliable studies were done on the bilayer $Bi_2Sr_2CaCu_2O_8$ ($Bi2212$) and its single layer counterpart $Bi_2Sr_2CuO_6$ ($Bi2201$), since these materials contains weakly coupled BiO planes with the longest interplane separation in the HTSC oxides. This results in a *natural cleavage* plane making these materials superior to others in ARPES experiments. After a drastic improvement of sample quality in others families of HTSC materials, became the ARPES technique a central method in theoretical considerations. Potentially, it gives information on the quasiparticle Green's function, i.e. on the quasiparticle spectrum and life-time effects. The ARPES can indirectly give information on the momentum and energy dependence of the pairing potential. Furthermore, the electronic spectrum of the HTSC oxides is highly *quasi-2D* which allows an unambiguous determination of the momentum of the initial state from the measured final state momentum, since the component parallel to the surface is conserved in photoemission. In this case the ARPES probes (under some favorable conditions) directly the single particle spectral function $A(\mathbf{k}, \omega)$.

In the following we discuss only those ARPES experiments which give us evidence for the importance of the EPI in HTSC oxides - see detailed reviews in [107], [108].

The *photoemission* measures a nonlinear response function of the electron system, since the photo-electron current $\langle \mathbf{j}(1) \rangle$ at the detector is proportional to the incident photon flux (square of the vector potential $\mathbf{A}$), i. e. schematically one has

$$\langle \mathbf{j}(1) \rangle \sim \langle \mathbf{j}(\bar{2})\mathbf{j}(1)\mathbf{j}(\bar{3}) \rangle \mathbf{A}(\bar{2})\mathbf{A}(\bar{3}), \tag{29}$$

and integration over bar ($1 = (\mathbf{x}, t)$ indices is understood. The correlation function $\langle \mathbf{j}(\bar{2})\mathbf{j}(1)\mathbf{j}(\bar{3}) \rangle$ describes all processes related to electrons, such as photon absorption, electron removal and electron detection, are treated as a single coherent process. In this case the bulk, surface and evanescent states, as well as surface resonances should be taken into account - the so called *one-step model*.

Under some conditions the one-step model can be simplified by an approximative, but physically plausible, *three-step model*. In this model the photoemission intensity

$$I_{tot}(\mathbf{k}, \omega) = I \cdot I_2 \cdot I_3 \tag{30}$$

is the product of three independent terms: (**1**) I - describes optical excitation of the electron in the bulk; (**2**) I_2 - the scattering probability of the travelling electrons; (**2**) I_3 -

the transmission probability through the surface potential barrier. The central quantity in the three-step model is $I(\mathbf{k}, \omega)$. To calculate it one assumes the *sudden approximation,* i.e. that the outgoing electron is moving so fast that it has no time to interact with the photo-hole - see more in [107],[108]. It turns out that $I(\mathbf{k}, \omega)$ can be written in the form [107], [108] (for $\mathbf{k} = \mathbf{k}_{\parallel}$)

$$I(\mathbf{k}, \omega) \simeq I_0(\mathbf{k}, \upsilon) f(\omega) A(\mathbf{k}, \omega). \tag{31}$$

$I_0(\mathbf{k}, \upsilon) \sim | \langle \psi_f | \mathbf{pA} | \psi_i \rangle |^2$ where $\langle \psi_f | \mathbf{pA} | \psi_i \rangle$ is the dipole matrix element and depends on $\mathbf{k}$, polarization and energy υ of the incoming photons. $f(\omega) = 1/(1 + \exp\{\omega/T\})$ is the Fermi function and $A(\mathbf{k}, \omega) = -\mathrm{Im}G(\mathbf{k}, \omega)/\pi$ is the quasiparticle spectral function. In reality because of finite resolution of experiments, in $\mathbf{k}$ and ω, $I(\mathbf{k}, \omega)$ should be convoluted by the ω-convolution function $R(\omega)$ and $\mathbf{k}$-convolution function $Q(\mathbf{k})$. It must be also added the extrinsic background B, which is due to secondary electrons (those which escape from the sample after having suffered inelastic scattering events coming out with reduced kinetic energy).

By measuring $A(\mathbf{k}, \omega)$ one can determine $\Sigma(\mathbf{k}, \omega) = \Sigma_1(\mathbf{k}, \omega) + i\Sigma_2(\mathbf{k}, \omega)$

$$A(\mathbf{k}, \omega) = -\frac{1}{\pi} \frac{\Sigma_2(\mathbf{k}, \omega)}{[\omega - \xi_0(\mathbf{k}) - \Sigma_1(\mathbf{k}, \omega)]^2 + [\Sigma_2(\mathbf{k}, \omega)]^2}. \tag{32}$$

$\xi_0(\mathbf{k}) = \varepsilon_{\mathbf{k}} - \mu$ is the bare quasiparticle energy. For instance in the case of the Landau-Fermi liquid $A(\mathbf{k}, \omega)$ can be separated into the coherent and incoherent part

$$A(\mathbf{k}, \omega) = Z_{\mathbf{k}} \frac{\Gamma_{\mathbf{k}}}{(\omega - \xi(\mathbf{k}))^2 + \Gamma_{\mathbf{k}}^2} + A_{inch}(\mathbf{k}, \omega), \tag{33}$$

where $Z_{\mathbf{k}} = 1/(1 - \partial\Sigma_1/\partial\omega)$, $\xi(\mathbf{k}) = Z_{\mathbf{k}}(\xi_0(\mathbf{k}) + \Sigma_1)$ and $\Gamma_{\mathbf{k}} = Z_{\mathbf{k}} | \Sigma_2 |$ calculated at $\omega = \xi(\mathbf{k})$. For small ω one has $\xi(\mathbf{k}) >> | \Sigma_2 |$ and $\Gamma_{\mathbf{k}} \sim [(\pi T)^2 + \xi^2(\mathbf{k})]$.

In some period of the HTSC era there were a number of controversial ARPES results and interpretations, due to bad samples and to the euphoria with exotic theories. For instance, a number of (now well) established results were *questioned* in the first ARPES measurements, such as: the shape of the Fermi surface, which is correctly predicted by the LDA band-structure calculations; bilayer splitting in *Bi*2212, etc.

We summarize here important ARPES results which were obtained recently, first in the *normal state* [107], [108]: (**N1**) There is well defined Fermi surface in the metallic state - with the topology predicted by the LDA; (**N2**) the spectral line are broad with $| \Sigma_2(\mathbf{k}, \omega) | \sim \omega$ (or $\sim T$ for $T > \omega$); (**N3**) there is a bilayer band splitting in *Bi*2212 (at least in the overdoped state); (**N4**) at temperatures $T_c < T < T^*$ and in the underdoped HTSC oxides there is a d-wave like pseudogap $\Delta_{pg}(\mathbf{k}) \sim \Delta_{pg,0}(\cos k_x - \cos k_y)$ in the quasiparticle spectrum; (**N5**) the pseudogap $\Delta_{pg,0}$ increases by lowering doping; (**N6**) there is evidence for the strong EPI interaction and *characteristic phonon* energy ω_{ph} - at $T > T_c$. Namely, in all HTSC oxides which are superconducting there are *kinks* in the quasiparticle dispersion in the nodal direction (along the $(0,0) - (\pi, \pi)$ line) at around $\omega_{ph}^{(70)} \sim (60 - 70)$ *meV* [43] - see Fig. 13, and around the anti-nodal point $(\pi, 0)$ at 40 meV [109] - see Fig. 14.
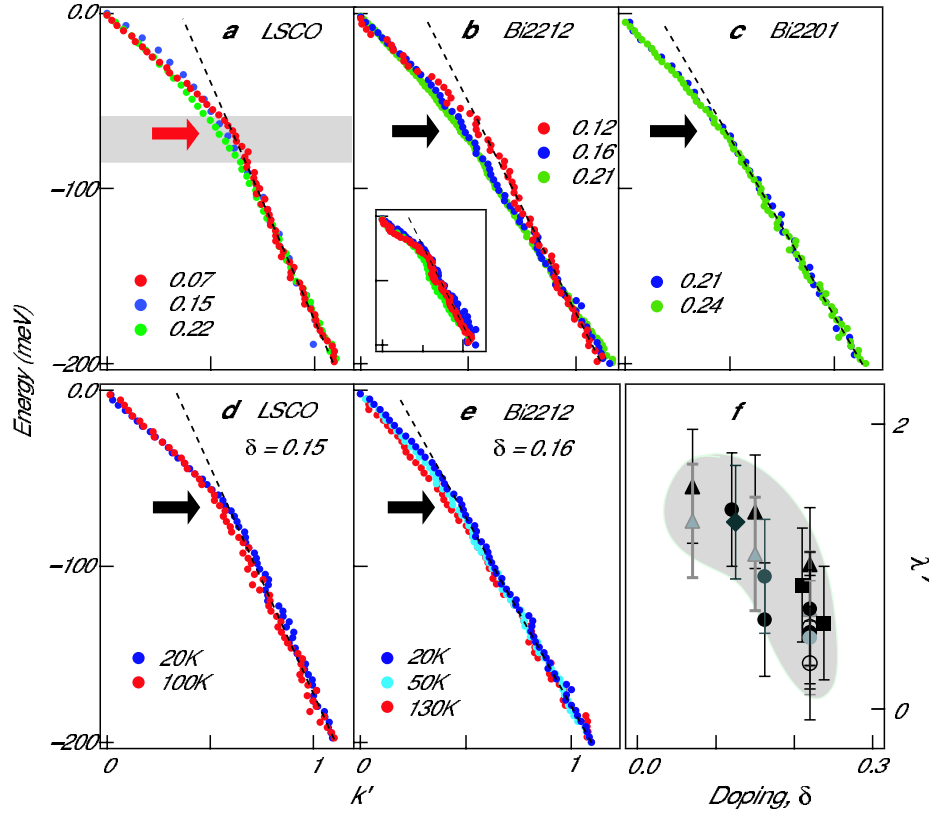
FIGURE 13. Quasiparticle dispersion of *Bi*2212, *Bi*2201 and *LSCO* along the nodal direction, plotted vs the momentum k for $(a) - (c)$ different doings, and $(d) - (e)$ different T; black arrows indicate the kink energy; the red arrow indicates the energy of the $q = (\pi, 0)$ oxygen stretching phonon mode; inset of (e)-T-dependent Σ' for optimally doped *Bi*2212; (f) - doping dependence of λ' along $(0,0) - (\pi, \pi)$ for the different HTSC oxides. From [43]

In the *superconducting state* ARPES results are the following [107], [108]: **(S1)** there is an anisotropic superconducting gap in most HTSC compounds, predominately of d-wave like, $\Delta_{sc}(\mathbf{k}) \sim \Delta_0(\cos k_x - \cos k_y)$ with $2\Delta_0/T_c \approx 5 - 6$; **(S2)** the dramatic changes in the spectral shapes near the point $(\pi, 0)$, i.e. a *sharp quasiparticle peak* develops at the lowest binding energy followed by a dip and a broader hump, giving rise to the so called *peak-dip-hump structure*; **(S3)** the kink at $(60 - 70)$ *meV* is surprisingly *unshifted* in the superconducting state -[43]. To remind the reader the standard Eliashberg theory the kink should be shifted to $\omega_{ph} + \Delta_0$. **(S4)** the anti-nodal kink at $\omega_{ph}^{(40)} \sim 40$ *meV* is shifted in the superconducting state by Δ_0, i.e. $\omega_{ph}^{(40)} \rightarrow \omega_{ph}^{(40)} + \Delta_0 = (65 - 70) meV$ since $\delta = (25 - 30) meV$ - see [109].
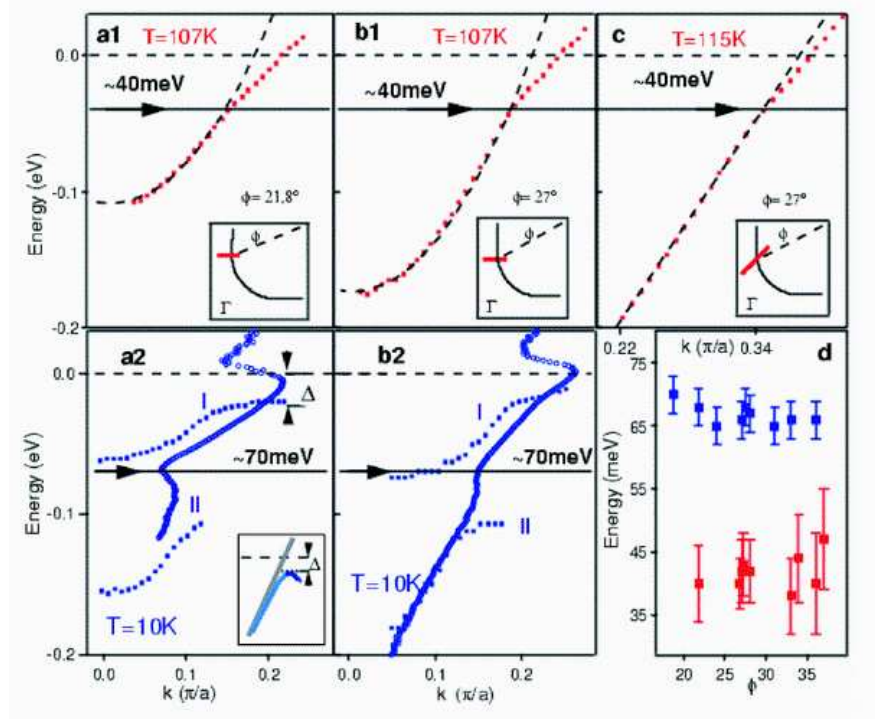
FIGURE 14. Quasiparticle dispersion $E(k)$ in the normal state (a1, b1, c), at 107 K and 115 K, along various directions ϕ around the anti-nodal point. The kink at $E = 40 meV$ is shown by the horizontal arrow. (a2 and b2) is $E(k)$ in the superconducting state at 10 K with the shifted kink to $70 meV$. (d) kink positions as a function of ϕ in the anti-nodal region. From [109]

2.6.2. Theory of the ARPES kink

We would like to point out that the breakthrough-experiments done by the Shen group [43], [109] shown in Fig. 13, Fig. 14, with the properties (**N6**), (**S3**) and (**S4**) - which we call the *ARPES shift-puzzle*, are the *smoking-gun* experiments for the microscopic theory of HTSC oxides. Namely, any theory which reflects to explain the pairing in HTSC oxides must solve the *shift-puzzle*.

In that respect the recent theory [44], which is based on the existence of the forward scattering peak (which is due to strong correlation in the EPI) in the EPI - the *FSP model*, was able to explain this puzzle in a consequent way. The FSP model (see more in [2], [44]) contains the following basic ingredients: *(i)* the electron-phonon interaction is dominant in HTSC and its spectral function $\alpha^2 F(\mathbf{k}, \mathbf{k}', \Omega) \approx \alpha^2 F(\varphi, \varphi', \Omega)$ (φ is the angle on the Fermi surface) has a pronounced forward scattering peak due to strong correlations. Its width is very narrow $| \mathbf{k} - \mathbf{k}' |_c \ll k_F$ even for overdoped systems [17], [18], [19]. In the leading order $\alpha^2 F(\varphi, \varphi', \Omega) \sim \delta(\varphi - \varphi')$; *(ii)* the dynamical part (beyond the Hartree-Fock) of the Coulomb interaction is characterized by the spectral function $S_C(\mathbf{k}, \mathbf{k}', \Omega)$. The ARPES shift puzzle implies that S_C is *either peaked* at small transfer momenta $| \mathbf{k} - \mathbf{k}' |$, *or it is so small* that the shift is weakly affected and is beyond the experimental resolution of ARPES. We assume that the former case is realized; *(iii)*

The scattering potential on non-magnetic impurities has pronounced forward scattering peak, which is also due to strong correlations [17], [18], [19]. The latter is characterized by two rates $\gamma_{1(2)}$. The case $\gamma_1 = \gamma_2$ mimics the extreme forward scattering, which does not affect pairing. On the other hand, $\gamma_2 = 0$ describes the isotropic exchange scattering - see discussion in

The Green's function is given by $G_k = 1/(i\omega_k - \xi_{\mathbf{k}} - \Sigma_k(\omega)) = -(i\tilde{\omega}_k + \xi_{\mathbf{k}})/(\tilde{\omega}_k^2 + \xi_{\mathbf{k}}^2 + \tilde{\Delta}_k^2)$ where in the $k = (\mathbf{k}, \omega)$. In the FSP model the equations for ω_k and $\tilde{\Delta}_k$ are [44]

$$\tilde{\omega}_{n,\varphi} = \omega_n + \pi T \sum_m \frac{\lambda_{1,\varphi}(n-m)\tilde{\omega}_{m,\varphi}}{\sqrt{\tilde{\omega}_{m,\varphi}^2 + \tilde{\Delta}_{m,\varphi}^2}} + \Sigma_{n,\varphi}^C, \tag{34}$$

$$\tilde{\Delta}_{n,\varphi} = \pi T \sum_m \frac{\lambda_{2,\varphi}(n-m)\tilde{\Delta}_{m,\varphi}}{\sqrt{\tilde{\omega}_{m,\varphi}^2 + \tilde{\Delta}_{m,\varphi}^2}} + \tilde{\Delta}_{n,\varphi}^C, \tag{35}$$

where

$$\lambda_{1(2),\varphi}(n-m) = \lambda_{ph,\varphi}(n-m) + \delta_{mn}\gamma_{1(2),\varphi}$$

with the electron-phonon coupling function

$$\lambda_{ph,\varphi}(n) = 2\int_0^\infty d\Omega \alpha_{ph,\varphi}^2 F_\varphi(\Omega) \frac{\Omega}{\Omega^2 + \omega_n^2}. \tag{36}$$

Since the EPI and $\Sigma_{n,\varphi}^C$ in Eq.(34-35) has a *local form* as a function of the angle φ, then the equation for $\tilde{\omega}_{n,\varphi}$ has also local form, which means that the different points on the Fermi surface are decoupled. In that case $\tilde{\omega}_{n,\varphi}$ depends on the local value of the gap $\tilde{\Delta}_{n,\varphi} \approx \Delta_0 \cos 2\varphi$. *Just this property is important in solving the ARPES shift puzzle*. So, in the *nodal point ($\varphi = \pi/4$)* one has $\tilde{\Delta}_{n,\varphi} = 0$ and the quasiparticle spectrum given by $E - \xi_{\mathbf{k}} - \Sigma_k(E, \tilde{\Delta}_{n,\varphi} = 0) = 0$ is *unaffected* by superconductivity, i.e. the kink is unshifted. This is exactly what is seen in the experiment of the Shen group [43] - see Fig. 13. In the case of the *antinodal point ($\varphi \approx \pi/2$)* there is a singularity at $40 meV$ in the quasiparticle spectrum (E_{sing}) in the normal state - see Fig. 14. The analytic and numeric calculations of Eq.(34) show that this singularity is *shifted* by Δ_0 in superconducting state, i.e. $E_{\text{sing}} \to E_{\text{sing}} + \Delta_0$. This is exactly what is seen in the recent experiment on BISCO [109] - see Fig. 14, where the singularity of the normal state spectrum at 40 meV is shifted to $(65 - 70)\ meV$ in the superconducting state, since $\Delta_0 \approx (25 - 30)\ meV$. The FSP model explains in the natural way also the *peak-dip-hump structure* in $A(\mathbf{k}, \omega)$ - for more details see [44].

2.6.3. ARPES and the EPI coupling constant λ

One can rise the question - is it possible to extract the coupling constant λ from ARPES measurements. As we have seen above, by assuming that the three-step model holds, where $I(\mathbf{k}, \omega) \sim A(\mathbf{k}, \omega)$, then one possibility is by measuring the kink in the quasiparticle renormalization, i.e. by measuring the real part of the self-energy $\Sigma_1(\mathbf{k}, \omega)$.

These measurements [43], [109] give $\lambda^{(1)}_{ARPES} \sim 1$ in both nodal and antinodal direction. Another possibility is by measuring the width ($\Delta k_{FW}(\omega)$) of the momentum distribution curves (MDCs) which give the imaginary part $\Sigma_2(\omega, T)$ via

$$\Sigma_2(\omega, T) \approx \frac{1}{2} v_F \Delta k_{FW}(\omega). \tag{37}$$

In that respect very indicative are recent measurements [45] of $\Sigma_2(\omega, T)$ around the *nodal point* in a number of HTSC compounds, such as the superstructure free $Bi_{2-x}Pb_xSr_2CaCu_2O_{8+\delta}$ $(Bi(Pb) - 2212)$, $Bi_2Sr_2CaCu_2O_{8+\delta}$ $(Bi - 2212)$ and $Bi_2Sr_{2-x}La_xCu_2O_{8+\delta}$ $(Bi - 2201)$. In the analysis of ARPES spectra the authors in [45] have assumed that there are two ω-dependent contributions to Σ - the Fermi liquid contribution Σ_{FL} and the part Σ_B due to the interaction via bosonic excitations (let say phonons and spin-fluctuations), i.e. $\Sigma_2 = \Sigma_{2,FL} + \Sigma_{2,B} + \Sigma_{2,imp}$ - see Fig. 15. We stress, that in [45] it is assumed that $v_F = 4\ eV$ Å.

In the framework of this procedure the theoretical analysis [46] gives small coupling $\lambda^{(2)}_{ARPES} < 0.2$, which is extracted from the slope of Σ_2 in the interval $0.05\ eV < \omega < 0.1$ eV - see the gray solid line in Fig. 15b). Such a small coupling gives very small T$_c$ and none of pairing mechanisms is effective. Furthermore, the small value of $\lambda^{(2)}_{ARPES}$ (most measurements give $\lambda^{(2)}_{max,ARPES} < 0.4$) - which is extracted from Σ_2, is a generic property of most ARPES measurements. This means, that we are *confronted with a trilemma*: (**1**) to abandon the boson-fermion separation procedure of $\Sigma(\omega)$ done in [45], (**2**) to abandon the Eliashberg theory, (**3**) to abandon the interpretation of ARPES data within the three-step model.

In some sense the situation in ARPES measurements with $\lambda^{(2)}_{ARPES} \ll \lambda$ resembles the one in transport measurements where $\lambda_{tr} \ll \lambda$, i.e. . This problem deserves further investigation.

3. EPI IN HTSC OXIDES

In the following we present briefly some elements of the general theory of the strong EPI and its low-energy version. In the latter, high-energy processes are integrated out and the low-energy phenomena are governed by the high-energy vertex functions Γ_c, the excitation potential Σ_0 (part of the self-energy due to the Coulomb interaction) and the EPI coupling constants $g_{EP,ren} \sim \Gamma_c$ - see more in [2]. However, this procedure was never performed in its full extent, because of difficulties to calculate Σ_0 and Γ_c. Therefore, the EPI coupling constant was as a rule calculated by some other methods. Usually in *LTSC* materials the EPI is calculated by using the local-density functional (*LDA*) method, which is suitable for ground state properties of crystals (matter) and which is based on an effective electronic crystal potential V_g. Since in principle V_g may significantly differ from Σ_0 then the *LDA* calculated coupling constant $g^{(LDA)}_{EP}$ can be also very different from the real coupling constant g_{EP}. The calculation of $g^{(LDA)}_{EP}$ is complicated, even in the *LDA* method, and further approximations are necessary, like for instance the rigid-ion (*RI*) and
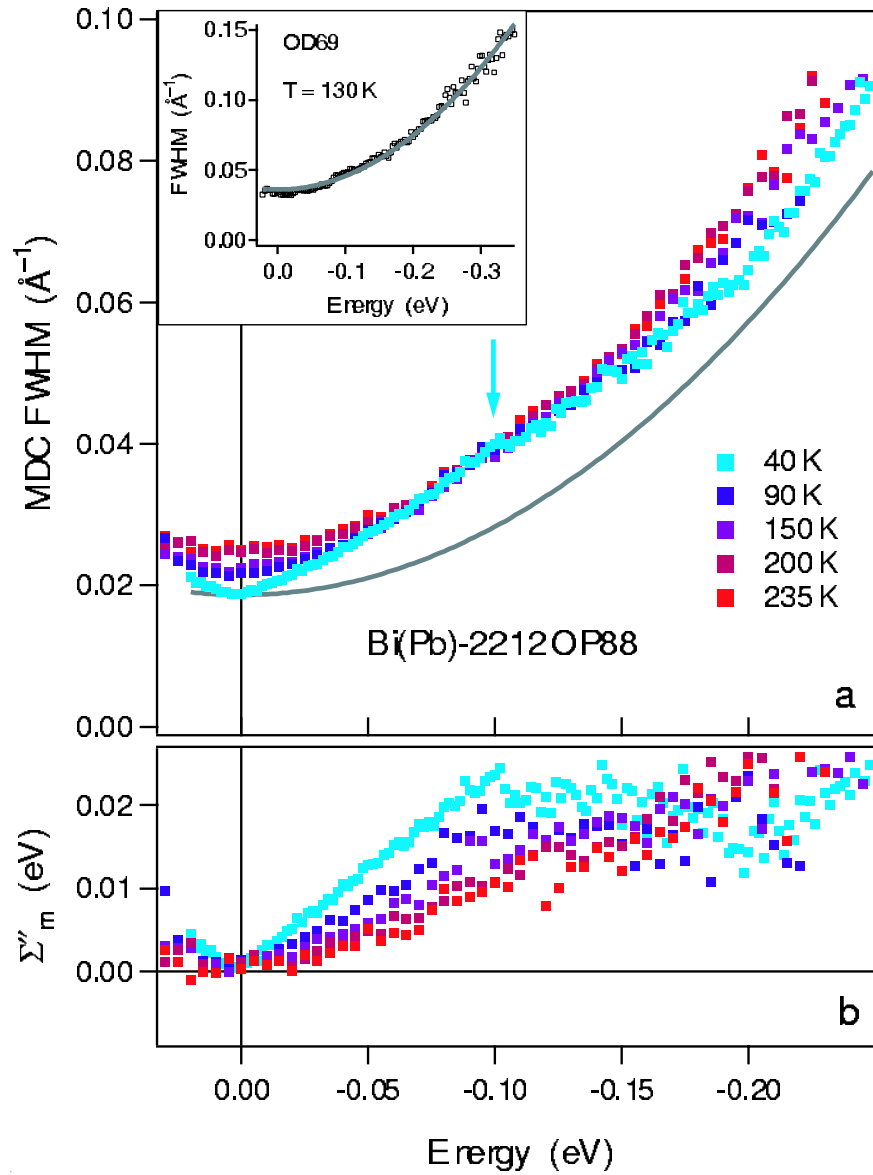
FIGURE 15. T- and ω-dependence of Σ_2 for the nodal quasiparticles in optimally doped Bi(Pb)-2212. (**a**) - the full width at half maximum of the ARPES intensity. The gray solid line is the Fermi liquid parabola obtained by fitting the data for highly overdoped sample (OD69) at 130 K (see inset). (**b**) - the bosonic part $\Sigma_{2,B}$ for various T. From [45]

rigid muffin-tin (*RMTA*) approximations. These approximation were justified in simple metals. However, these approximations are inadequate for HTSC oxides, because they fail to take into account correctly the *long-range forces* (Madelung energy - see below) and *strong electronic correlations*. Strictly speaking the EPI does not have meaning in the *LDA* method - see more in [2], because the latter treats the ground state properties of materials, while the EPI is due to excited states and inelastic processes in the system.

3.1. General strong coupling theory of the EPI

It is based on the fully microscopic electron-ion Hamiltonian for the interacting electrons and ions in a crystal - see for instance [110], [111], [112], and comprises electrons interacting between themselves as well as with ions and ionic vibrations. In order to describe superconductivity the Nambu-spinor $\hat{\psi}^\dagger(\mathbf{r})$ is introduced which operates in the electron-hole space $\hat{\psi}^\dagger(\mathbf{r}) = (\hat{\psi}^\dagger_\uparrow(\mathbf{r})\ \hat{\psi}^\dagger_\downarrow(\mathbf{r}))$ (analogously for the column $\hat{\psi}(\mathbf{r})$) with $\hat{\psi}_\uparrow(\mathbf{r})$, $\hat{\psi}^\dagger_\uparrow(\mathbf{r})$ as annihilation and creation operators for spin up, respectively etc. The microscopic Hamiltonian which in principle should describe the normal and superconducting state of the system contains three parts $\hat{H} = \hat{H}_e + \hat{H}_i + \hat{H}_{e-i}$. The *electronic Hamiltonian* $\hat{H}_e$, which describes the kinetic energy and the Coulomb interactions of electrons, is given in the second-quantization by

$$\hat{H}_e = \int d^3r\,\hat{\psi}^\dagger(\mathbf{r})\hat{\tau}_3\varepsilon_0(\hat{p})\hat{\psi}(\mathbf{r})+$$

$$+\frac{1}{2}\int d^3r d^3r'\,\hat{\psi}^\dagger(\mathbf{r})\hat{\tau}_3\hat{\psi}(\mathbf{r})V_c(\mathbf{r}-\mathbf{r}')\hat{\psi}^\dagger(\mathbf{r}')\hat{\tau}_3\hat{\psi}(\mathbf{r}'), \tag{38}$$

where $\varepsilon_0(\hat{p}) = \hat{p}^2/2m$ is the kinetic energy of electron and $V_c(\mathbf{r}-\mathbf{r}') = e^2/\mid \mathbf{r}-\mathbf{r}'\mid$ is the electron-electron Coulomb interaction. Note, that in the electron-hole space the pseudo-spin (Nambu) matrices $\hat{\tau}_i$, $i=0,1,2,3$ are Pauli matrices.

The *lattice Hamiltonian* (describes lattice vibrations $\hat{u}_{\alpha n}$ of ions enumerated by n) is given by

$$\hat{H}_i = \frac{1}{2}\sum_n M(\frac{d\hat{\mathbf{u}}_n}{dt})^2 + \frac{1}{2}\sum_{n,m,\alpha} V_{ii}(\mathbf{R}^0_n - \mathbf{R}^0_m) + \frac{1}{2}\sum_{n,m}(\hat{u}_{\alpha n} - \hat{u}_{\alpha m})\nabla_\alpha V_{ii}(\mathbf{R}^0_n - \mathbf{R}^0_m)+$$

$$+\frac{1}{2}\sum_{n,m,\alpha,\beta}(\hat{u}_{\alpha n} - \hat{u}_{\alpha m})(\hat{u}_{\beta n} - \hat{u}_{\beta m})\nabla_\alpha\nabla_\beta V_{ii}(\mathbf{R}^0_n - \mathbf{R}^0_m) + \hat{H}^{anh}_i. \tag{39}$$

The first term in Eq.(39) is the kinetic energy of vibrating ions (with charge Ze), $V_{ii}(\mathbf{R}^0_n - \mathbf{R}^0_m) = Z^2 e^2/\mid \mathbf{R}^0_n - \mathbf{R}^0_m\mid$ is the bare ion-ion interaction in equilibrium, while the third and fourth terms describe the change of V_{ii} by lattice vibrations with the ion-displacement is $\hat{u}_n = \mathbf{R}_n - \mathbf{R}^0_n$. The term $\hat{H}^{anh}_i$ describes higher anharmonic terms with respect to $\hat{u}^\beta_n$. The theory which we describe below holds for any kind of anharmonicity.

The *electron-ion Hamiltonian* describes the interaction of electrons with the equilibrium lattice and with its vibrations, respectively

$$\hat{H}_{e-i} = \sum_n \int d^3r V_{e-i}(\mathbf{r}-\mathbf{R}^0_n)\hat{\psi}^\dagger(\mathbf{r})\hat{\tau}_3\hat{\psi}(\mathbf{r}) + \int d^3r\,\hat{\Phi}(\mathbf{r})\hat{\psi}^\dagger(\mathbf{r})\hat{\tau}_3\hat{\psi}(\mathbf{r}), \tag{40}$$

$$\hat{\Phi}(\mathbf{r}) = \sum_n[V_{e-i}(\mathbf{r}-\mathbf{R}^0_n - \hat{\mathbf{u}}_n) - V_{e-i}(\mathbf{r}-\mathbf{R}^0_n).$$

Here, $V_{e-i}(\mathbf{r}-\mathbf{R}^0_n)$ is the electron-ion potential - see [2]. The second term which depends on the lattice distortion operator $\hat{\Phi}(\mathbf{r})$ describes the interaction of electrons with harmonic ($\sim \hat{u}_{\alpha n}$) (or anharmonic $\sim \hat{u}^k_{\alpha n}$, $k=2,3...$) lattice vibrations.

Based on the above Hamiltonian one can in principle calculate the electron and phonon Green's functions

$$\hat{G}(1,2) = -\langle T\hat{\psi}(1)\hat{\psi}^\dagger(2)\rangle \tag{41}$$

and

$$\tilde{D}(1-2) = -\langle T\hat{\Phi}(1)\hat{\Phi}(2)\rangle, \tag{42}$$

respectively. The solution of these equations is written in the form of Dyson's equations

$$\hat{G}^{-1}(1,2) = \hat{G}_0^{-1}(1,2) - \hat{\Sigma}(1,2) \tag{43}$$

and

$$\tilde{D}^{-1}(1,2) = \tilde{D}_0^{-1}(1,2) - \tilde{\Pi}(1,2), \tag{44}$$

where $\hat{G}_0^{-1}(1,2)$ and $\tilde{D}_0^{-1}(1,2)$ are the bare inverse electron and phonon Green's function, respectively. The nontrivial effects of interactions are hidden in the self-energies $\hat{\Sigma}(1,2)$ and $\tilde{\Pi}(1,2)$. Here, $1 = (\mathbf{r}_1, \tau_1)$, where τ_1 is the imaginary time. The calculation of $\hat{\Sigma}$ is simplified by using the *Migdal adiabatic approximation* [139], which incorporates the experimental fact that in most metals the characteristic phonon (Debye) energy of lattice vibrations ω_D is much smaller than the characteristic electronic Fermi energy E_F ($\omega_D \ll E_F$). Using this fact Migdal formulated a theorem which claims that in the self-energy Σ one should keep explicitly terms linear in the phonon propagator $\tilde{D}$ only. As the result one obtains the *Migdal-Eliashberg theory* for

$$\hat{\Sigma} = \hat{\Sigma}_c + \hat{\Sigma}_{EP}, \tag{45}$$

where

$$\hat{\Sigma}_c(1,2) = -V_c^{sc}(1,\bar{1})\hat{\tau}_3\hat{G}(1,\bar{2})\hat{\Gamma}_c(\bar{2},2;\bar{1}). \tag{46}$$

$V_c^{sc}(1,2) = V_c(1,\bar{2})\varepsilon_e^{-1}(\bar{2},2)$ is the screened Coulomb interaction. The part which is due to the EPI has the following form

$$\hat{\Sigma}_{EP}(1,2) = -V_{EP}(\bar{1},\bar{2})\hat{\Gamma}_c(1,\bar{3};\bar{1})\hat{G}(\bar{3},\bar{4})\hat{\Gamma}_c(\bar{4},2;\bar{2}), \tag{47}$$

where

$$V_{EP}(1,2) = \varepsilon_e^{-1}(1,\bar{1})\tilde{D}(\bar{1},\bar{2})\varepsilon_e^{-1}(\bar{2},2)$$

is the screened EPI and ε_e is the electronic dielectric function. Note, $\hat{\Sigma}_{EP}(1,2)$ depends now quadratically on the vertex function $\hat{\Gamma}_c$, due to the adiabatic theorem. If $\hat{\Gamma}_c$ (which is a functional of $\hat{G}$) is known then the quasiparticle dynamics can be in principle determined. In that respect the central question is: (**1**) how to calculate $\hat{\Gamma}_c$ - which contains all information on Coulomb interaction and electronic correlations? This is a difficult task and practically never realized in its full extent for real systems. However, this program is realized recently in the t-J model with the EPI interaction in the framework of the X-method - see below and [2]; (**2**) how to calculate the effective EPI potential $V_{EP} \sim g_{EP}^2/\varepsilon_e^2$, or more precisely the coupling constant g_{EP} and the electronic dielectric function ε_e? In absence of a better theory these quantities are usually calculated in the framework of the LDA band-structure theory.

3.2. LDA calculations of λ in HTSC oxides

The LDA method considers electrons in the ground state (there is a generalization to finite T), whose energy can be calculated by knowing the spectrum $\{\varepsilon_k\}$ of the Kohn-Sham (Schrödinger like) equation

$$[\frac{\hat{\mathbf{p}}^2}{2m} + V_g(\mathbf{r})]\psi_k(\mathbf{r}) = \varepsilon_k \psi_k(\mathbf{r}), \qquad (48)$$

which depends on the *effective one-particle potential*

$$V_g(\mathbf{r}) = V_{ei}(\mathbf{r}) + V_H(\mathbf{r}) + V_{XC}(\mathbf{r}). \qquad (49)$$

Here. V_{ei} is the electron-lattice potential, V_H is the Hartree term and V_{XC} describes exchange-correlation effects - see [2]. Because the EPI depends on the excited states (above the ground state) of the system this means, that in principle the LDA method can not describe it - see [2]. However, by using an analogy with the microscopic Migdal-Eliashberg theory one can define the EPI coupling constant $g^{(Mig)} = g\Gamma_c/\varepsilon$ also in the LDA theory - see [2]. It reads

$$g_{\alpha,ll'}^{(LDA)}(\mathbf{k},\mathbf{k}') = \sum_n g_{\alpha,nll'}^{(LDA)}(\mathbf{k},\mathbf{k}') = \langle \psi_{\mathbf{k}l} \mid \sum_n \frac{\delta V_g(\mathbf{r})}{\delta R_{n\alpha}} \mid \psi_{\mathbf{k}'l'}\rangle, \qquad (50)$$

where n means summation over the lattice sites, $\alpha = x,y,z$ and the wave function $\psi_{\mathbf{k}l}$ is the solution of the Kohn-Sham equation. Formally one has $\delta V_g/\delta\mathbf{R}_n = \Gamma_{LDA}\varepsilon_e^{-1}\nabla V_{ei}$. Even in such a simplified approach it is difficult to calculate $g_{\alpha,ll'}^{(LDA)} = g_{\alpha,n}^{RMTA} + g_{\alpha,n}^{nonloc}$ because it contains the short-range (local) coupling

$$g_{\alpha,n}^{RMTA} \sim g_{\alpha,n}^{RMTA}(\mathbf{k},\mathbf{k}') \sim \langle Y_{lm} \mid \hat{r}_\alpha \mid Y_{l'm'}\rangle \qquad (51)$$

with $\Delta l = 1$, and the long-range coupling

$$g_{\alpha,n}^{nonloc}(\mathbf{k},\mathbf{k}') \sim \langle Y_{lm} \mid (\mathbf{R}_n^0 - \mathbf{R}_m^0)_\alpha \mid Y_{l'm'} \qquad (52)$$

with $\Delta l = 0$. In most calculations the local term $g_{\alpha,n}^{RMTA}$ is calculated only, which is justified in simple metals only but not in the HTSC oxides. In HTSC oxides the latter gives very small EPI coupling $\lambda^{RMTA} \sim 0.1$, which is apparently much smaller than the experimental value $\lambda > 1$ giving rise to the pessimistically small T$_c$ [113]. The small λ^{RMTA} was also one of the reasons for abandoning the EPI as pairing mechanism in HTSC oxides. At the beginning of the HTSC era the electron-phonon spectral function $\alpha^2 F(\omega)$ for the case $La_{2-x}Sr_xCuO_4$ was calculated in [114] by using the first-principles band structure calculations and the nonorthogonal tight-binding theory of lattice dynamics. It was obtained $\lambda = 2.6$ and for assumed $\mu^* = 0.13$ gave $T_c = 36\ K$. However, these calculations predict a lattice instability for the oxygen breathing mode near $La_{1.85}Sr_{0.15}CuO_4$ that is never observed. Moreover, the same method was applied to $YBa_2Cu_3O_7$ in [115] where it was found $\lambda = 0.5$ which leads at most to $T_c = (19-30)\ K$. In fact the calculations in [114], [115] do not take into account the Madelung coupling (i.e. neglect the matrix elements with $\Delta l = 0$).

However, because of the weak screening of the ionic (long-range) Madelung coupling in HTSC oxides - especially for vibrations along the c-axis, it is necessary to include the nonlocal term $g_{\alpha,n}^{nonloc}$. This goal was achieved in the LDA approach by the Pickett's group [51], where the EPI coupling for $La_{2-x}M_xCuO_4$ is calculated in the *frozen-in phonon* (*FIP*) method. They have obtained $\lambda = 1.37$ and $\omega_{\log} \approx 400\,K$ and for $\mu^* = 0.1$ one has $T_c = 49\,K$ ($T_c \approx \omega_{\log}\exp\{-1/[(\lambda/(1+\lambda)) - \mu^*]\}$). For more details see Ref. [2] and references therein. We point out, that some calculations which are based on the tight-binding parametrization of the band structure in $YBa_2Cu_3O_7$ gave rather large EPI coupling $\lambda \approx 2$ and $T_c = 90\,K$

Recently, a new *linear-response full-potential linear-muffin-tin-orbital* (*LR-LMTO*) method for the calculation of λ^{LDA} was invented in [116]. It is very efficient in explaining the physics of elemental metals, like $Al, Cu, Mo, Nb, Pb, Pd, Ta$ and V with disagreements by only $10 - 30\%$ of theoretical and experimental results (obtained from tunnelling and resistivity measurements) for the EPI coupling constants λ and λ_{tr}. However, the *LR-LMTO* method applied to the doped HTSC oxide $(Ca_{1-x}Sr_x)_{1-y}CuO_2$ for $x \sim 0.7$ and $y \sim 0.1$ with $T_c = 110\,K$ gives surprisingly small *EPI* coupling $\lambda_s \approx 0.4$ for $s-wave$ pairing and $\lambda_d \leq 0.3$ for $d-wave$ pairing [117]. Although this finding, that λ_d is of the similar magnitude as λ_s ($\lambda_d \approx \lambda_s$), is interesting and encouraging it seems that this method misses some ingredients of the ionic structure of the layered structure [52], [53].

We point out, that the model calculations which take into account the long-range ionic Madelung potential appropriately [47], [48], [50] gave also rather large coupling constant $\lambda \sim 2$, what additionally hints to the importance of the long-range forces in the EPI.

Since in HTSC oxides the plasma frequency along the c-axis, ω_{pl}^c, is of the order (or even less) of some characteristic c-axis vibration mode, it is necessary to include the *nonadiabatic effects* in the EPI coupling constant, i.e. its frequency dependence $g_{\alpha,n} \sim g^0/\varepsilon_{cc}(\omega)$. This non-adiabaticity is partly accounted for in the Falter group [52], [53] by calculating the electronic dielectric function along the c-axis $\varepsilon_{cc}(\mathbf{k},\omega)$ in the RPA approximation. The result is that $g_{\alpha,n}$ is increased appreciable beyond its (well screened) metallic part, what gives a large increase of the EPI coupling not only in the phonon modes but also in the plasmon one. This question deserves much more attention than it was in the past.

3.3. Lattice dynamics and EPI coupling

The calculation of the phonon frequencies ω_{ph}, which are obtained from

$$D_0^{-1}(\mathbf{q},\omega_{ph}) - \hat{\Pi}(\mathbf{q},\omega_{ph}) = 0, \tag{53}$$

is in principle even more complicated problem than the calculations of the electronic properties. It lies on the difficulty to calculate the phonon polarization operator $\hat{\Pi}$ - see more in [2]. Schematically one has

$$\hat{\Pi} \sim (\nabla_\alpha V_{e-i})^2 \hat{\chi}_c, \tag{54}$$

where $\hat{\chi}_c$ is the *electronic charge susceptibility*. V_{e-i} is the bare electron-lattice interactions. $\hat{\chi}_c$ is schematically given by $\hat{\chi}_c = \hat{P}\hat{\varepsilon}_e^{-1}$ and the electronic *polarization operator* $\hat{P} = \hat{G}\hat{\Gamma}_c\hat{G}$. As we see the phonon frequencies depends crucially on the screening properties of electrons. The screening effects in HTSC oxides are determined by the specificity of the metallic-ionic structure and strong electronic correlations. At present there is a controllable theory for the electronic properties in the t-J model [17], [18], [19], [20], [2] only, where these two ingredients are successfully incorporated in the theory. However, until now there is no controllable theory for the lattice dynamics which incorporates these two ingredients, in spite the fact that the X-method (see below) offers well defined and procedure. There were a number of interesting attempts to calculate renormalization of some specific phonons [54], [55], [56], such as for instance of the half-breathing phonon mode along the $(1,0,0)$ direction - which is strongly softened. In spite of some alleged theoretical confirmation of the experimental softening in YBCO and LASCO, none of these calculations are reliable, because none of them take into account the screening due to strong correlations (the charge vertex $\hat{\Gamma}_c$ and the dielectric function $\hat{\varepsilon}_e$) in a controllable way. That is the reason that all attempts until were unable to extract the reliable magnitude of the coupling constant with a specific phonon. Even more, by playing only with a single phonon mode, and with a particular wave-vector in the Brillouin zone, *one can not get large EPI* and large λ - see [2]. The latter claim is confirmed by tunnelling experiments, which demonstrate that almost all phonons (for instance 39 modes in *YBCO*) contribute to λ. No particular mode can be singled out in the spectral function $\alpha^2 F(\omega)$ as being the only one which dominates in pairing mechanism in HTSC oxides.

4. THEORY OF STRONG ELECTRONIC CORRELATIONS

The well established fact is that *strong electronic correlations* are pronounced in HTSC oxides, at least in underdoped systems. However, the LDA theory fails to capture effects of strong correlations by treating they as a local perturbation. This is, as we shall see later, an unrealistic approximation in HTSC oxides, where strong correlations introduce non-locality. The shortcoming of the *LDA* is that in the half-filling case (with $n = 1$ and one particle per lattice site) it predicts metallic state missing the existence of the *Mott insulating state*. In the latter, particles are localized at lattice sites independent of the (non)existence of the *AF* order and the localization is due to the large Coulomb repulsion U at a given lattice site, i.e. $U \gg W$ where W is the band width. Some properties in the metallic state can not be described by the simple canonical Landau-Fermi liquid concept. For instance, recent ARPES photoemission measurements [122] on the hole doped samples show a well defined Fermi surface in the one-particle energy spectrum, which contains $1 - \delta$ electrons in the Fermi volume (δ is the hole concentration), but the band width is $(2-3)$ times smaller than the *LDA* band structure calculations predict. The latter is consistent with the Luttinger theorem as well as with the *LDA* band structure calculations. However, experimental data on the dynamical conductivity (spectral weight of the Drude peak), Hall measurements etc. indicate that in transport properties a low density of hole-like charge carriers (which is proportional to δ) participates

predominantly. These carriers suffer strong scattering and their inverse lifetime is proportional to the temperature (at $T > T_c$) as we discussed earlier. It is worth of mentioning here that the local moments on the Cu sites, which are localized in the parent AF compound, are counted as part of the Fermi surface area when the system is doped by small concentration of holes in the metallic state. The latter fact gives rise to a *large Fermi surface* which scales with the number (per site) of electrons $1 - \delta$. At the same time the conductivity sum-rule is proportional to the number of doped holes δ, instead of $1 - \delta$ as in the canonical Landau-Fermi liquid. These two properties tell us that we deal with a *correlated state*, and the latter must be due to the specific electronic structure of HTSC oxides (cuprates). The common ingredient of all cuprates is the presence of the Cu atoms. In order to account for the absence of Cu^{3+} ionic configuration (the charge transfer $Cu^{2+} \rightarrow Cu^{3+}$ costs large energy $U \sim 10 \ eV$, i.e. the occupation of the Cu site with two holes with opposite spins is unfavorable) P. W. Anderson [61] proposed the Hubbard model as the basic model for quasiparticle properties in these compounds. For some parameter values it can be derived from the (minimal) microscopic *three-band model*. Besides the hopping t_{pd} between the d-orbitals of Cu and p-orbitals of O ions (as well as t_{pp}) - the Emery model [123], it includes also the strong Coulomb interaction U_{Cu} on the Cu ions as well as interaction between p- and d-electrons. The main two parameters are $U_{Cu} \sim (6-10) \ eV$ and the charge transfer energy $\Delta_{pd} \equiv \varepsilon_d^0 - \varepsilon_p^0 \sim (2.5-4)$ eV, where $\varepsilon_d^0, \varepsilon_p^0$ are energies of the d- and p-level, respectively. In HTSC oxides the case $U_{Cu} >> \Delta_{pd}$ is realized, i.e. they belong to the class of *charge transfer materials*. This allows us to project the complicated three-band Hamiltonian onto the low-energy sector, and to obtain an effective single-band Hubbard Hamiltonian with an effective hopping parameter t and the effective repulsion $U \approx \Delta_{pd}$. It turns out that the case $U >> t$ is realized, since $\Delta_{pd} \gg t = t_{pd}^2/\Delta_{pd}$. The effective and minimal Hamiltonian which describes the low-energy physics of HTSC oxides comprises also the long-range Coulomb interaction $\hat{V}_C$ and the EPI $\hat{V}_{EPI}$ - see [7], [2]

$$\hat{H} = -\sum_{i,j,\sigma} t_{ij} c_{i\sigma}^\dagger c_{j\sigma} + U \sum_i n_{i\uparrow} n_{i\downarrow} + \hat{V}_C + \hat{V}_{EPI}. \tag{55}$$

The effective repulsion $U \approx 4 \ eV$ has its origin in the charge-transfer gap of the three-band model, while the nearest neighbor and next-nearest neighbor hopping t and t' , respectively are estimated to be $t = 0.3 - 0.5 \ eV$ and t'/t equal -0.15 in La compounds and $-0.45 \ YBCO$. Since $(U/t) \gg 1$ the above Hamiltonian is again in the regime of strong electronic correlations, where the doubly occupancy of a given lattice site is strongly suppressed, i.e. $\langle n_{i\uparrow} n_{i\downarrow} \rangle \ll 1$. The latter restricts charge fluctuations of electrons (holes) on a given lattice site are allowed, since $n_i = 0, 1$ is allowed only, while processes with $n_i = 2$ are (practically) forbidden. Note, that in (standard) weakly correlated metals all charge fluctuation processes ($n_i = 0, 1, 2$) are allowed, since $U \ll W$ in these systems. From the Hamiltonian in Eq.(55), which is the 2D model for the low-energy physics in the CuO_2 plane, comes out that in the *undoped* system there is one particle per lattice - the so called half-filled case (in the band language) with $\langle n_i \rangle = 1$. It is an insulator because of large U and even antiferromagnetic insulator at $T = 0 \ K$. The effective exchange interaction (with $J = 4t^2/U$) between spins is Heisenberg-like. By doping the system by holes (with the hole concentration $\delta (< 1)$), means that particles are taken

out from the system in which case there is on the average $\langle n_i \rangle = 1 - \delta$ particles per lattice site. Above some (small) critical doping $\delta_c \sim 0.01$ the *AF* order is destroyed and the system is strongly correlated metal. For some *optimal* doping $\delta_{op}(\sim 0.1)$ the system is metallic with the large Fermi surface and can exhibit even high-T_c superconductivity in the presence of the EPI, as it will demonstrated below. The latter interaction and its interplay with strong correlations is the central subject in the following sections.

4.1. X-method for strongly correlated systems

Since $U >> t$ one can put with good accuracy $U \to \infty$, i.e. the system is in the *strongly correlated regime* where the doubly occupancy $n_i = 2$ is excluded. One of the ways to cope with such strong correlations is to introduce the (fermionic like) creation and annihilation operators ($\hat{X}_i^{\sigma 0}$ and $\hat{X}_i^{0\sigma} = (\hat{X}_i^{\sigma 0})^\dagger$)

$$\hat{X}_i^{\sigma 0} = c_{i\sigma}^\dagger (1 - n_{i,-\sigma}), \tag{56}$$

which respect the condition $n_{i,\sigma} + n_{i,-\sigma} \le 1$ on each lattice site. The latter means that there is no more than one electron (hole) at a lattice site, i.e. the doubly occupancy is forbidden. The bosonic like operators

$$\hat{X}_i^{\sigma_1 \sigma_2} = \hat{X}_i^{\sigma_1 0} \hat{X}_i^{0\sigma_2} \tag{57}$$

(with $\sigma_1 \ne \sigma_2$) create a spin fluctuation at the $i - th$ site. Here, the spin projection parameter $\sigma = \uparrow, \downarrow$ and $-\sigma = \downarrow, \uparrow$ and the operator $\hat{X}_i^{\sigma\sigma}$ has the meaning of the electron (hole) number on the i-th site. In the following we shall use the convention that when $\hat{X}_i^{\sigma\sigma} \mid 1 \rangle = 1 \mid 1 \rangle$ there is a fermionic particle ("electron") on the i-th site, while for $\hat{X}_i^{\sigma\sigma} \mid 0 \rangle = 0 \mid 0 \rangle$ the site is empty, i.e. there is a hole on it. It is useful to introduce the hole number operator

$$\hat{X}_i^{00} = \hat{X}_i^{0\sigma} \hat{X}_i^{\sigma 0} \tag{58}$$

at a given lattice site, i.e. if $\hat{X}_i^{00} \mid 0 \rangle = 1 \mid 0 \rangle$ the i-th site is empty - there is one hole on it, while for $\hat{X}_i^{00} \mid 1 \rangle = 0 \mid 1 \rangle$ it is occupied by an "electron" and there is no hole. They fulfill the non-canonical commutation relations

$$\left[\hat{X}_i^{\alpha\beta}, \hat{X}_j^{\gamma\lambda} \right]_\pm = \delta_{ij} \left[\delta_{\gamma\beta} \hat{X}_i^{\alpha\lambda} \pm \delta_{\alpha\lambda} \hat{X}_i^{\gamma\beta} \right]. \tag{59}$$

Here, $\alpha, \beta, \gamma, \lambda = 0, \sigma$ and δ_{ij} is the Kronecker symbol. The (anti)commutation relations in Eq.(59) are rather different from the canonical Fermi and Bose (anti)commutation relations.

Since $U \to \infty$ the doubly occupancy is excluded, i.e. $\hat{n}_{i\uparrow} \hat{n}_{i\downarrow} \mid \psi \rangle (= \hat{X}_i^{22} \mid \uparrow \downarrow \rangle) = 0$, and by construction the $\hat{X}$ operators satisfy the *local constraint* (the completeness relation)

$$\hat{C}_X(i) \equiv \hat{X}_i^{00} + \sum_{\sigma=1}^{N} \hat{X}_i^{\sigma\sigma} = 1. \tag{60}$$

This condition tells us that at a given lattice site there is either one hole ($\hat{X}_i^{00} \, | \, hole \rangle = 1 \, | \, hole \rangle$) ore one electron ($\hat{X}_i^{\sigma\sigma} \, | \, elec \rangle = 1 \, | \, elec \rangle$). Note, if Eq.(60) is obeyed then both commutation and anticommutation relations hold also in Eq.(59) at the same lattice site, which is due to the projection properties of the Hubbard operators $\hat{X}^{\alpha\beta}\hat{X}^{\gamma\mu} = \delta_{\beta\gamma}\hat{X}^{\alpha\mu}$.

For further purposes, i.e. for the study of low-energy excitations in a controllable way, the number of spin projections is *generalized* to be N , i.e. $\sigma = 1, 2, ...N$. This way of generalization was very useful in describing heavy fermion physics, where for some Ce compounds N means the number of projections of the total angular momentum, for instance when $j = 5/2$ then $N = 2j + 1 = 6$ ($N \gg 1$). For some Yb compounds one has $j = 7/2$, i.e. $N = 2j + 1 = 8$ ($N \gg 1$). By projecting out the doubly occupied (high energy) states from the Hamiltonian in Eq.(55) one obtains the generalized $t - J$ model. The details of this derivation are given in Appendix and here we give the final expression for the Hamiltonian which excludes the doubly occupancy

$$\hat{H} = \hat{H}_t + \hat{H}_J = -\sum_{i,j,\sigma} t_{ij}\hat{X}_i^{\sigma 0}\hat{X}_j^{0\sigma} + \sum_{i,j,} J_{ij}(\mathbf{S}_i \cdot \mathbf{S}_j - \frac{1}{4}\hat{n}_i\hat{n}_j) + \hat{H}_3. \tag{61}$$

The first term describes the hopping of the "electron" by taking into account that the doubly occupancy of sites are excluded. The second term describes the Heisenberg-like exchange energy of almost localized "electrons". $\hat{H}_3$ contains three-sites hopping which is usually omitted believing it is not important. For effects related to charge fluctuation processes it is plausible to omit it, while for spin-fluctuation processes it may be questionable approximation. The spin and number operators can be expressed via the Hubbard operators [125]

$$\mathbf{S} = \hat{X}_i^{\bar{\sigma}_1 0}(\vec{\sigma})_{\bar{\sigma}_1\bar{\sigma}_2}\hat{X}_i^{0\bar{\sigma}_2}; \; \hat{n}_i = \hat{X}_i^{\bar{\sigma}\bar{\sigma}} \tag{62}$$

where summation over bar indices is understood.

The basic idea behind the *X-method* is that the Dyson's equation for the electron Green's function can be effectively obtained by introducing *external potentials* (sources) $u^{\sigma_1\sigma_2}(1)$. The source Hamiltonian $\hat{H}_s$ is used in the form

$$\int \hat{H}_s \, d\tau = \int \sum_{\sigma_1,\sigma_2} u^{\sigma_1\sigma_2}(1)\hat{X}^{\sigma_1\sigma_2}(1)\, d1 \equiv u^{\bar{\sigma}_1\bar{\sigma}_2}(\bar{1})\hat{X}^{\bar{\sigma}_1\bar{\sigma}_2}(\bar{1}) , \tag{63}$$

where $1 \equiv (\mathbf{l}, \tau)$ and $\int(..)d1 \equiv \int(..)d\tau\sum_{\mathbf{l}}$ and τ is the Matsubara time. Here and in the following, integration over bar variables($\bar{1}, \bar{2}..$) and a summation over bar spin variables($\bar{\sigma}..$) is understood. The sources $u^{\sigma_1\sigma_2}(1)$ are useful in generating higher correlation functions entering the self-energy. The electronic Green's function is defined by [2] ($\hat{T}$ is the time-ordering operator)

$$G^{\sigma_1\sigma_2}(1,2) = \frac{-\langle \hat{T}\left(\hat{S}\hat{X}^{0\sigma_1}(1)\hat{X}^{\sigma_2 0}(2)\right)\rangle}{\langle \hat{T}\hat{S}\rangle}, \tag{64}$$

where $\hat{S} = \hat{T}\exp\{-\int \hat{H}_s(1)d1\}$ and the corresponding Dyson's equation reads

$$\left[G_{0,u}^{-1,\sigma_1\bar{\sigma}_2}(1,\bar{2}) - \Sigma_G^{\sigma_1\bar{\sigma}_2}(1,\bar{2})\right]G^{\bar{\sigma}_2\sigma_2}(\bar{2},2) = Q^{\sigma_1\sigma_2}(1)\delta(1-2), \tag{65}$$

$$G_{0,u}^{-1,\sigma_1\sigma_2}(1,2) = (-\frac{\partial}{\partial t_1})\delta^{\sigma_1\sigma_2}\delta(1-2) - u^{\sigma_1\sigma_2}(1)\delta(1-2) \tag{66}$$

The so called Hubbard spectral weight is given by

$$Q^{\sigma_1\sigma_2}(1) = \delta^{\sigma_1\sigma_2}\langle\hat{X}^{00}(1)\rangle + \langle\hat{X}^{\sigma_1\sigma_2}(1)\rangle. \tag{67}$$

$\Sigma_G^{\sigma_1\sigma_2}(1,2)$ is a functional of the Green's function $G^{\sigma_1\sigma_2}(1,2)$. The latter describes the *composite* (correlated) particle (in the language of the *SB* theory it describes the combined "spinon + holon"). For further analysis it is useful to introduce the quasiparticle Green's $g^{\sigma_1\sigma_2}$ (something analogous to the "spinon" Green's function in the *SB* approach) and the vertex functions $\gamma_{\sigma_3\sigma_4}^{\sigma_1\sigma_2}(1,2;3)$, respectively

$$g^{\sigma_1\sigma_2}(1,2) = G^{\sigma_1\bar{\sigma_2}}(1,2)Q^{-1,\bar{\sigma_2}\sigma_2}(2) \tag{68}$$

$$\gamma_{\sigma_3\sigma_4}^{\sigma_1\sigma_2}(1,2;3) = -\frac{\delta g^{-1,\sigma_1\sigma_2}(1,2)}{\delta u^{\sigma_3\sigma_4}(3)}, \tag{69}$$

respectively. Note, that $\gamma_{\sigma_3\sigma_4}^{\sigma_1\sigma_2}(1,2;3)$ are the *three-point vertex function*, which also renormalizes the ionic EPI coupling constant - as we shall see below. $g^{\sigma_1\sigma_2}(1,2)$ is the solution of the equation

$$\left[G_{0,u}^{-1,\sigma_1\bar{\sigma_2}}(1,\bar{2}) - \Sigma_g^{\sigma_1\bar{\sigma_2}}(1,\bar{2})\right]g^{\bar{\sigma_2}\sigma_2}(\bar{2},2) = \delta^{\sigma_1\sigma_2}\delta(1-2), \tag{70}$$

where $\Sigma_g^{\sigma_1\sigma_2}(1,2)$ depends on the "quasiparticle" Green's function $g^{\sigma_1\sigma_2}(1,2)$. Note, that in Eq.(70) the Hubbard spectral weight $Q^{\sigma\sigma}$ disappears from the right hand side.

Since in the following we study *nonmagnetic (paramagnetic) normal state* one has $\Sigma_g^{\sigma\sigma}(1,2) \equiv \Sigma_g(1,2)$ for $\sigma = 1,..N$, as well as $Q^{\sigma\sigma}(\equiv Q)$. In [17], [18], [19], [20] it is shown that in that case Σ_g can be expressed via two vertex functions - the *charge vertex*

$$\gamma_c(1,2;3) \equiv \gamma_{\sigma\sigma}^{\sigma\sigma}(1,2;3) \tag{71}$$

and the *spin vertex*

$$\gamma_s(1,2;3) \equiv \gamma_{\sigma\sigma}^{\bar{\sigma}\sigma}(1,2;3), \tag{72}$$

i.e. Σ_g is given by

$$\Sigma_g(1-2) = -\frac{t_0(1-2)}{N}Q(1) + \delta(1-2)\frac{J_0(1-\bar{1})}{N} < \hat{X}^{\sigma\sigma}(\bar{1}) > -$$

$$-\frac{t_0(1-\bar{1})}{N}g(\bar{1}-\bar{2})\gamma_c(\bar{2},2;1)+$$

$$+\frac{t_2(1,\bar{1},\bar{3})}{N}g(\bar{1}-\bar{2})\gamma_s(\bar{2},2;\bar{3}) + \Sigma_Q(1-2), \tag{73}$$

where $t_2(1,2,3) = \delta(1-2)t_0(1-3) - \delta(1-3)J_0(1-2)$. The notation $t_0(1-2)$ (and $J_0(1-2)$) means $t_0(1-2) = t_{0,i_1j_2}\delta(\tau_1 - \tau_2)$. The first two terms in Eq.(73) represent an effective kinetic energy of quasiparticles in the lower Hubbard band. As we shall

see below they give rise to the band narrowing and to the shift of the band center, respectively. The third and fourth terms describe the kinematic and dynamic interaction of quasiparticles with charge and spin fluctuations, respectively, while the very important term proportional to $\Sigma_Q(1,2)$ takes into account the counterflow of surrounding quasiparticles which takes place in order to respect the local constraint (absence of doubly occupancy). It reads

$$\Sigma_Q(1,2) = \frac{t_0(1-\bar{1})}{N}\frac{g(\bar{1}-\bar{2})}{Q}\left[\frac{\delta Q(\bar{2})}{\delta u^{\bar{\sigma}\bar{\sigma}}(1)} - \frac{\delta Q^{\bar{\sigma}\sigma}(\bar{2})}{\delta u^{\bar{\sigma}\sigma}(1)}\right]g^{-1}(\bar{2}-2).$$

Σ depends on the vertex functions $\gamma_c(1,2;3)$ and $\gamma_s(1,2;3)$ and it does not contain a small expansion parameter, like the interaction energy in weakly interacting systems, because the hopping parameter t describes at the same time the kinetic energy and *kinematic interaction* of quasiparticles. This means that there is no controllable perturbation technique, due to the lack of small parameter. There are various decoupling procedures and mean-field like techniques - the path integral method, or $1/N$ expansion in various slave-boson approaches [2].

What is the advantage of the *X-method* expressed by Eq.(68-73). It turns out that it allows to formulate a controllable $1/N$ expansion for Σ_g by including also the EPI [17], [18], [19], [20] - see below. For that purpose it is necessary to generalize the *local constraint* condition

$$\hat{C}_{X_N}(i) \equiv \hat{X}_i^{00} + \sum_{\sigma=1}^{N}\hat{X}_i^{\sigma\sigma} = \frac{N}{2}, \tag{74}$$

where $N/2$ replace the unity in Eq.(60). It is apparent from Eq.(60) that for $N = 2$ it coincides with Eq.(60) and has the meaning that maximally half of all spin states at a given lattice site can be occupied.

The spectral function $A(\mathbf{k},\omega) = -\mathrm{Im}G(\mathbf{k},\omega)/\pi$ must obey the generalized Hubbard sum rule which respects the new local constraint in Eq.(74).

$$\int d\omega A(\mathbf{k},\omega) = \frac{1 + (N-1)\delta}{2} \tag{75}$$

The $N > 2$ generalization of the local constraint allows us to make a *controllable $1/N$ expansion* of the self-energy with respect to the small quantity $1/N$ (when $N \gg 1$). Physically this procedure means that we select a *class of diagrams* in the self-energy and response functions which might be important in some parameter regime. By careful inspection of Eq.(73) one concludes that for large N there is $1/N$ expansion for various quantities - for instance

$$g = g_0 + \frac{g_1}{N} + ...; Q = Nq_0 + Q_1 + ..., \tag{76}$$

$$\Sigma_g = \Sigma_0 + \frac{\Sigma_1}{N} + ...; \gamma_c = \gamma_{c0} + \frac{\gamma_{c1}}{N} + ..., \tag{77}$$

$$\gamma_s(1,2;3) = N\delta(1-2)\delta(1-3) + \gamma_{s1} + ...$$

As a result of this expansion one obtains Σ_0 and g_0 in *leading O(1)-order* - see details in [2], [17], [18], [19], [20] (Σ_Q in Eq.(73) is of O(1/N) order)

$$g_0(\mathbf{k}, \omega) \equiv \frac{G_0(\mathbf{k}, \omega)}{Q_0} = \frac{1}{\omega - [\varepsilon_0(\mathbf{k}) - \mu]}, \qquad (78)$$

where the *quasiparticle energy* $\varepsilon_0(\mathbf{k}) = \varepsilon_c - q_0 t_0(\mathbf{k}) - \sum_{\mathbf{p}} J_0(\mathbf{k} + \mathbf{p}) n_F(\mathbf{p})$, and the *level shift* $\varepsilon_c = \sum_{\mathbf{p}} t_0(\mathbf{p}) n_F(\mathbf{p})$. Here, $t_0(\mathbf{k})$ and $J_0(\mathbf{k})$ are Fourier transforms of $t_{0,ij}$ and $J_{0,ij}$, respectively. For $t' = 0$ one has $t_0(\mathbf{k}) = 2t_0(\cos k_x + \cos k_y)$ and $J_0(\mathbf{k}) = 2J_0(\cos k_x + \cos k_y)$. In the equilibrium state ($u^{\sigma_1 \sigma_2} \to 0$) and in leading order one has

$$Q_0 = < \hat{X}_i^{00} > = N q_0 = N \delta / 2. \qquad (79)$$

The chemical potential μ is obtained from the condition

$$1 - \delta = 2 \sum_{\mathbf{p}} n_F(\mathbf{p}). \qquad (80)$$

Let us summarize the main results which were obtained by the *X-method* in leading $O(1)$-order and compare these results with corresponding results of the *SB*-method [17], [18], [19], [20]: (**1**) In the $O(1)$ order the Green's function $g_0(\mathbf{k}, \omega)$ describes the *coherent motion* of quasiparticles whose contribution to the total spectral weight of the Green's function $G_0(\mathbf{k}, \omega)$ is $Q_0 = N\delta/2$. Note, $G_0(\mathbf{k}, \omega) = Q_0 g_0(\mathbf{k}, \omega)$ in leading order. The dispersion of the quasiparticle energy is dominated by the exchange parameter if $J_0 > \delta t_0$. In the case when $J_0 = 0$ there is a band narrowing by lowering the hole doping δ, where the band width is proportional to the hole concentration δ, i.e. $W = z \cdot \delta \cdot t_0$. (**2**) The X-method respects the local constraint at each lattice site and in each step of calculations. (**3**) In the important paper [126] - which is based on the theory elaborated in [17], [18], [19], [20], it is shown that in the superconducting state the anomalous self-energy (which is of $O(1/N)$-order in the $1/N$ expansion) of the *X*- and *SB*-methods *differ* substantially. As a consequence, the *SB*-method [127] predicts false superconductivity in the $t - J$ model (for $J = 0$) with large T_c (due to the kinematical interaction), while the X-method gives extremely small $T_c(\approx 0)$ [126]. The reason for this discrepancy between the two methods is that calculations done in the *SB*-method miss a class of compensating diagrams, which are on the other hand taken automatically in the X-method. So, although the two approaches yield some similar results in leading $O(1)$-order their implementation in the next leading $O(1/N)$-order make that they are different. Note, that the $1/N$ expansion in the X-method is well-defined and transparent. (**4**) By explicit calculation and comparison of the two methods in [18] it is shown that the renormalization of the EPI coupling constant is different in the two approaches even in the large N-limit - see below; (**5**) Very interesting behavior as a function of doping concentration exhibits the optical conductivity $\sigma(\omega, \mathbf{q} = 0) \equiv \sigma(\omega)$ which scales with the doping δ. Note, the volume below the Fermi surface in the case of strong correlations scales with $n = 1 - \delta$, like in the usual Fermi liquid. The above analysis clearly demonstrate shows difference in response functions of strongly correlated systems and the canonical Landau-Fermi liquid.

4.2. Forward scattering peak in the charge vertex γ_c

The three-point *charge vertex* $\gamma_c(1,2;3)$ plays important role in the renormalization all charge processes, such as the EPI, Coulomb scattering and the scattering on non-magnetic impurities. It was shown in [17], [18], [19], [20], [2] that $\gamma_c(1,2;3)$ can be calculated exactly in the leading $O(1)$ order (and in all other orders) of the $t-J$ model. The integral equation in the $O(1)$ order reads

$$\gamma(1,2;3) = \delta(1-2)\delta(1-3) + t(1-2)g_0(1,\bar{1})g_0(\bar{2},1^+)\gamma(\bar{1},\bar{2};3)$$

$$+\delta(1-2)t(1-\bar{1})g_0(\bar{1},\bar{2}))g_0(\bar{3},1)\gamma(\bar{2},\bar{3};3$$

$$-J(1-2)g_0(1,\bar{1}))g_0(\bar{2},2)\gamma(\bar{1},\bar{2};3. \tag{81}$$

The analytical solution of Eq.(81) is given by [2], [20]

$$\gamma_c(\mathbf{k},q) = 1 - \sum_{\alpha=1}^{6} \sum_{\beta=1}^{6} F_\alpha(\mathbf{k})[\hat{1}+\hat{\chi}(q)]_{\alpha\beta}^{-1}\chi_{\beta 2}(q), \tag{82}$$

where

$$\chi_{\alpha\beta}(q) = \sum_p G_\alpha(p,q)F_\beta(\mathbf{p}), \tag{83}$$

$$G_\alpha(p,q) = [1, t(\mathbf{p}+\mathbf{q}), \cos p_x, \sin p_x, \cos p_y, \sin p_y]\Pi(p,q),$$

$$F_\alpha(\mathbf{k}) = [t(\mathbf{k}), 1, 2J_0\cos k_x, 2J_0\sin k_x, 2J_0\cos k_y, 2J_0\sin k_y],$$

where $\Pi(k,q) = -g(k)g(k+q)$ and $q = (\mathbf{q}, iq_n)$, $q_n = 2\pi nT$, $p = (\mathbf{p}, ip_m)$, $p_m = \pi T(2m+1)$. Note, the frequency sum over p_m in $\chi_{\alpha\beta}(q)$ in Eq.(82) involves only Π and can easily be carried out $\sum_{p_m} \Pi(p,q) = [n_F(\xi_{\mathbf{q}+\mathbf{p}}) - n_F(\xi_{\mathbf{p}})]/[\xi_{\mathbf{p}} - \xi_{\mathbf{q}+\mathbf{p}} - iq_n]$.

We stress that $\gamma_c(\mathbf{k},q)$ describes a specific screening of the charge potential due to of strong correlations. In the presence of perturbation (external source u) there is change of the band width, as well as of the local chemical potential, which comes from the suppression of doubly occupancy. The central result of the X-method is that for momenta $\mathbf{k}$ laying at (and near) the Fermi surface $\gamma_{c0}(\mathbf{k}, \mathbf{q}, \omega = 0)$ has very pronounced *forward scattering peak* at $\mathbf{q} = 0$) at low doping concentration $\delta(\ll 1)$, while the backward scattering is substantially suppressed - see Fig. 17. The latter means that charge fluctuations are strongly suppressed (correlated) at small distances. Such a behavior of the vertex function means that a quasiparticle moving in the strongly correlated medium digs up a *giant correlation hole* with the radius $\xi_{ch} \approx a/\delta$, where a is the lattice constant - see Fig. 16.

However, in the highly doped systems with $\delta > 0.1$ - which corresponds to the overdoped HTSC oxides, the effects of strong correlations is progressively suppressed and the screening mechanism due to strong correlations is less effective. We stress that when $J < t$ then the last term in Eq.(81) for $\gamma_{c0}(\mathbf{k}_F, \mathbf{q})$ is unimportant. On the other hand both terms, the second (due to band narrowing) and the third (due band shifting) one, are in conjunction responsible for the development of the forward scattering peak at lower doping. If we omit in Eq.(81) the band shifting term (the third one) we get very
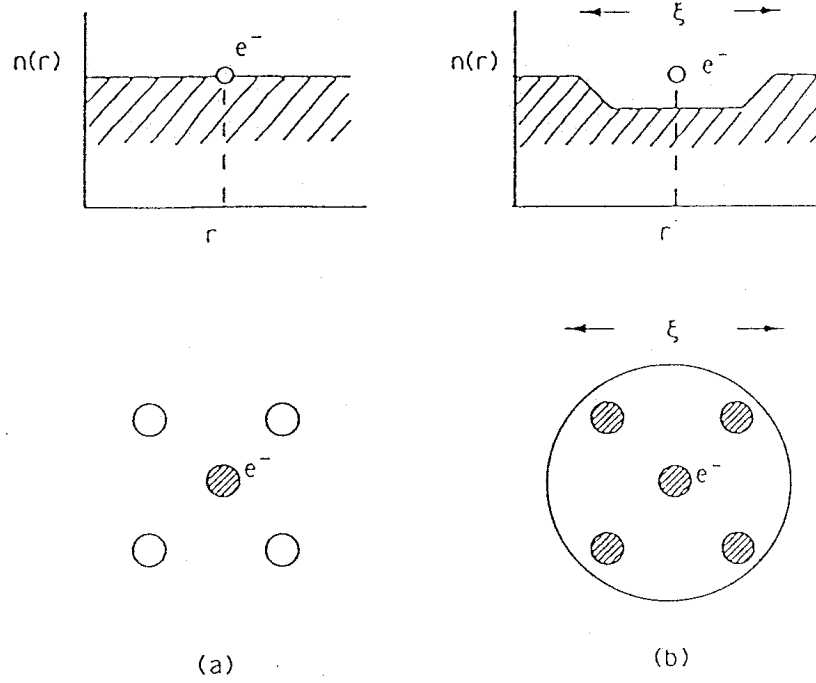
FIGURE 16. Schematic picture of electron correlation hole and the $E - P$ interaction for uncorrelated (weakly correlated) (a) and strongly correlated (b) electron. In the case (a) the electron does not perturb the electronic density $n(r)$ and it interacts with the vibrations of a single atom (shaded). In the case (b) an electron is accompanied by a large correlation hole of size $\xi \sim 1/\delta$ (δ is doping) and it will interact with atoms within this zone. From [120].

weak forward scattering peak, while omitting the band narrowing term (the first one) $\gamma_{c0}(\mathbf{k}_F, \mathbf{q})$ is practically constant in a broad region of $\mathbf{q}$.

Finally, since the real physics is characterized by $N = 2$ one can put the question - what is the *reliability* of the results for the quasiparticle properties obtained by the $1/N$ expansion (and $N \to \infty$) within the X-method? First, the exact diagonalization of the charge correlation function $N(\mathbf{k}, \omega)$ in the $t - J$ model [124] shows clearly that the low-energy charge scattering processes at large momenta $\mid \mathbf{k} \mid \approx 2k_F$ are strongly suppressed compared to the small transferred momenta ($\mid \mathbf{k} \mid \ll 2k_F$). These calculations confirm unambiguously the results obtained by the X-method in [17], [18], [19] on the suppression of the backward scattering in the vertex. Second, very recent Monte Carlo (numerical) calculations in the Hubbard model with finite U [21] show clear development of the forward scattering peak in $\gamma_c(\mathbf{k}_F, \mathbf{q})$ by increasing U, thus confirming the theoretical predictions in [17], [18], [19].
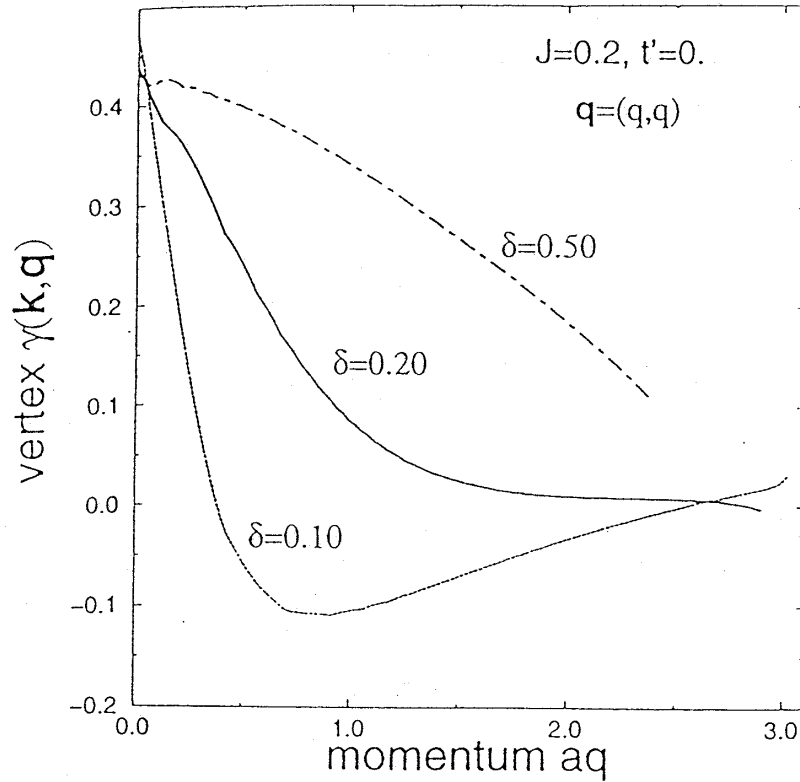
FIGURE 17. Zero-frequency vertex function $\gamma(\mathbf{k}_F, \mathbf{q})$ of the $t-J$ model as a function of the momentum aq with $\mathbf{q} = (q, q)$ for three different doping δ - from [19].

5. RENORMALIZATION OF THE EPI BY STRONG CORRELATIONS

In preceding Sections arguments we argued that because $\lambda_{tr} \ll \lambda$ the standard Migdal-Eliashberg EPI theory must be corrected in order to take into account screening properties of strongly correlated system. This analysis is done in the framework of the X-method in a series of papers [17], [18], [19] which we briefly discuss below. The renormalization of the EPI by strong correlations has been studied also by the *SB*-method [128], [121], [129], [130] by the $1/N$ expansion in the partition function, or by using the mean-field approach [131] where also the non-Migdal correction due to the EPI is considered. We stress that at present there are no systematic and controllable calculations within the *SB*-method for the EPI. From that point of view the *X*-method is of indispensable value.

5.1. The forward scattering peak in the EPI

The minimal model Hamiltonian for the HTSC oxides contains besides the $t-J$ terms also the EPI, i.e. $\hat{H} = \hat{H}_{tJ} + \hat{H}_{EP}$ where $\hat{H}_{EP} = \hat{H}_{EP}^{ion} + \hat{H}_{EP}^{cov}$

$$\hat{H} = -\sum_{i,j,\sigma} t_{ij}\hat{X}_i^{\sigma 0}\hat{X}_j^{0\sigma} + \sum_{i,j,}J_{ij}(\mathbf{S}_i\cdot\mathbf{S}_j - \frac{1}{4}n_i n_j) +$$

$$+\sum_{i,\sigma}\varepsilon_{a,i}^0\hat{X}_i^{\sigma\sigma} + \hat{H}_{ph} + \hat{H}_{EP} + \hat{V}_{LC}, \qquad (84)$$

where the ionic contribution to the EPI is

$$\hat{H}_{EP}^{ion} = \sum_{i,\sigma}\hat{\mathbf{\Phi}}_i(\hat{X}_i^{\sigma\sigma} - \langle\hat{X}_i^{\sigma\sigma}\rangle) + \hat{H}_{EP}^{cov}. \qquad (85)$$

Here, $\hat{\mathbf{\Phi}}_i$ (given by Eq.(40)) describes the change of the atomic energy $\varepsilon_{a,i}^0$ due to the long-range Madelung energy, where L and κ enumerate unit lattice vectors and atoms in the unit cell, respectively. $Z_{L\kappa}$ is the effective charge of an ion at the site $L\kappa$. Note, in Eq.(85) we do not assume small displacement $\hat{\mathbf{u}}_i$ and the following analysis holds in principle also for an *anharmonic* EPI. The term proportional to $\langle\hat{X}_i^{\sigma\sigma}\rangle$ in Eq.(85) is introduced in order to have $\langle\hat{\mathbf{\Phi}}_i\rangle = 0$ in the equilibrium state. Note, that there is also covalent contribution to the *EPI* in Eq.(84) due to the change of the hopping (t) and exchange energy (J) by the ion displacements

$$\hat{H}_{EP}^{cov} = -\sum_{i,j,\sigma}\frac{\partial t_{ij}}{\partial(\mathbf{R}_i^0 - \mathbf{R}_j^0)}(\hat{\mathbf{u}}_i - \hat{\mathbf{u}}_j)\hat{X}_i^{\sigma 0}\hat{X}_j^{0\sigma} +$$

$$+\sum_{i,j,}\frac{\partial J_{ij}}{\partial(\mathbf{R}_i^0 - \mathbf{R}_j^0)}(\hat{\mathbf{u}}_i - \hat{\mathbf{u}}_j)\mathbf{S}_i\cdot\mathbf{S}_j. \qquad (86)$$

The treatment of the first term is similar to the Madelung term in Eq.(85) although the equation for the *four-point vertex function* $\gamma_c(1,2;3,4)$ is different than Eq.(86). We stress, that the X-method has advantage also in the treatment of the covalent term, because it peaks up straightforwardly all important contributions in γ_c, due to strong correlations. On the other side the corresponding treatment by the *SB* method is complicated and not well defined, giving sometimes wrong results. For instance, in [121] several terms in the vertex equation are omitted leading to incorrect results for the covalent EPI coupling. We stress, that the covalent part contributes approximately $20-30$ K to the critical temperature in HTSC oxides as the band structure calculations in [114], [115] have shown (partly discussed in Section 3.). Its renormalization by strong correlations will be studied elsewhere. The second term in $\hat{H}_{EP}^{cov}$ is due to the change of the exchange energy by phonon vibrations. Since it is second order with respect to t_{ij} it is much smaller than the first covalent term and accordingly contributes very little to the total EPI.

After technically lengthy calculations, which are performed in [17], [18] the expression for the ionic part of the EPI (frequency-dependent) part of the self-energy reads

$$\Sigma_{EP}^{(dyn)}(1,2) = -V_{EP}(\bar{1}-\bar{2})\gamma_c(1,\bar{3};\bar{1})g_0(\bar{3}-\bar{4})\gamma_c(\bar{4},2;\bar{2}), \tag{87}$$

where analogously to Eq.(47) one has $V_{EP}(1-2) = \varepsilon_e^{-1}(1-\bar{1})V_{EP}^0(\bar{1}-\bar{2})\varepsilon_e^{-1}(\bar{2}-2)$. The propagator of the bare EPI $V_{EP}^0(1-2) = -\langle T\hat{\Phi}(1)\hat{\Phi}(2)\rangle$ comprises in principle also the anharmonic contribution. From Eq.(87) it is seen that in strongly correlated systems the ionic part of the EPI is proportional to the square of the *three-point charge vertex* $\gamma_c(1,2;3)$ (due to correlations). The self-energy is given by

$$\Sigma_{EP}^{(dyn)}(\mathbf{k},\omega) = \int_0^\infty d\Omega \langle \alpha^2 F(\mathbf{k},\mathbf{k}',\Omega)\rangle_{\mathbf{k}'} R(\omega,\Omega), \tag{88}$$

where $R(\omega,\Omega)$ is given in [2], [17], [18]. The (momentum-dependent) Eliashberg spectral function is defined by

$$\alpha^2 F(\mathbf{k},\mathbf{k}',\omega) = N_{sc}(0)\sum_\nu \mid g_{eff}(\mathbf{k},\mathbf{k}-\mathbf{k}',\nu) \mid^2 \times$$

$$\times \delta(\omega - \omega_\nu(\mathbf{k}-\mathbf{k}'))\gamma_c^2(\mathbf{k},\mathbf{k}-\mathbf{k}'). \tag{89}$$

$n_B(\Omega)$ is the Bose distribution function and ψ is di-gamma function, while $g_{eff}(\mathbf{k},\mathbf{p},\nu)$ is the EPI coupling constant for the ν-the mode, where the renormalization by long-range Coulomb interaction is included, i.e. $g_{eff}(\mathbf{k},\mathbf{p},\nu) = g(\mathbf{k},\mathbf{p},\nu)/\varepsilon_e(\mathbf{p})$. $N_{sc}(0)$ is the density of states renormalized by strong correlations where $N_{sc}(0) = N_0(0)/q_0$ and $q_0 = \delta/2$ in the $t-t'$ model ($J=0$). In the $t-J$ model $N_{sc}(0)$ has another form which does not diverge for $\delta \to 0$ but one has $N_{sc}(0)(\sim 1/J_0) > N_0(0)$, where the bare density of states $N_0(0)$ is calculated, for instance by the *LDA* scheme.

5.2. Pairing and transport EPI coupling constants

Depending on the symmetry of the superconducting order parameter $\Delta(\mathbf{k},\omega)$ ($s-$, $d-wave$ pairing) various averages (over the Fermi surface) of $\alpha^2 F(\mathbf{k},\mathbf{k}',\omega)$ enter the Eliashberg equations. Assuming that the superconducting order parameter transforms according to the representation Γ_i ($i=1,3,5$) of the point group C_{4v} of the square lattice (in the CuO_2 planes) the appropriate symmetry-projected spectral function is given by

$$\alpha^2 F_i(\tilde{\mathbf{k}},\tilde{\mathbf{k}}',\omega) = \frac{N_{sc}(0)}{8}\sum_{\nu,j} \mid g_{eff}(\tilde{\mathbf{k}},\tilde{\mathbf{k}}-T_j\tilde{\mathbf{k}}',\nu) \mid^2 \times$$

$$\times \delta(\omega - \omega_\nu(\tilde{\mathbf{k}}-T_j\tilde{\mathbf{k}}')) \mid \gamma_c(\tilde{\mathbf{k}},\tilde{\mathbf{k}}-T_j\tilde{\mathbf{k}}') \mid^2 D_i(j). \tag{90}$$

$\tilde{\mathbf{k}}$ and $\tilde{\mathbf{k}}'$ are momenta on the Fermi line in the irreducible Brillouin zone which is $1/8$ of the total Brillouin zone. T_j, $j=1,..8$, denotes the eight point-group transformations forming the symmetry group of the square lattice. This group has five irreducible

representations which we distinguish by the label $i = 1, 2, ...5$. In the following the representations $i = 1$ and $i = 3$, which correspond to the $s-$ and $d - wave$ symmetry of the full rotation group, respectively, will be of importance. $D_i(j)$ is the representation matrix of the $j - th$ transformation for the representation i. By assuming that the superconducting order parameter $\Delta(\mathbf{k}, \omega)$ does not vary much in the irreducible Brillouin zone one can average over $\tilde{\mathbf{k}}$ and $\tilde{\mathbf{k}}'$ in the Brillouin zone. For each symmetry one obtains the corresponding spectral function $\alpha^2 F_i(\omega)$

$$\alpha^2 F_i(\omega) = \langle\langle \alpha^2 F_i(\tilde{\mathbf{k}}, \tilde{\mathbf{k}}', \omega)\rangle_{\tilde{\mathbf{k}}}\rangle_{\tilde{\mathbf{k}}'} \tag{91}$$

which (in the first approximation determines) the transition temperature for the order parameter with the symmetry Γ_i. In the case $i = 3$ the electron-phonon spectral function $\alpha^2 F_3(\omega)$ in the *d-channel* is responsible for $d - wave$ superconductivity represented by the irreducible representation Γ_3 (or sometimes labelled as B_{1g}).

Performing similar calculations (as above) for the phonon-limited resistivity one finds that the latter is related to the *transport spectral function $\alpha^2 F_{tr}(\omega)$* which is given by

$$\alpha^2 F_{tr}(\omega) = \frac{\langle\langle \alpha^2 F(\mathbf{k}, \mathbf{k}', \omega)[\mathbf{v}(\mathbf{k}) - \mathbf{v}(\mathbf{k}')]^2\rangle_{\mathbf{k}}\rangle_{\mathbf{k}'}}{2\langle\langle \mathbf{v}^2(\mathbf{k})\rangle_{\mathbf{k}}\rangle_{\mathbf{k}'}}. \tag{92}$$

$\mathbf{v}(\mathbf{k})$ is the Fermi velocity. The effect of strong correlations on the EPI was discussed in [17] and more extensively in [18] within the model where the phonon frequencies $\omega(\tilde{\mathbf{k}} - \tilde{\mathbf{k}}')$ and $g_{eff}(\mathbf{k}, \mathbf{p}, \lambda)$ are weakly momentum dependent - due to the long-range screening (RPA). In order to illustrate the effect of strong correlations on $\alpha^2 F_i(\omega)$ we consider the latter functions at zero frequency ($\omega = 0$) which are then reduced to the (so called) "enhancement" functions

$$\Lambda_i = \frac{1}{8} \frac{N_{sc}(0)}{N_0(0)} \sum_{j=1}^{8} \langle\langle | \gamma_c(\tilde{\mathbf{k}}, \tilde{\mathbf{k}} - T_j\tilde{\mathbf{k}}') |^2\rangle_{\tilde{\mathbf{k}}}\rangle_{\tilde{\mathbf{k}}'} D_i(j) \tag{93}$$

Note, in the case $J = 0$ one has $N_{sc}(0)/N_0(0) = q_0^{-1}$, where q_0 is related to the doping concentration, i.e. $q_0 = \delta/2$. Similarly, the correlation effects in the resistivity $\rho(T)(\sim \Lambda_{tr})$ renormalize the transport coupling constant Λ_{tr})

$$\Lambda_{tr} = \frac{N_{sc}(0)}{N_0(0)} \frac{\langle\langle | \gamma_c(\tilde{\mathbf{k}}, \tilde{\mathbf{k}} - T_j\tilde{\mathbf{k}}') |^2 [\mathbf{v}(\mathbf{k}) - \mathbf{v}(\mathbf{k}')]^2\rangle_{\mathbf{k}}\rangle_{\mathbf{k}'}}{2\langle\langle \mathbf{v}^2(\mathbf{k})\rangle_{\mathbf{k}}\rangle_{\mathbf{k}'}} \tag{94}$$

Note, that for quasiparticles with the isotropic band the absence of correlations implies that $\Lambda_1 = \Lambda_{tr} = 1$, $\Lambda_i = 0$ for $i > 1$.

The averages in Λ_1, Λ_3 and Λ_{tr} were performed numerically in [18] by using the realistic anisotropic band dispersion in the $t - t' - J$ model and the corresponding charge vertex. The results for Λ_1, Λ_3 and Λ_{tr} are shown in Fig. 18 as functions of doping concentration in the t and $t - t'$ and $t - t' - J$ models, respectively. The three curves are multiplied with a common factor so that Λ_1 approaches 1 in the empty-band limit $\delta \to 1$, when strong correlations are absent. Note, that T_c in the weak coupling limit and
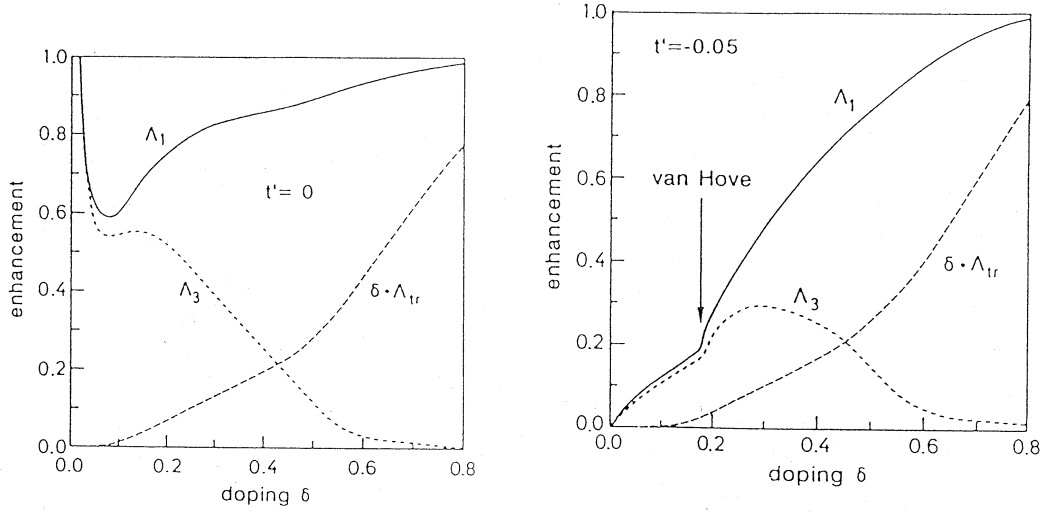
FIGURE 18. **(a)** - Enhancements Λ_1 and Λ_3 and $\delta \cdot \Lambda_{tr}$ as a function of doping δ for $t' = 0$ and $J = 0$ - from [18]. **(b)** Enhancements Λ_1 and Λ_3 and $\delta \cdot \Lambda_{tr}$ as a function of doping δ for $t' = -0.05$ and $J = 0$ - from [18].

in the $i - th$ channel scales like

$$T_c^{(i)} \approx \langle \omega \rangle \exp(-1/(\Lambda_i - \mu_i^*)), \tag{95}$$

where μ_i^* is the Coulomb pseudopotential in the i-th channel and $\langle \omega \rangle$ averaged phonon frequency.

Several interesting results, which are seen in Fig. 18, should be stressed.

First, in the empty-band limit $\delta \to 1$ the $d - wave$ coupling constant Λ_3 is much smaller than the $s - wave$ coupling constant Λ_1, i.e. $\Lambda_3 \ll \Lambda_1$. Furthermore, the totally symmetric function Λ_1 decreases with decreasing doping.

Second, in both models Λ_1 and Λ_3 meet each other (note $\Lambda_1 > \Lambda_3$ for all δ) at some small doping $\delta \approx 0.1 - 0.2$ where $\Lambda_1 \approx \Lambda_3$ but still $\Lambda_1 > \Lambda_3$. By taking into account a residual Coulomb repulsion of quasiparticles with $\mu_d^* \ll \mu_s^*$ one gets that the $s - wave$ superconductivity (which is governed by the coupling constant Λ_1) is suppressed, while the $d - wave$ superconductivity (governed by Λ_3) is only weakly affected. In that case the $d - wave$ superconductivity due to the EPI becomes more stable than the $s - wave$ superconductivity at sufficiently small doping δ, i.e. $T_c^{(d)} > T_c^{(s)}$. Experimentally, this occurs in underdoped, optimally doped an overdoped HTSC oxides [34]. This transition between s- and $d - wave$ superconductivity is triggered by electronic correlations because in the calculations it is assumed that the bare EPI coupling is momentum independent, i.e. the bare coupling constant contains the $s - wave$ symmetry only.

Third, the calculations are performed in the *adiabatic approximation*, where Λ_1 is less and Λ_{tr} much more suppressed by strong correlations. In the *nonadiabatic regime* $\omega > \mathbf{p} \cdot \mathbf{v}_F(\mathbf{p})$ i.e. for $\omega < \mathbf{p} \cdot \mathbf{v}_F(\mathbf{p})$ the vertex function grows by decreasing q finally reaching $\gamma_c(\mathbf{k}_F, \mathbf{p} = \mathbf{0}, \omega) = 1$. Due to the latter effect the enhancement function $\gamma_c^2(\mathbf{k}_F, \mathbf{p}, \omega)/q_0$ may be substantially larger compared to the adiabatic. This means that different phonons

will be differently affected by strong correlations. For a given frequency the coupling to phonons with momenta $p < p_c = \omega/v_F$ will be *enhanced*, while the coupling to those with $p > p_c = \omega/v_F$ is substantially reduced due to the suppression of the backward scattering by strong correlations.

Fourth, the *transport coupling constant* Λ_{tr} (not properly normalized in Fig. 18 - see correction in [19]) is reduced in the presence of strong correlations, especially for lower doping where $\Lambda_{tr} < \Lambda/3$. This is very important result because it resolves the experimental puzzle that λ_{tr} (which enters resistivity $\rho(T) \sim \lambda_{tr}T$) is much smaller than the coupling constant λ (which enters the self-energy Σ and T_c), i.e. why $\lambda_{tr} << \lambda$. The answer lies in strong correlations which causes the forward scattering peak in charge scattering processes - the *FSP theory*.

As we already said, Monte Carlo (numerical) calculations if the Hubbard model at finite U - performed by Scalapino Group [21], show that the forward scattering peak in the EPI coupling constant (and the charge vertex) develops by increasing U. The latter effect is more pronounced at lower doping. The similar (to Monte Carlo) results were obtained quite recently in [22] in the framework of the Rückenstein-Kotliar (four slave-boson) model. These numerical results prove the *correctness of the EPI theory* based on the X-method.

We stress that contrary to the X-method, where the systematic $1/N$ calculations of the EPI self-energy is uniquely done, this is still a problem for the *SB* (Barnes) method where the $1/N$ expansion of the partition function $Z(T,\mu)$ is usually performed [121]. The existing expression (in the literature) for the vertex function in the SB method is different than that in the X-method [18], [18]. It seems that such a not well-controlled procedure omits a class of diagrams giving inadequate behavior of the coupling constant λ as a function of doping. Additionally, the vertex function in the *SB* approach is peaked not at $q = 0$ but at some finite q_{max}, where $q_{max} \to 0$ only for doping $\delta \to 0$ - see [23].

6. FSP THEORY AND NOVEL EFFECTS

There are a number of effects which are predicted by the FSP theory. We have already explained the effects of the forward scattering peak on the EPI. In Section 2. the shift-puzzle in ARPES was also explained by the FSP theory (model). We discuss briefly some other predictions of the FSP theory containing parts not comprised in [2].

6.1. Nonmagnetic impurities and robustness of d-wave pairing

In the presence of strong correlations the impurity potential is also renormalized and the effective potential in the Born approximation is given by $u^2(\mathbf{q}) = \gamma_c^2(k_F, \mathbf{q})u_0^2(\mathbf{q})$, where $u_0(\mathbf{q})$ is the single impurity scattering potential in the absence of strong correlations [142]. Since the charge vertex $\gamma_c(\mathbf{p}_F, \mathbf{q})$ is peaked at $\mathbf{q} = \mathbf{0}$ the potential $u(\mathbf{q})$ is also peaked at $\mathbf{q} = \mathbf{0}$. This means that the scattering amplitude contains not only the s-channel (as usually assumed in studying impurity effects in HTSC oxides), but also the *d-channel*, etc. Based on this property the FSP theory succeeded in explaining some

experimental facts, such as: (**i**) the suppression of the residual resistivity ρ_i [17], [18]. It is observed in the optimally doped $YBCO$, where the resistivity $\rho(T)$ at $T = 0\ K$ has a rather small value $< 10\ \mu\Omega cm$.; (**ii**) the robustness of $d - wave$ pairing [142]. The previous theories [140], which assume $u(\mathbf{q}) = const$, i.e. the s-wave scattering channel only, predict that $T_c(\rho_{i,c}) = 0$ at much smaller residual resistivity $\rho_{i,c}^{(s)} \sim 50\ \mu\Omega cm$, while the experimental range is $200\ \mu\Omega cm < \rho_{i,c}^{\exp} < 1500\ \mu\Omega cm$ [141]. The latter experimental fact means that d-wave pairing in HTSC is much more robust than the standard theory predicts, and it is one of the smoking gun experiments in testing the concept of the forward scattering peak in the charge scattering potential. It is worth of mentioning that in a number of papers the pair-breaking effect of non-magnetic impurities in HTSC was analyzed in terms of the impurity concentration n_i, i.e. the dependence $T_c(n_i)$. However, n_i is not the parameter which governs this pair-breaking effect. The more appropriate parameter for discussing the robustness of d-wave pairing is the impurity scattering amplitude $\Gamma(\theta, \theta')$, which can be related to the measured residual resistivity ρ_i which leads to the dependence of $T_c(\rho_i)$. The robustness of d-wave pairing in HTSC can be revealed only by studying the experimental curve $T_c(\rho_i)$, what has been first recognized experimentally in [141] and theoretically in [17], [142].

The theory of the robustness of d-wave pairing in HTSC was elaborated first in [142], where the FSP theory [17], [18] is applied to this problem. We shall not go into details - which are given in [142], [2], but we give here a general formula for the $T_c(\rho_i)$ dependence in anisotropic (including unconventional) superconductors, only. We assume that in anisotropic superconductivity the superconducting order parameter has the form $\Delta(\theta) = \Delta_0 Y(\theta)$ and generally one has $\langle Y(\theta) \rangle \neq 0$ ($\langle Y^*(\theta) \rangle Y(\theta) \rangle = 1$) where the momentum dependent impurity scattering amplitude is $\Gamma(\theta, \theta') = \Gamma_s(\theta, \theta') + \Gamma_d Y_d(\theta) Y_d(\theta') + ...$

$$\ln \frac{T_c}{T_{c0}} = \Psi(\frac{1}{2}) - \Psi(\frac{1}{2} + (1 - \beta)x) - \langle Y(\theta) \rangle^2 [\Psi(\frac{1}{2}) - \Psi(x + \frac{1}{2})]. \qquad (96)$$

Here, $x = \Gamma_s/4\pi T_c$, $\beta = \Gamma_d/\Gamma_s$ and $\langle Y(\theta) \rangle$ means an averaging over the Fermi surface. Note, Eq.(96) holds independently of the scattering strength Γ_s, Γ_d, i.e. it holds in the Born as well as in the unitary limit. The residual resistivity ρ_i can be related to the transport scattering rate by $\rho_i = 4\pi \Gamma_{tr}/\omega_{pl}^2$, while the s-wave amplitude is related to Γ_{tr} by $\Gamma_s = p\Gamma_{tr}$. The parameter $p > 1$ can be obtained from the microscopic model (for instance in the t-J model $p \approx 2 - 3$) or can be treated as a fitting parameter - see more in [2]. In the case of an unconventional pairing one has $\langle Y(\theta) \rangle = 0$ and the last term drops. For the s-scattering only ($\Gamma_d = 0$) one has $\beta = 0$ and $T_c(\rho_i)$ should be suppressed very strongly contrary to the experimental results [141] - see Fig. 20.

The FSP theory of the impurity scattering in the t-J model [142] gives that the s-channel and d-channel almost equally contribute to the impurity scattering amplitude, since $\beta \approx 0.75 - 0.85$ for doping $\delta \approx 0.1 - 0.2$. The dependence of $\beta(\delta)$ is calculated for the t-J model - see Fig. 19.

Since the d-channel in scattering is not detrimental for d-wave pairing the FSP theory predicts that $T_c(\rho_i)$ vanishes at much larger $\rho_{i,c}$, i.e. $\rho_{i,c}^{(FSP)} >> \rho_{i,c}^{(s)}$, what is in the good agreement with experiments - as shown in Fig. 20.
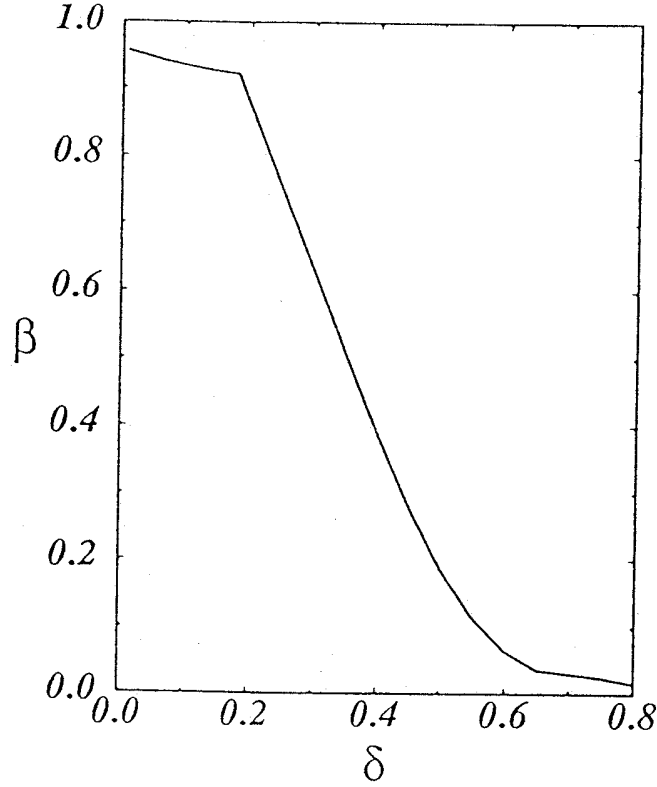
FIGURE 19. The anisotropy scattering parameter β as a function of doping δ in the t-J model. From [142].

6.2. Transport properties and superconductivity

The EPI was studied in the past in the *extreme limit* of the forward scattering peak in the Einstein model with the phonon frequency Ω [119], where in leading order the spectral function is singular, i.e. $\alpha^2 F(\mathbf{k}, \mathbf{k}', \omega) \sim \delta(\mathbf{k} - \mathbf{k}')\delta(\omega - \Omega)$. Numerical calculations of the Eliashberg equations in the normal state [119] give very interesting behavior of the *density of states* $N(\omega)$, where a strong renormalization of $N(\omega)$ is present, but which is absent in the standard theory of the isotropic EPI. *First*, $N(\omega = 0) > N_{bare}(\omega = 0)$, where $N_{bare}(\omega = 0)$ is the density of states in the absence of the EPI - see Fig. 21.

There is a "pseudogap"-like feature in the region $(\Omega/5) < \omega \leq \Omega$ where $N(\omega) < N_{bare}(\omega)$. The "pseudogap" feature disappears at T comparable with the phonon energy Ω. Note, that the usual isotropic EPI does not renormalize the density of states in the normal state, i.e. $N(\omega) = N_{bare}(\omega)$. As a consequence of the pseudogap behavior of $N(\omega)$ the transport properties are very peculiar. For instance, the resistivity $\rho(T)$ is linear in T starting at very low temperatures, i.e. $\rho(T) \sim T$ for $(\Omega/30) \leq T$ and extends
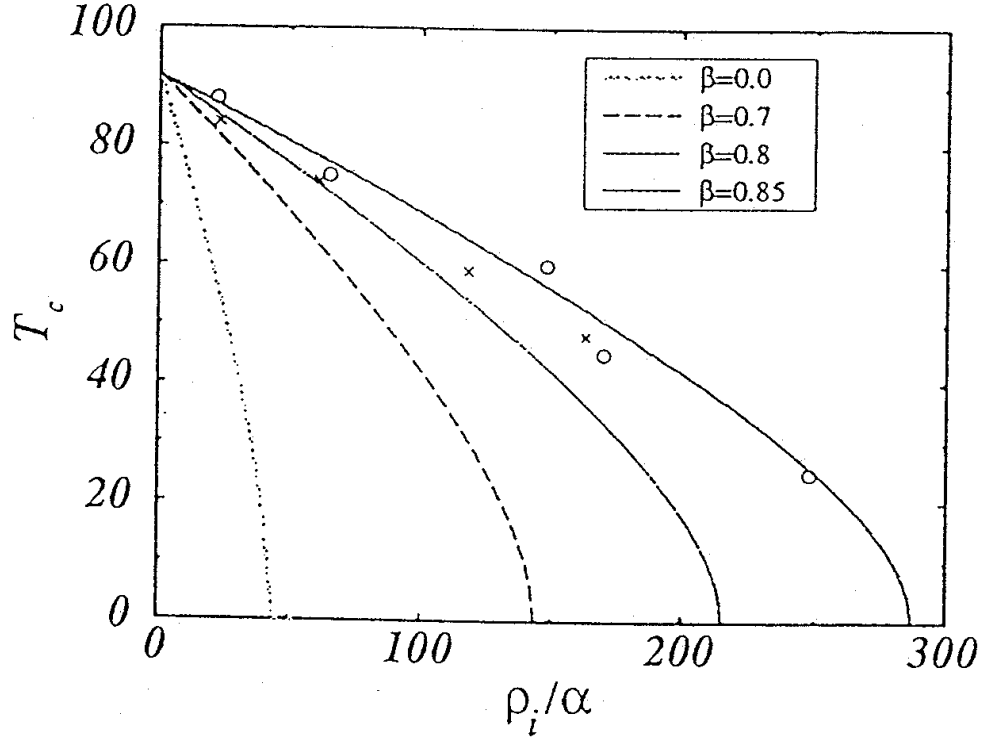
FIGURE 20. The critical temperature $T_c[K]$ of d-wave superconductor as a function of the experimental parameter $\rho_i/\alpha_c[K]$, ρ_i is the residual resistivity and α is defined in the text. The case $\beta = 0$ corresponds to the prediction of the standard d-wave theory with isotropic scattering [140]. The experimental data [141] are given by crosses - $YBa_2(Cu_{1-x}Zn_x)_3O_{7-\delta}$, and circles - $Y_{1-y}Pr_yBa_2Cu_3O_{7-\delta}$ - from [142].

up to several Ω - as it is seen in Fig. 22. The dynamical conductivity $\sigma_1(\omega)$ shows the (extended) Drude-like behavior with the Drude width $\Gamma_{tr} \sim T$, for $\omega < T$ - see Fig. 22. The above numbered properties are in a qualitative agreement with experimental results in HTSC oxides, as discussed in Section 2.

In this extreme forward scattering peak limit one can calculate T_c. In leading order w.r.t. $(\Omega/T_c << 1)$ one has

$$T_{c0} \approx N(0)V_{EP} = \lambda N(0)/4, \tag{97}$$

where $\lambda = N(0)V_{EP}$. In that case the maximal superconducting gap is given by $\Delta_0 = 2T_c$ which is reached on the Fermi surface, while away from it the gap decreases, i.e.

$$\Delta_k = \Delta_0\sqrt{1 - (\xi_k/\Delta_0)^2}. \tag{98}$$

The expression for T_c tells us that it can be large even for $\lambda < 0.1$, since in HTSC oxides the bare density of states is $N_{bare}(0) \sim 1states/eV$. It is apparent that in this order there is no isotope effect, i.e. $\alpha = 0$. We stress that such an extreme limit is never realized in nature, but for the self-energy it is a good starting point, since the effects of the finite
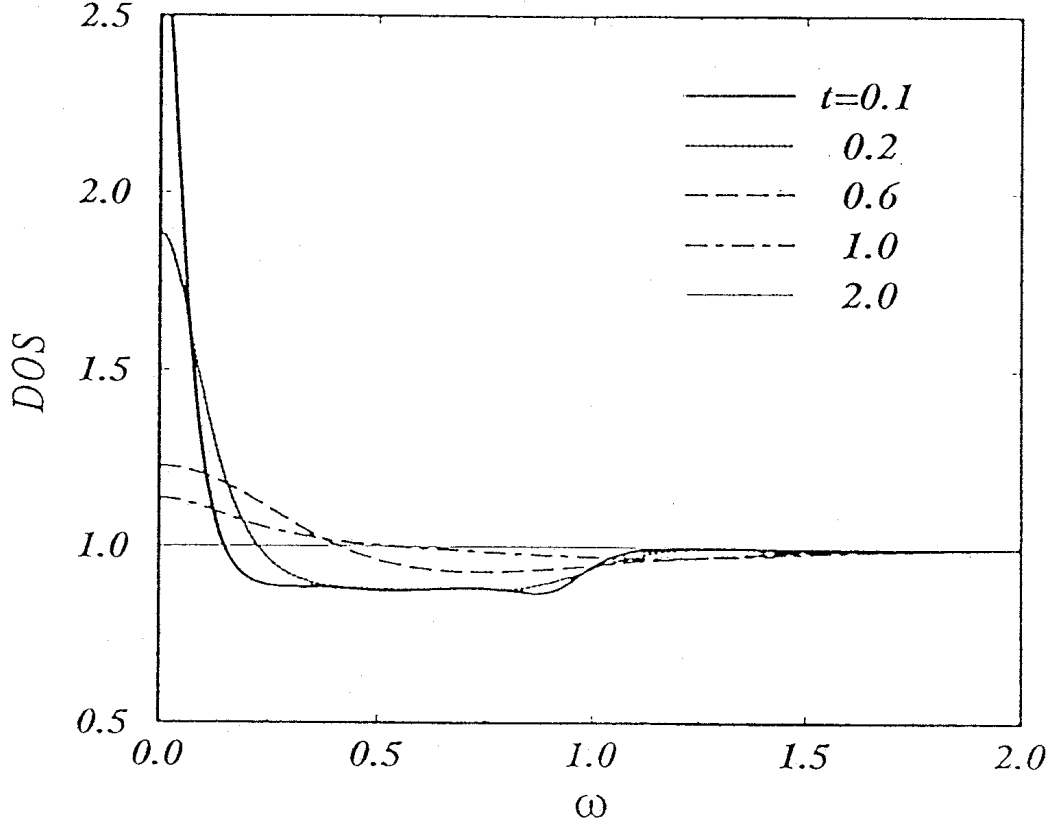
FIGURE 21. The density of states $N(\omega)$ in the FSP model for the EPI. with the dimensionless coupling $l(= V_{EP}/\pi\Omega) = 0.1$ for various $t(= \pi T/\Omega)$. From [119].

width (k_c) of $\alpha^2 F(\mathbf{k}, \mathbf{k}', \omega)$, whenever $k_c \ll k_F$, change mainly the quantitative picture - see [119]. In case when $k_c v_F \ll \Omega$ the reduction of T_c is given by

$$T_c = T_{c0}\left(1 - \frac{7\zeta(3)k_c v_F}{4\pi^2 T_{c0}}\right). \tag{99}$$

Very interesting calculations in the more realistic FSP model with the finite width k_c, but $k_c \ll k_F$, were done in [134], where the FSP theory for the EPI and the SFI theory (based on spin-fluctuation mechanism of pairing) were compared. For instance, the FSP theory can explain the appreciable increase of the anisotropy ratio $R \equiv \Delta(\pi, 0)/\Delta(\pi/2, \pi/2)$ when $T \to T_c$, while the SFI is unable. Furthermore, the FSP theory of the EPI can explain the pronounced orthorhombic ($a \neq b$) effect in $YBCO$ on the gap ratio Δ_a/Δ_b, penetration depth anisotropy λ_a^2/λ_b^2 and supercurrent ratio in the c-axis $Pb - YBCO$ junction. On the other hand, the SFI theory is ineffective, since it predicts at least one order of magnitude smaller effects - [134], [2].
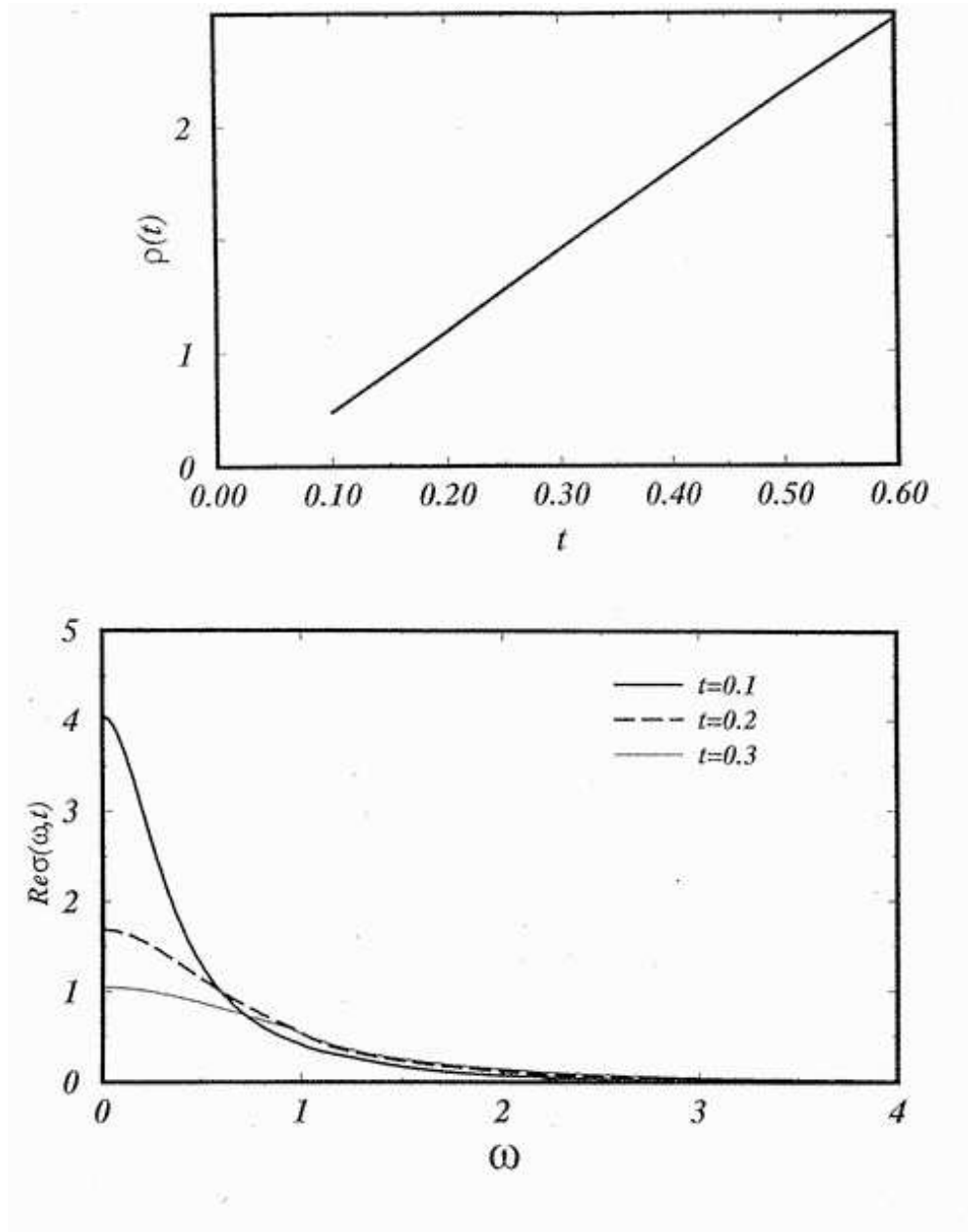
FIGURE 22. $\rho(T)$ (upper part) and $\sigma_1(\omega)$ in the FSP model for the EPI. with the dimensionless coupling $l(=V_{EP}/\pi\Omega)=0.1$ for various $t(=\pi T/\Omega)$. From [119].

6.3. Nonadiabatic corrections of T_c

HTSC oxides are characterized not only by strong correlations but also by relatively small Fermi energy E_F, which is not much larger than the characteristic (maximal) phonon frequency ω_{ph}^{max}, i.e. $E_F \simeq 0.1 - 0.3$ eV, $\omega_{ph}^{max} \simeq 80$ meV. The situation is even more pronounced in *fullerene compounds* A_3C_{60}, with $T_c = 20 - 35$ K, where

$E_F \simeq 0.2\ eV$ and $\omega_{ph}^{\max} \simeq 0.16\ eV$. This fact implies a possible breakdown of the Migdal's theorem [139], [9], which asserts that the relevant vertex corrections due to the $E - P$ interaction are small if $(\omega_D/E_F) \ll 1$. In that respect a comparison of the intercalated graphite KC_8 and the fullerene A_3C_{60} compounds, given in [120], is very instructive, because both compounds have a number of similar properties. However, the main difference in these systems lies in the ratio ω_D/E_F, since $(\omega_D/E_F) \ll 1$ in KC_8, while it is rather large $(\omega_D/E_F) \sim 1$ in A_3C_{60}. Due to the appreciable magnitude of ω_D/E_F in the fullerene compounds and in HTSC oxides it is necessary to correct the Migdal-Eliashberg theory by vertex corrections due to the EPI. It is well-known that these vertex corrections lower T_c in systems with isotropic EPI. However, the vertex corrections in systems with the forward scattering peak and with the cut-off $q_c << k_F$ the increases of T_c appreciable. The calculations by the Pietronero group [120] gave two important results: (**1**) there is a drastic increase of T_c by lowering $Q_c = q_c/2k_F$, for instance $T_c(Q_c = 0.1) \approx 4 T_c(Q_c = 1)$; (**2**) Even small values of $\lambda < 1$ can give large T_c. The latter results open a new possibility in reaching high T_c in systems with appreciable ratio ω_D/E_F and with the forward scattering peak. The difference between the Migdal-Eliashberg and non-Migdal theories can be explained qualitatively in the framework of an approximative McMillan formula for T_c (for not too large λ) which reads

$$T_c \approx \langle \omega \rangle e^{-1/[\tilde{\lambda} - \mu^*]}. \tag{100}$$

The *Migdal-Eliashberg theory* predicts

$$\tilde{\lambda} \approx \frac{\lambda}{1 + \lambda}, \tag{101}$$

while the non-Migdal theory [120] gives

$$\tilde{\lambda} \approx \lambda(1 + \lambda). \tag{102}$$

For instance $T_c \sim 100\ K$ in HTSC oxides can be explained by the Migdal-Eliashberg theory for $\lambda \sim 2$, while in the non-Migdal theory much smaller coupling constant is needed, i.e. $\lambda \sim 0.5$ as it is seen in Fig. 23. The pioneering approach done in [120] deserves more attention in the future.

6.4. Pseudogap behavior in the FSP model for the EPI

In this review we did not discuss a number of interesting topics such as the possible existence of stripes, the properties of the pseudogap state, etc.. There is a believe that the understanding of these properties might give some hints for pairing mechanism in HTSC oxides. Especially, the pseudogap (PG) problem is a very intriguing one and is not surprising at all, that a number of theoretical approaches were proposed for explaining the PG. We are not going to discuss it but only quote some of them. The *first* one is based on the assumption that the PG phase represents pre-formed pairs [143], and the true critical temperature T_c is smaller than the mean-field one T_c^{MF}. In the region $T_c < T < T_c^{MF}$ pre-formed pairs exist giving rise to the dip in the density of states $N(\omega)$. This approach
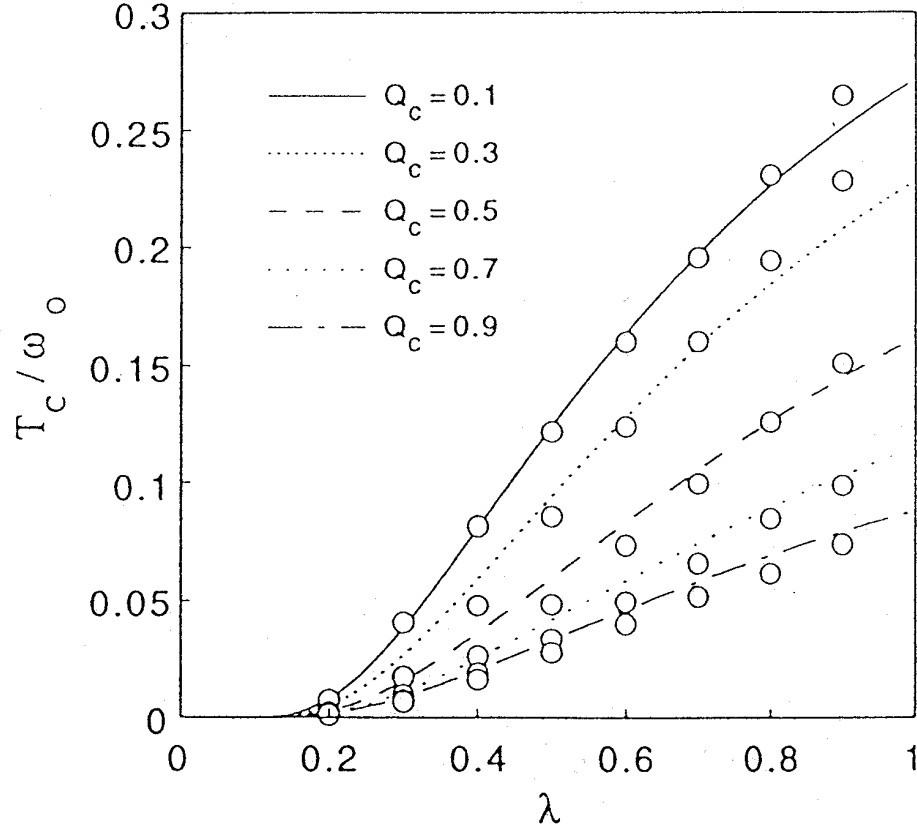
FIGURE 23. The approximative analytic (solid lines) and numerical (circles) solution of $T_c(\lambda)$ in the first nonadiabatic approximation for various cutoff Q_c and for $m = (\omega_D/E_F) = 0.2$. From [120].

is physically plausible having in mind that HTSC oxides are characterized by the short coherence length and quasi-two dimensionality. From the experimental side there are some supports. For instance, the specific heat measurements [144] point to the non-mean field character of the superconducting phase transition, particularly for the underdoped systems. As we have already mentioned in the Introduction the ARPES measurements show that the PG has a d-wave like form

$$\Delta_{pg}(\mathbf{k}) \approx \Delta_{pg,0}(\cos k_x - \cos k_y) \tag{103}$$

(like the superconducting gap) and $\Delta_{pg,0}$ increases by lowering doping. The *second* approach assumes that the PG is due to a competing order, but usually without the long-range order, such as due to "spin-density wave" alias for strong antiferromagnetic fluctuations [145], [146]. There are other approaches which are based on the RVB and orbital current model, d-wave order, etc., but we shall not discussed it here.

However, the FSP theory, which predicts the long-range force due to the renormalization of the EPI by strong correlations, opens an additional possibility for the PG. As we

discussed in Section 6.2, due to the forward scattering peak the critical temperature has a non-BCS dependence, i.e. $T_c^{MF} = V_{EP}/4$. However, this is the mean-field value, which is inevitably reduced by phase and internal Cooper pair fluctuations present in systems with long-range attractive forces, i.e. with the forward scattering peak.

The interesting problem of fluctuations in systems with long-range attractive forces was recently studied in [147]. It was shown there, that such a long-ranged superconductor exhibits a class of fluctuations in which the internal structure of the Cooper pair is soft. This leads to a "pseudogap" behavior in which the actual transition temperature T_c is greatly depressed from its mean-field value T_c^{MF}. We stress that these fluctuations are not the standard phase fluctuations in superconductors. Since the problem is very interesting and deserve much more attention in the future we discuss it here briefly. In the following the weak coupling limit is assumed, where the pairing Hamiltonian has the form

$$H = \sum_\sigma \int d\mathbf{x}\psi_\sigma^\dagger(\mathbf{x})\xi(\hat{\mathbf{p}})\psi_\sigma(\mathbf{x})$$

$$- \int d\mathbf{x}d\mathbf{x}'V(\mathbf{x}-\mathbf{x}')\psi_\uparrow^\dagger(\mathbf{x})\psi_\downarrow^\dagger(\mathbf{x}')\psi_\downarrow(\mathbf{x}')\psi_\uparrow(\mathbf{x}). \tag{104}$$

In the MFA the order parameter $\Delta(\mathbf{x},\mathbf{x}')$ is given by

$$\Delta(\mathbf{x},\mathbf{x}') = V(\mathbf{x}-\mathbf{x}')\langle\psi_\downarrow(\mathbf{x}')\psi_\uparrow(\mathbf{x})\rangle. \tag{105}$$

$\Delta(\mathbf{x},\mathbf{x}')$ depends in fact on the internal coordinate $\mathbf{r} = \mathbf{x} - \mathbf{x}'$ and the center of mass $\mathbf{R} = (\mathbf{x}+\mathbf{x}')/2$, i.e. $\Delta(\mathbf{x},\mathbf{x}') = \Delta(\mathbf{r},\mathbf{R})$. In usual superconductors with the short-range pairing potential $V_{sr}(\mathbf{x}-\mathbf{x}') \approx V_0\delta(\mathbf{x}-\mathbf{x}')$ one has $\Delta(\mathbf{r},\mathbf{R}) = \Delta(\mathbf{R})$ and therefore there are practically the spatial ($\mathbf{R}$) fluctuations of the order parameter, only. In the case of long-range pairing potential there are additional fluctuations of the internal ($\mathbf{r}$) degrees of freedom. In the following we sketch the analysis given in [147].

When the range of the pairing potential is large, i.e. $r_c > \xi$ (the superconducting coherence length), fluctuations of the internal Cooper wave-function are important since they give rise to a tremendous reduction of the mean-field quantities. In order to make the physics of internal wave-function fluctuations we study much simpler Hamiltonian the so called reduced BCS Hamiltonian,

$$H = \sum_{\mathbf{k}\sigma} \xi_{\mathbf{k}}c_{\mathbf{k}\sigma}^\dagger c_{\mathbf{k}\sigma} - \sum_{\mathbf{k},\mathbf{k}'} V_{\mathbf{k}-\mathbf{k}'}c_{\mathbf{k}\uparrow}^\dagger c_{-\mathbf{k}\downarrow}^\dagger c_{-\mathbf{k}'\downarrow}c_{\mathbf{k}'\downarrow}. \tag{106}$$

Since we shall study excitations around the ground state we assume that there are no unpaired electrons which allows us to study the problem in the pseudo-spin Hamiltonian [148]

$$H = \sum_{\mathbf{k}\sigma} 2\xi_{\mathbf{k}}S_{\mathbf{k}\sigma}^z - \frac{1}{2}\sum_{\mathbf{k},\mathbf{k}'} V_{\mathbf{k}-\mathbf{k}'}(S_{\mathbf{k}}^+S_{\mathbf{k}'}^- + S_{\mathbf{k}'}^+S_{\mathbf{k}}^-)$$

$$= \sum_{\mathbf{k}\sigma} 2\xi_{\mathbf{k}}S_{\mathbf{k}\sigma}^z - \sum_{\mathbf{k},\mathbf{k}'} V_{\mathbf{k}-\mathbf{k}'}(S_{\mathbf{k}}^x S_{\mathbf{k}'}^x + S_{\mathbf{k}'}^y S_{\mathbf{k}}^y), \tag{107}$$

where the pseudo-spin 1/2 operators $S^z_{\mathbf{k}\sigma}$, $S^+_{\mathbf{k}\sigma} = (S^-_{\mathbf{k}\sigma})^\dagger$ are given by

$$S^z_{\mathbf{k}\sigma} = \frac{1}{2}(c^\dagger_{\mathbf{k}\uparrow}c_{\mathbf{k}\uparrow} - c^\dagger_{-\mathbf{k}\downarrow}c_{-\mathbf{k}\downarrow} - 1),$$

$$S^+_{\mathbf{k}\sigma} = c^\dagger_{\mathbf{k}\uparrow}c^\dagger_{-\mathbf{k}\downarrow}. \tag{108}$$

We see that Eq.(107) belongs to the class of the Heisenberg ferromagnetic ($V_{\mathbf{k}-\mathbf{k}'} > 0$) Hamiltonian formulated on the lattice in the Brillouin zone. The mean-field approximation (MFA) for this Hamiltonian is given by

$$H_{MFA} = -\sum_k \mathbf{h_k S_k} \tag{109}$$

with the mean-field $\mathbf{h_k}$ given by

$$\mathbf{h_k} = -2\xi_\mathbf{k}\mathbf{z} + \sum_{\mathbf{k}'} V_{\mathbf{k}-\mathbf{k}'}\langle S^x_{\mathbf{k}'}\mathbf{x} + S^y_{\mathbf{k}'}\mathbf{y}\rangle, \tag{110}$$

where $\mathbf{x}, \mathbf{y}$ and $\mathbf{z}$ are unit vectors. Since x- and y-axis are equivalent one can searches $\mathbf{h_k}$ in the form $\mathbf{h_k} = -2\xi_\mathbf{k}\mathbf{z} + 2\Delta_\mathbf{k}\mathbf{x}$, where the order parameter $\Delta_\mathbf{k}$ is the solution of the equation

$$\Delta_\mathbf{k} = \sum_{\mathbf{k}'} V_{\mathbf{k}-\mathbf{k}'}\langle S^x_{\mathbf{k}'}\rangle = \sum_{\mathbf{k}'} V_{\mathbf{k}-\mathbf{k}'}\frac{V_{\mathbf{k}-\mathbf{k}'}\Delta_{\mathbf{k}'}}{2E_\mathbf{k}}\tanh\frac{\beta E_\mathbf{k}}{2}, \tag{111}$$

with $E_\mathbf{k} = \sqrt{\xi^2_\mathbf{k} + \Delta^2_\mathbf{k}}$.

In the case of *short-range BCS-like forces* $V_{BCS}(\mathbf{x} - \mathbf{x}') \approx V_0\delta(\mathbf{x} - \mathbf{x}')$ one has $V_{\mathbf{k}-\mathbf{k}'} = V_0$ for all momenta. This "long-range force" in the momentum space it is the "long-range force" means that the MFA is good approximation with the standard BCS solution of Eq.(111).

For the *long-range attractive forces* the function $V_{\mathbf{k}-\mathbf{k}'}$ is peaked at $\mid \mathbf{k} - \mathbf{k}' \mid = 0$, for instance in the extreme forward scattering peak case (see Section 6.2) one has $V_{\mathbf{k}-\mathbf{k}'} = V_0\delta(\mathbf{k} - \mathbf{k}')$. In the following we analyze s-wave pairing only where the solution of Eq.(111) gives $T^{MF}_c = V_0/4$ and $\Delta_0 = 2T^{MF}_c$. (Note, that in the BCS case one has $\Delta_0 = 1.76T^{MF}_c$.). The coherence length is defined by $\xi = v_F/\pi\Delta_0$. The important fact is that in the case of long-ranged superconductors the Heisenberg like Hamiltonian in the momentum space is short-ranged giving rise to low-laying spin-wave spectrum. The latter spectrum are in fact the low-energy bound states (excitons) which loosely correspond to the low-energy collective modes (in the true many-body theory based on Eq.(104)). This problem is studied in [147] for the long-range (but finite) potential $V(r) = V_0\exp\{-r^2/2r^2_c\}$ (its Fourier transform is $V_k = (2\pi r^2_c)V_0\exp\{-k^2r^2_c/2\}$) where it was found a large number $N_{cm} \sim \pi k_F r_c/6\xi$ (for $r_c \gg \xi$) of the excitonic like collective modes ω^{exc}_{mn} at zero momentum. These excitonic modes lie between the ground state and the two particle continuum for $\omega > 2\Delta_0$. Note, that since we assume that $\Delta_0 \ll E_F$ the system is far from the Bose-Einstein condensation limit.

The above analysis is useful for physical understanding, but the fully many-body fluctuation problem, which is based on the Hamiltonian in Eq.(104), is studied in [147]

where the Ginzburg-Landau (G-L) equation is derived for the long-ranged superconductor. Due to the fluctuations of the internal wave-function the G-L free-energy functional $F\{\Delta(\mathbf{R},\mathbf{k})\}$ for the order parameter $\Delta(\mathbf{R},\mathbf{k}) = \int d\mathbf{r}\Delta(\mathbf{R}-\mathbf{r}/2,\mathbf{R}+\mathbf{r}/2)\exp\{-i\mathbf{kr}\}$ has much more complicated form

$$F\{\Delta(\mathbf{R},\mathbf{k})\} = \sum_k \int d\mathbf{R}\{A_{\mathbf{k}} \mid \Delta(\mathbf{R},\mathbf{k}) \mid^2 + B_{\mathbf{k}} \mid \Delta(\mathbf{R},\mathbf{k}) \mid^2$$

$$+\frac{1}{2M} \mid \partial_{\mathbf{k}}\Delta(\mathbf{R},\mathbf{k}) \mid^2 + \frac{1}{2m_{\mathbf{k}}} \mid \partial_{\mathbf{R}}\Delta(\mathbf{R},\mathbf{k}) \mid^2\}, \tag{112}$$

where $M = r_c^2 V_0$ and

$$A_{\mathbf{k}} = \frac{1}{V_0} - \frac{\tanh(\beta\xi_{\mathbf{k}}/2)}{2\xi_{\mathbf{k}}}$$

$$\frac{1}{2m_{\mathbf{k}}} = \frac{\beta^2 v_F^2 \sinh(\beta\xi_{\mathbf{k}}/2)}{32\xi_{\mathbf{k}}\cosh^3(\beta\xi_{\mathbf{k}}/2)}$$

$$B_{\mathbf{k}} = \frac{\tanh(\beta\xi_{\mathbf{k}}/2)}{8\xi_{\mathbf{k}}^3} - \frac{\beta}{16\xi_{\mathbf{k}}^2\cosh^3(\beta\xi_{\mathbf{k}}/2)}. \tag{113}$$

The term due to the partial derivative $\partial_{\mathbf{k}}$ is a direct consequence of the long-ranged pairing potential, and it describes of fluctuations of the internal Cooper wave-function. The effect of these fluctuations, described by the free-energy functional in Eq.(112), is studied in the Hartree-Fock approximation in the limit $r_c \gg \xi$, where it is found the large reduction of the mean-field critical temperature

$$T_c \sim \frac{T_c^{MF}}{(r_c/\xi)}. \tag{114}$$

The latter result means that T_c in the long-ranged superconductors is *controlled by thermal fluctuations of collective modes* which is in contrast with the short-range (BCS-like) superconductivity. In the temperature interval $T_c < T < T_c^{MF}$ the system is in the pseudogap regime where the electrons are paired but there is no long-range phase coherence. The latter sets in only at $T < T_c$. We shall not further discuss this interesting approach but only stress that it can be generalized by including the repulsive interaction due to spin fluctuations, what shall be discussed elsewhere.

In conclusion, the forward scattering peak in the EPI gives rise to the long-ranged superconductivity in which the soft excitonic modes of the internal Cooper wave function reduce T_c strongly. In the region $T_c < T < T_c^{MF}$ the pseudogap (PG) phase is realized. In this approach the PG has the same symmetry as the superconducting gap.

7. ELECTRON-PHONON INTERACTION VS SPIN-FLUCTUATIONS

7.1. Interaction via spin fluctuations (SFI) and pairing

At present one of the possible candidates in explaining experimental results in HTSC oxides appears to be the theory based on the spin fluctuation pairing mechanism - the SFI theory. The latter is usually described by the single band Hubbard model, or on the phenomenological level by the postulated form of the self-energy (written below)[29], [136], [135], [83], [84], [137]. In the approach of Pines-school to the SFI the effective potential $V_{eff}(\mathbf{k}, \omega)$ (see Eq.(5) in Sections 2.) depends on the imaginary part of the spin susceptibility $Im\chi(\mathbf{k} - \mathbf{k}', \omega)$ (ω real). According to this school, the shape and the magnitude of $Im\chi(\mathbf{q}, \omega)$, which is peaked at $\mathbf{Q} = (\pi, \pi)$, plays an important role in obtaining T_c in this mechanism. There are two phenomenological approaches, which can be theoretically justified in a very weak coupling limit $g_{sf} \ll 1$ only, where $Im\chi(\mathbf{q}, \omega)$ is inferred from different experiments:

(**1**) From *NMR* experiments at very low ω - the *MMP model* [29], [136], [135], where $Im\chi_{MMP}$ is modelled by

$$Im\chi_{MMP}(\mathbf{q}, \omega + i0^+) = \frac{\omega}{\omega_{sf}} \frac{\chi_Q}{[1 + \xi_M^2 \mid \mathbf{q} - \mathbf{Q} \mid^2 + (\omega/\omega_{sf})^2]^2} \Theta(\omega_c^{MMP} - \mid \omega \mid), \quad (115)$$

with the frequency cutoff $\omega_c^{MMP} = 400 \, meV$. They fit the *NMR* experiments by assuming very large value for $\chi_Q \approx (30 - 40)\chi_0 \sim 100 \, eV^{-1}$. From Fig. 24 it is seen that the imaginary susceptibility is peaked at low frequency $\omega_{peak} \approx 5 - 10 \, meV$.

(**2**) From the neutron scattering experiments [83], [84]) - the *RULN model*, where $Im\chi_{RULN}$ is modelled by

$$Im\chi_{RULN}(\mathbf{q}, \omega + i0^+) = C[\frac{1}{1 + J_0[\cos q_x + \cos q_y]}]^2 \times$$

$$\times \frac{3(T + 5)\omega}{1.5\omega^2 - 60 \mid \omega \mid + 900 + 3(T + 5)^2} \Theta(\omega_c^{RULN} - \mid \omega \mid), \quad (116)$$

where $\omega_c^{RULN} = 100 \, meV$, $J_0 = 0.3$, $C = 0.19 \, eV^{-1}$ with T and ω measured in *meV*. From Fig. 25 it is seen that $Im\chi_{RULN}$ is peaked around 30 meV, which is much larger than in the MMP model.

By knowing $Im\chi$ one can calculate the effective pairing potential $V_{eff}(\mathbf{k}, \omega)$ from Eq.(5) and the spectral function for the d-wave pairing $\alpha_d^2 F(\omega)$

$$\alpha_d^2 F(\omega) = -\frac{\langle\langle Y_d(\mathbf{k})Y_d(\mathbf{k}')V_{SF}(\mathbf{k} - \mathbf{k}', \omega + i0^+)\rangle\rangle}{\langle Y_d^2(\mathbf{k})\rangle}. \quad (117)$$

Here, $Y_d(\mathbf{k}) = \cos k_x - \cos k_y$ is the $d-wave$ pairing function ($\Delta(\mathbf{k}, \omega) \approx \Delta(\omega)Y_d(\mathbf{k})$). The bracket means an average over the Fermi surface. The spectral function $\alpha_d^2 F(\omega)$ for two models is shown in Fig. 26, where it is seen that $\alpha_d^2 F(\omega)^{RULN}$ is much narrower
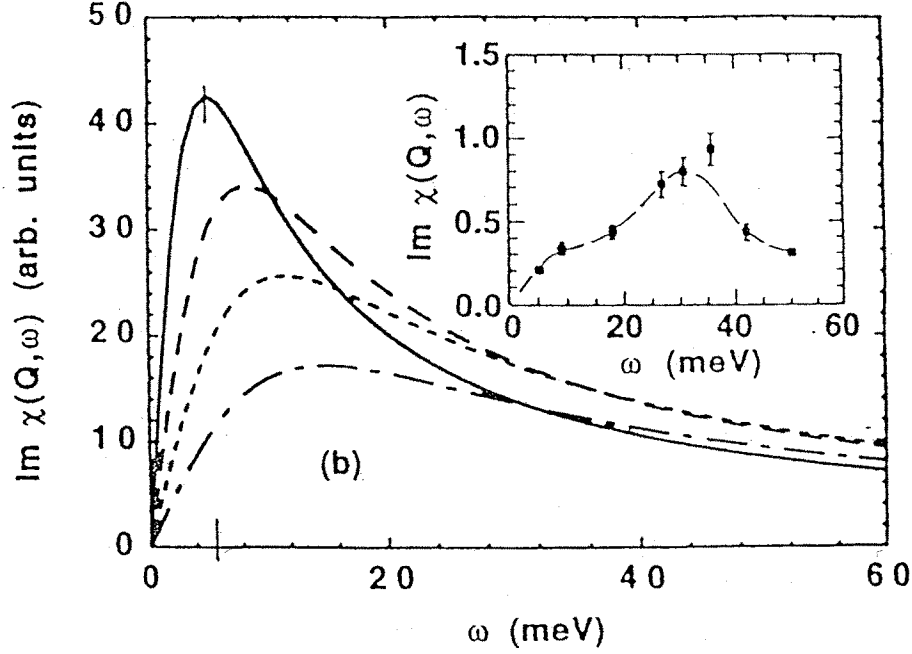
FIGURE 24. Spectral function $\text{Im}\chi(,\omega)$ for the *MMP model* of spin-mediated interactions $\text{Im}\chi(,\omega)$ in $YBa_2Cu_3O_{7-\delta}$. The spectral function is calculated at $= (\pi,\pi)$ and $T = 0$ K (solid line), 100 K (long-dashed line), 200 K (short dashed line), and 300 K (dot-dashed line). Inset: experimental data of $YBa_2Cu_3O_{6.6}$ at $T = 100$ K - the line is to guide the eye. From [83], [84].

function than $\alpha_d^2F(\omega)^{MMP}$. The latter is peaked almost at the same ω as $\alpha_d^2F(\omega)^{RULN}$, while $\alpha_d^2F(\omega)^{MMP}$ is much broader than $\alpha_d^2F(\omega)^{RULN}$.

Due to different shapes of the susceptibility and of $\alpha_d^2F(\omega)$ in these two approaches the calculated (from Eliashberg equations) critical temperatures are also very different. Since the MMP spectral function is much broader than the RULN one it turns out that $T_c^{(MMP)}$ can reach 100 K for rather large value of $g_{SF} \sim 0.64$ eV, while $T_c^{(RULN)}$ saturates already at 50 K even for $g_{SF} \gg 1$. From the physical pint of view the RULN model is more plausible than the MMP one, since the former is based on the neutron scattering measurements which comprise much larger frequencies than the NMR measurements. Note, that a valid model for HTSC oxides must be able to explain the high values of T_c (which needs $\lambda_{sf}(= 2 \int (\alpha_d^2F(\omega)/\omega)d\omega) \sim 2$) and the resistivity $\rho(T)$ (and its slope ρ' with small $\lambda_{tr} \sim 0.6$). It turns out that $T_c^{(MMP)}$ can fit $T_c \approx 100$ K on the expense of large coupling $g_{sf}^{(MMP)} \sim 0.64$ eV and $\lambda_{sf}^{(MMP)} \sim 2.5$. However, the value $g_{sf}^{(MMP)} \sim 0.64$ eV gives much larger value for $\rho(T)$ and ρ' than the experiments do. On the other hand if one fits $\rho(T)$ and ρ' with the MMP model one gets very small $T_c < 7$ K, thus making the MMP model ineffective in HTSC oxides.

In the physically more plausible *RULN model* $T_c^{(RULN)}$ saturates at 50 K even for $g_{sf}^{(RULN)} \gg 1$ eV. If one chooses an appropriate value for $g_{sf}^{(neut)}$ to fit $\rho(T)$ and ρ' one
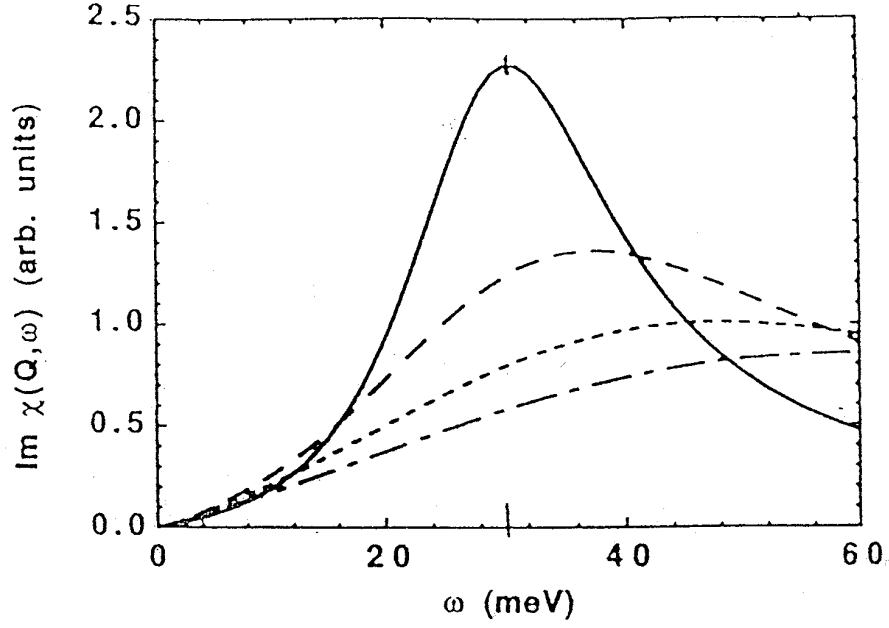
FIGURE 25. Spectral function $\mathrm{Im}\chi(,\omega)$ for the *RULN model* of spin-mediated interactions $\chi(,\omega)$ in $YBa_2Cu_3O_{7-\delta}$. The spectral function is calculated at $= (\pi,\pi)$ and $T = 0$ K (solid line), 100 K (long-dashed line), 200 K (short dashed line), and 300 K (dot-dashed line). Inset: experimental data of $YBa_2Cu_3O_{6.6}$ at $T = 100$ K - the line is to guide the eye. From [83], [84].
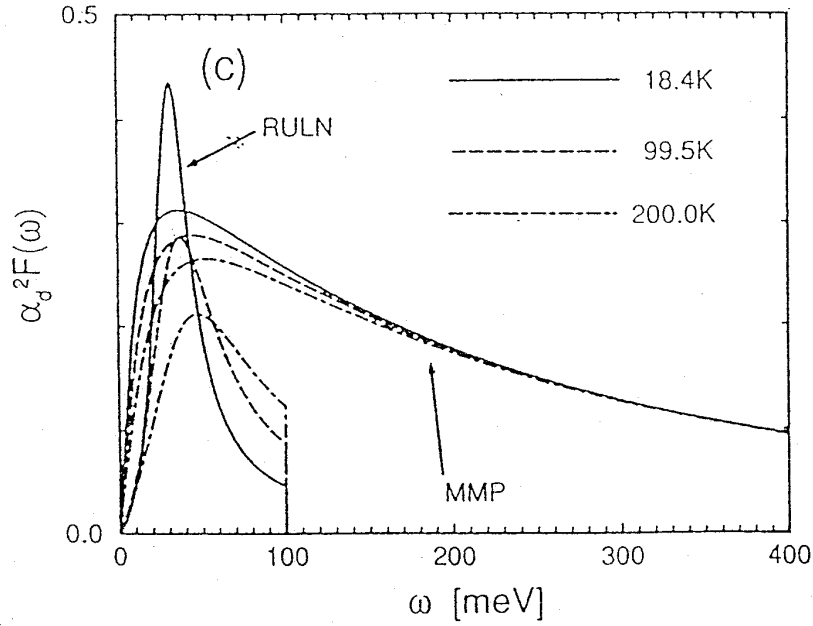

FIGURE 26. The spectral function $\alpha_d^2 F(\omega)$ in the $d - wave$ pairing channel for the *MMP* and *RULN* model at different temperature - from [137].

gets $T_c^{(RULN)} \approx 7\ K$. This analysis gives a convincing evidence that the existing SFI theories are ineffective in HTSC oxides.

We stress again, that the large effective coupling constant, assumed in the SFI theories, $g_{sf} \sim 0.64\ eV$, is difficult to justify theoretically (if at all). By analyzing theoretically the possible strength of the coupling constant g_{sf}, in both the weak ($N(0)U \ll 1$) and strong ($N(0)U \gg 1$) coupling limit, one obtains that $g_{sf} < 0.2\ eV$ and $\lambda_{sf} < 0.2$ (note $\lambda_{sf} \sim g_{sf}^2$), which means that $\lambda_{sf} \ll \lambda_{sf}^{(MMP)}$ and $T_c^{(sf)} \ll T_c^{(MMP)}$ [2]. This analysis is supported by the recent theoretical results where $g_{sf} < 0.2\ eV$ is extracted from the calculation : **1.** of the width of the magnetic resonance peak at 41 *meV* [68]; **2.** of the small magnetic moment ($\mu < 0.1\ \mu_B$) in the antiferromagnetic order, which coexists with superconductivity in $La_{2-x}Sr_xCuO_4$ [69].

7.2. Are the EPI and SFI compatible in d-wave pairing?

The phenomenological SFI theories (MMP, RULN, FLEX approximation [149]] became popular because they can produce d-wave pairing, due to the repulsive character of spin-fluctuations (in the momentum space.) which are peaked in the backward ($q = Q$) scattering. However, as we have argued in previous Sections, a number of experiments point to a large EPI with $\lambda > 1$. On the other hand if one assumes that the EPI is momentum independent (isotropic), like in the standard Migdal-Eliashberg theory, then it is strongly pair-breaking for d-wave pairing. So, if one assumes (for the moment) that superconductivity in HTSC oxides is due to the SFI with $\lambda_{sf} \approx 2$, then in that case $T_c^{(sf)}$ would be drastically reduced (to almost zero) by the isotropic EPI even for moderate $\lambda_{EP} \sim 1$. The latter was shown in [138] where the Eliashberg equations are solved for the SFI treated in the FLEX approximation [149] and the EPI in the Einstein model with various momentum dependent $V_{EP}(\vec{k}, \omega)$. This result means, that if the SFI would be the basic pairing interaction in the presence of the isotropic and momentum independent EPI, then in order to reach $T_c \sim 100\ K$ the bare critical temperature should be $T_c^{(sf)} \sim (600 - 700)\ K$, which needs unrealistically large λ_{sf}. This is not only highly improbable, but would give enormous large resistivity and its slope, in contrast to experiments. The similar results were obtained in [11].

The calculations in [138] show that the SFI interaction is dominant in (d-wave) pairing if some strong constraints are realized, such as: (**1**) very large SFI coupling constant $\lambda_{sf} \approx 2$; (**2**) a strong forward scattering peak in the EPI with small EPI coupling $\lambda \ll 1$. Both these conditions are incompatible with experiments and theoretical analysis - see also Section 2.1. The way out from this controversy is that the EPI with the forward scattering peak is inevitably dominant interaction in the quasiparticle scattering and pairing in HTSC oxides. As we already discussed in Section 5. the forward scattering peak in the EPI gives rise to the large coupling constant in the d-wave channel, which is of the order of the one in the s-wave channel in the range of doping around the optimal one, i.e. $\lambda_{EP,d} \approx \lambda_{EP,s}$. This means that the residual Coulomb repulsion (by including also the SFI with the backward scattering peak (BSP)) with $\lambda_c < \lambda_{EP,d}$ *triggers* d-wave pairing.

8. IS THERE HIGH-TEMPERATURE SUPERCONDUCTIVITY IN THE HUBBARD AND T-J MODEL?

8.1. Hubbard model

There are a number of papers dealing with numerical calculations, such as Monte Carlo, exact Lanczos diagonalization, in the 2-dimensional (2D) single-band and three-band Hubbard model. One can say that the single-band Hubbard model does very well in describing the magnetic properties of HTSC oxides. Concerning the existence of superconductivity the situation is not definitely resolved. So far the calculations are done on finite clusters and rather high temperatures $T > 0.1t$ [150], [7] which show no tendency to superconductivity. It is worth of mentioning that most of these calculations deal with the pairing susceptibility - see Eq.(126) below, defined in terms of the bare electron operators $c_{mathbf k\sigma}$ in Eq.(128). Since superconducting pairing is realized on quasiparticles with the weight $z < 1$ there is a last hope that the accuracy of the present numerical calculations is not sufficient to pick up the suppressed pairing susceptibility. In that respect a very important approach to the problem of superconductivity (in any microscopic model), which is formulated without using any order parameter, was given by the Scalapino group [151]. The method of calculations is based on the two most important hallmarks of superconductivity: **(i)** *ideal diamagnetism* (the Meissner effect) and **(ii)** *ideal conductivity*. In that respect they study the superfluid density D_s (proportional to λ^{-2}, λ is the penetration depth) and the Drude weight D in the single-band n.n. (nearest neighbors) Hubbard model. The dynamical conductivity along the x-axis is given by

$$\sigma_{xx}(\omega) = -\frac{e^2}{i} \frac{\langle -T_x \rangle - \Lambda_{xx}(\mathbf{q} = 0, \omega)}{\omega + i\delta}. \tag{118}$$

Here, $\langle -T_x \rangle = \langle -T \rangle / 2$ where T is the kinetic energy in the n.n. tight-binding model - see Eq.(18), where the current-current response function $\Lambda_{xx}(\mathbf{q}, \omega)$ is obtained from

$$\Lambda_{xx}(\mathbf{q}, i\omega_m) = \frac{1}{N} \int_0^\beta d\tau e^{i\omega_m \tau} \langle j_x^p(\mathbf{q}, \tau) j_x^p(-\mathbf{q}, 0) \rangle, \tag{119}$$

with $\omega_m = 2\pi mT$, by the standard analytic continuation $i\omega_m \rightarrow \omega + i\delta$ and

$$j_x^p(\mathbf{q}, \tau) = it \sum_{l,\sigma} e^{-i\mathbf{q}\mathbf{l}} (c^\dagger_{l+x\sigma} c_{l\sigma} - c^\dagger_{l\sigma} c_{l+x\sigma}). \tag{120}$$

In the pure Hubbard model $\sigma_{xx}(\omega)$ contains the delta function contribution

$$\sigma_{xx}(\omega) = D\delta(\omega) + \sigma_{reg}(\omega), \tag{121}$$

where the Drude weight $D(\equiv (n/m)^*$, which measures the ratio of the density of the mobile charge carriers to their mass, is defined by

$$\frac{D}{\pi e^2} = \langle -T_x \rangle - \Lambda_{xx}(\mathbf{q} = 0, \omega \rightarrow 0). \tag{122}$$

The Meissner effect is the current response to a static and transverse gauge potential $\mathbf{q} \cdot \mathbf{A}(\mathbf{q}, \omega = 0) = 0$. In the small $\mathbf{q}$ limit one has

$$\langle j_\alpha(\mathbf{q} \to \mathbf{0}) \rangle = -\frac{D_s}{\pi}(\delta_{\alpha\beta} - q_\alpha q_\beta / q^2)A_\beta \tag{123}$$

where $D_s(\equiv (n_s/m)^*$

$$D_s = \langle -T_x \rangle - \Lambda_{xx}(q_x = 0, q_y \to 0, \omega = 0). \tag{124}$$

Based on the above definitions of D and D_s we can study various phases of the system: (**1**) D=D_s=0 - an *isolator*; (**2**) D$\neq$0 and D_s=0 - a *nonsuperconducting metal*; (**3**) $D_s \neq$0, D$\neq$0 - a *superconducting metal*.

The numerical Monte Carlo calculation in the repulsive Hubbard model (U=4t>0) [151] on an 8$\times$8 lattice show that D_s=0 and D$\neq$0 in a broad range of the filling 0.5<n<0.9 and for $T > 0.1t$. This means that there is no tendency to high-temperature superconductivity in the single-band Hubbard model. This conclusion is supported by the projector-QMC calculations [152] for the quarter filling case n=0.5 and at T=0. That these results ($D_s = 0$) are not a finite size effect confirm the calculations on the attractive Hubbard model (U=-4t<0), also on an 8$\times$8 lattice, where the clear tendency to superconductivity is found, since $D_s \neq$0, D$\neq$0 already at T<0.2t.

The paper [151] is of great importance numerical studies of pairing in model systems, not only because it hints on the absence of superconductivity in the repulsive Hubbard model, but also because of the following two reasons: (**1**) It uses the general and unbiased criterion for superconductivity, which is independent on the type of the pairing amplitude; (**2**) It shows that the attractive interaction is more favorable for (high-temperature) superconductivity than the repulsion.

8.2. t-J model

The SFI phenomenological approaches root on their basic $t - J$ Hamiltonian Eq.(61). On can put a legitimate question - is there superconductivity in the t-J model? In the past there were various approaches confronting with this important problem. In spite of a number of controversial statements it seems that the results converge to the unique answer - *there is no superconductivity with appreciable T_c*. If superconductivity exists T_c is very low. As the strong support of this claim serve the recent calculations based on the high-temperature expansion in the t-J-V model [70],

$$\hat{H} = -\sum_{i,j,\sigma} t_{ij}\hat{X}_i^{\sigma 0}\hat{X}_j^{0\sigma} + \sum_{i,j=n.n.} [J(\mathbf{S}_i \cdot \mathbf{S}_j) + (V - \frac{J}{4})n_i n_j)]. \tag{125}$$

Here, the V-term mimic the screened Coulomb interaction which is always present in metals, where one expects that $V > J$. In [70] it was calculated the uniform susceptibility for the superconducting pairing

$$\chi_{SC} \equiv \frac{1}{N}\int_0^\beta d\tau \langle\langle \hat{T}_\tau e^{H\tau}O_{SC}e^{-H\tau}O_{SC}^\dagger \rangle\rangle \tag{126}$$
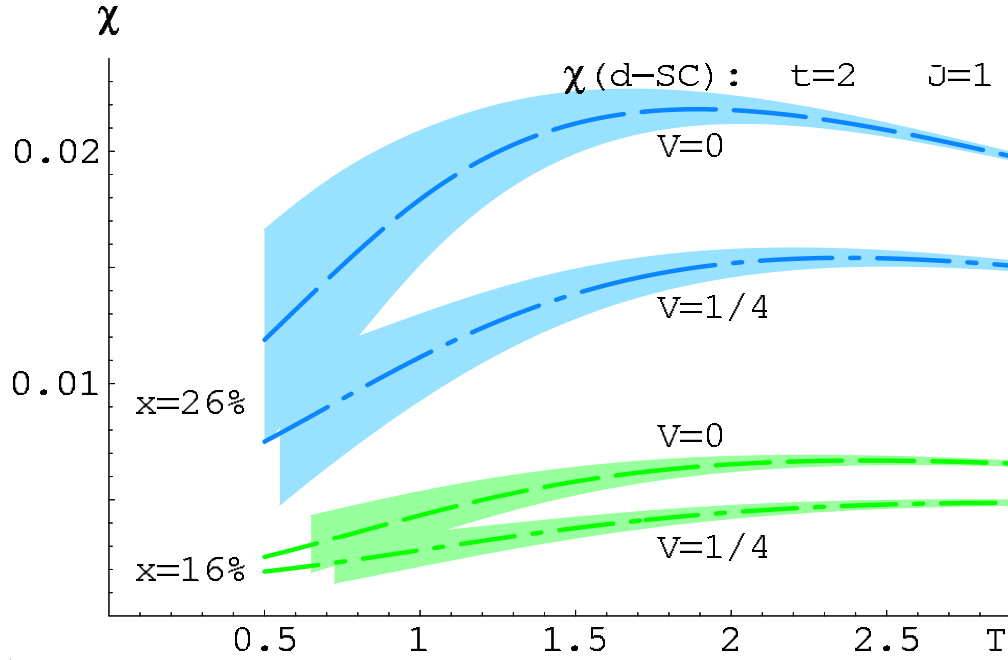
FIGURE 27. Superconducting (d-wave) susceptibility $\chi(d-Sc)(T)$ for $t=2J$. Pairing correlations are already weak for $V=0$, dashes, and decreases further by increasing V-n.n. repulsion (dot-dash). From [70]

$$O_{SC} = \frac{1}{2}\sum_{\mathbf{r}}(\Delta_{\mathbf{r},\mathbf{r}+\mathbf{x}} \pm \Delta_{\mathbf{r},\mathbf{r}+\mathbf{y}}) \qquad (127)$$

$$\Delta_{ij} \equiv c_{i\uparrow}c_{j\downarrow} + c_{j\uparrow}c_{i\downarrow}. \qquad (128)$$

where + sign holds for the s-Sc and the - sign for d-Sc.

In the physical region of parameters $t > J$ both χ_{s-SC} and χ_{d-SC} are small and further decrease by decreasing T. For rather small $V = J/4$, which is even much smaller than expected, the superconducting susceptibilities are drastically decreased as it is seen in Fig. 27. This means that in the more realistic models for HTSC oxides, such as the t-J-V, *there is no tendency to high-temperature superconductivity*. If superconductivity exists at all its T_c must be very low.

9. SUMMARY AND CONCLUSIONS

A number of experiments, such as optics (*IR* and Raman), transport, tunnelling, ARPES, neutron scattering, give convincing evidence that the electron-phonon interaction (EPI) in HTSC oxides is sufficiently strong and contributes to pairing. These experiments give also evidence for the presence of strong correlations which modify the EPI not only quantitatively but also qualitatively. The most spectacular result of the *EP*I theory in strongly correlated systems is the appearance of the *forward scattering peak* in the EPI,

as well as in other charge scattering processes such as the residual Coulomb interaction and scattering on non-magnetic impurities - the FSP *theory* [17], [18], [19], [20] [2]. The forward scattering peak is especially pronounced at lower doping δ. This fundamental result allows us to resolve a number of experimental facts which can not be explained by the old theory based on th isotropic Migdal-Eliashberg equations for the EPI. The most important predictions of the FSP theory of the EPI and other charge scattering processes are: (**1**) the transport coupling constant λ_{tr} (entering the resistivity, $\rho \sim \lambda_{tr}T$) is much smaller than the pairing one λ, i.e. $\lambda_{tr} < \lambda/3$; (**2**) the strength of pairing in HTSC oxides is basically due to the EPI, while the residual Coulomb repulsion (including spin–fluctuations) *triggers* d-wave pairing; (**3**) d-wave pairing is very robust in the presence of non-magnetic impurities; (**4**) the nodal kink in the quasiparticle spectrum is unshifted in the superconducting state, while the anti-nodal singularity is shifted.

We stress the following two facts coming from the theoretical analysis: (**i**) the forward scattering peak in the EPI of strongly correlated systems is a general phenomenon by *affecting electronic coupling to all phonons*; (**ii**) the existence of the forward scattering peak in the EPI is confirmed numerically by the Monte Carlo calculations for the Hubbard-Holstein model with finite U [21], by exact diagonalization [124], as well as by some other methods [22].

Tunnelling experiments and ARPES measurements of the real part of the self-energy give evidence that the EPI coupling constant $\lambda > 1$. At present there are no reliable microscopic calculations of λ in HTSC oxides, which properly include (**a**) the ionic-metallic coupling (due to the long-range Madelung energy) and covalent coupling and (**b**) strong electronic correlations.

In the last several years a large number of published papers were devoted to the study of spin-fluctuation (SFI) interaction as a mechanism of pairing in HTSC oxides. In spite of many efforts and well financed theoretical projects (headed by the greatest authorities in the field), which have opened some new research directions in the theory of electron magnetism, there is no theoretical evidence for the effectiveness of the non-phononic mechanism of pairing. Until now superconductivity could not been proved in the repulsive single-band Hubbard model as well as in its derivative the $t - J$ model. Just opposite, quite recent numerical calculations [70] show in a convincing way, that there is no high-temperature superconductivity in the t-J model. If it exists its T_c is extremely low. Finally, the numerical calculations in the Hubbard model [151] show that the repulsive Hubbard interaction is unfavorable for high-temperature superconductivity, contrary to the attractive interaction which favors it.

The explanation of the high critical temperature in HTSC oxides should be searched in the electron-phonon interaction which is renormalized by strong electronic correlations.

To conclude, *one can not avoid unavoidable*.

10. APPENDIX: DERIVATION OF THE T-J MODEL

10.1. Hubbard model for finite U in terms of Hubbard operators

For simplicity we study the nearest neighbor (n.n.) Hubbard model [153]

$$H = -t \sum_{m \neq n\sigma} \hat{c}_{m\sigma}^{\dagger} \hat{c}_{n\sigma} + U \sum_{m} \hat{n}_{m\uparrow} \hat{n}_{m\downarrow}, \tag{129}$$

where the operator $\hat{c}_{m\sigma}^{\dagger}$ creates an electron at the m-th site with the spin projection σ.

The Hilbert space at the given lattice site contains four states $\{| \alpha > \Longrightarrow | 0 >, | 2 >, | \uparrow >, | \downarrow >\}$. Let us introduce the Hubbard projection operators $X^{\alpha\beta}$; $\alpha, \beta = 0, 2, \sigma$ (where $\sigma = \uparrow (+), \sigma = \downarrow (-)$)

$$X^{\alpha\beta} = | \alpha > < \beta | . \tag{130}$$

They fulfill the projection properties

$$X^{\alpha\beta} X^{\gamma\delta} = \delta_{\beta\gamma} X^{\alpha\delta}, \tag{131}$$

and rather "ugly" (anti)commutation algebra

$$X_i^{\alpha\beta} X_j^{\gamma\delta} \pm X_j^{\gamma\delta} X_i^{\alpha\beta} = \delta_{ij} (\delta_{\beta\gamma} X_i^{\alpha\delta} \pm \delta_{\delta\alpha} X^{\gamma\beta}). \tag{132}$$

The completeness relation of the Hilbert space reads

$$X_i^{00} + X_i^{22} + \sum_{\sigma} X_i^{\sigma\sigma} = 1. \tag{133}$$

The Hubbard operators describe the composite object. There is a connection between $\hat{c}_{i\sigma}$ and $X^{\alpha\beta}$ (if $\sigma = \uparrow \Longrightarrow \bar{\sigma} = \downarrow$)

$$\hat{c}_{i\sigma} = X_i^{0\sigma} + \sigma X_i^{\bar{\sigma}2}; \hat{c}_{i\sigma}^{\dagger} = X_i^{\sigma 0} + \sigma X_i^{2\bar{\sigma}} \tag{134}$$

$$n_i = 1 - X_i^{00} + X_i^{22} \tag{135}$$

$$S_i^+ = \hat{c}_{i\uparrow}^\dagger \hat{c}_{i\downarrow} = X_i^{+-} = (S_i^-)^\dagger = (X_i^{-+})^\dagger$$

$$S_i^z = \frac{1}{2}(\hat{c}_{i\uparrow}^\dagger \hat{c}_{i\uparrow} - \hat{c}_{i\downarrow}^\dagger \hat{c}_{i\downarrow}) = \frac{1}{2}(X_i^{++} - X_i^{--}), \tag{136}$$

and vice versa

$$X^{\sigma 0} = \hat{c}_\sigma^\dagger (1 - \hat{n}_{\bar{\sigma}}) \tag{137}$$

$$X^{\sigma\sigma} = \hat{n}_\sigma (1 - \hat{n}_{\bar{\sigma}}); \ \ X^{\sigma\bar{\sigma}} = \hat{c}_\sigma^\dagger \hat{c}_{\bar{\sigma}} \tag{138}$$

$$X^{00} = (1 - \hat{n}_\uparrow)(1 - \hat{n}_\downarrow) \tag{139}$$

$$X^{2\sigma} = \sigma \hat{c}_{\bar{\sigma}}^\dagger \hat{n}_\sigma; \ \ X^{20} = \sigma \hat{c}_{\bar{\sigma}}^\dagger \hat{c}_\sigma \tag{140}$$

$$X^{22} = n_\uparrow n_\downarrow \tag{141}$$

The Hubbard Hamiltonian $H = H_1 + H_{12} + H_0$ in terms of $X^{\alpha\beta}$ is given by

$$H_1 = -t \sum_{ij\sigma} (X_i^{\sigma 0} X_j^{0\sigma} + X_i^{2\sigma} X_j^{\sigma 2}) \tag{142}$$

$$H_{12} = -t \sum_{ij\sigma} \sigma (X_i^{\sigma 0} X_j^{\bar{\sigma} 2} + X_i^{2\bar{\sigma}} X_j^{0\sigma}) \tag{143}$$

$$H_0 = U \sum_i X_i^{22} \tag{144}$$

The first term in H_1 describes the motion of single electron in the lower (L) Hubbard band, while the second term describes the motion of the doubly occupied electrons from j-th to the i-th side in the upper (U) Hubbard band. The term H_0 is the repulsive energy of two electrons on the i-th site. Finally, H_{12} connects the two (lower and upper) bands.

10.2. Effective Hamiltonian for $U \gg t$

There are various ways to obtain the effective Hamiltonian in the case $U \gg t$. Because of its generality and simplicity we use here the canonical transformation method [153], where the operator S mixes lower and upper band. Under the action of S the Hamiltonian is transformed into $H_{eff} = e^S H e^{-S}$

$$H_{eff} = H + [S, H] + \frac{1}{2}[S, [S, H]] + .. \tag{145}$$

with S in the form

$$S = \kappa \sum_{ij\sigma} (X_i^{\sigma 0} X_j^{\bar{\sigma} 2} - X_i^{2\bar{\sigma}} X_j^{0\sigma}). \tag{146}$$

Now, we choose κ so that all first-order in t processes between the L- and U-band disappear from H_{eff}, i.e. one has

$$H_{12} + [S, H_2] = 0. \tag{147}$$

The solution of Eq.(147) is $\kappa = -t/U$, and H_{eff} reads

$$H_{eff} = -t \sum_{ij\sigma} X_i^{\sigma 0} X_j^{0\sigma} + H_{3s}$$

$$+ J \sum_{ij\sigma} (\mathbf{S}_i \mathbf{S}_j - \frac{1}{4}\hat{n}_i \hat{n}_j) + H_2, \tag{148}$$

where $J = 2t^2/U$ is the exchange energy.

The term H_2 describes motion of "doublons" in the U-band

$$H_2 = U \sum_i X_i^{22} - t \sum_{ij\sigma} X_i^{2\sigma} X_j^{\sigma 2}, \tag{149}$$

while H_{3s} describes the three-sites hopping.

$$H_{3s} = \frac{J}{2} \sum_{ijl\sigma} (X_i^{\bar{\sigma}0} X_l^{\sigma\bar{\sigma}} X_j^{0\sigma} - X_i^{\sigma 0} X_l^{\bar{\sigma}\bar{\sigma}} X_j^{0\sigma}). \tag{150}$$

Usually this term is neglected in the t-J model.

However, it may have tremendous effect on superconductivity by strongly suppressing it [154]. By projecting H_{eff} onto the lower Hubbard band one gets the famous t-J model Hamiltonian $H_{tJ} = P H_{eff} P$

$$H_{tJ} = -t \sum_{ij\sigma} X_i^{\sigma 0} X_j^{0\sigma} + + J \sum_{ij\sigma} (\mathbf{S}_i \mathbf{S}_j - \frac{1}{4}\hat{n}_i \hat{n}_j)$$

$$= -t \sum_{ij\sigma} X_i^{\sigma 0} X_j^{0\sigma} + \frac{J}{2} \sum_{ij\sigma} (X_i^{\sigma\bar{\sigma}} X_j^{\bar{\sigma}\sigma} - X_i^{\sigma\sigma} X_j^{\bar{\sigma}\bar{\sigma}}). \tag{151}$$

Before we are going to discuss some representations for non-canonical operators $X_i^{\sigma 0}$ in terms of bosons and fermions let us stress that the so called "spin" operators $S^{\pm}, S^z$ do not describe correctly the electron spin. Although they satisfy the correct spin-commutation relations

$$[S_i^+, S_j^-] = 2\delta_{ij} S_i^z$$

$$[S_i^z, S_j^{\pm}] = \pm\delta_{ij} S_i^{\pm}, \tag{152}$$

they describe a particle with spins $S = 0, 1/2$ at the lattice site, since $\mathbf{S}_i^2$ fulfills

$$\mathbf{S}_i^2 = \frac{3}{4}\hat{n}_i \neq \frac{3}{4}. \tag{153}$$

Since $X^{\alpha\beta}$ obey the non-canonical ("ugly") algebra the question is how to treat the Hamiltonian H_{tJ} ? In Section 4.-5. we have shown that one can study directly with these operators by using the functional technique and $1/N$ expansion for the self-energy. However, there are very popular approaches which represent $X^{\alpha\beta}$ in terms of bosons and fermions with canonical commutation relations.

Slave boson (SB) method.   Here, one introduces the fermion with spin (spinon) $F_{i\sigma}$ and the boson without spin (holon) B_i operators, where $X^{0\sigma} = F_\sigma B^\dagger$. The *constraint* on the SB Hilbert space (completeness), at the given lattice site, is given by $B^\dagger B + \sum_\sigma F_\sigma^\dagger F_\sigma = 1$ and the t-J Hamiltonian reads

$$H_{tJ} = -t \sum_{ij\sigma} F_{i\sigma}^\dagger F_{j\sigma} B_i B_j^\dagger + \frac{J}{2} \sum_{ij\sigma\sigma'} F_{i\sigma}^\dagger F_{j\sigma} F_{j\sigma'}^\dagger F_{i\sigma'}. \tag{154}$$

We stress that the *constraint* strongly limits the SB Hilbert space of bosons and fermions (at the given lattice site) which effectively means their strong interaction. In that respect any uncontrollable decoupling in the SB method (as in some RVB approaches) leads to a spin-charge (spinon-holon) separation, which is not realized in 2D and 3D systems. In order to correct this one introduces the so called gauge fields which keep the spin and charge together. We already discussed the difficulties of the SB method in studying the electron-phonon interaction.

Slave fermion (SF) method.   In the SF method the boson has spin and fermion not, i.e. $X^{0\sigma} = B_\sigma^\dagger F$ with the constraint on the Hilbert space $F^\dagger F + \sum_\sigma B_\sigma^\dagger B_\sigma = 1$.

Spin fermion method.   Here, the real fermion $\hat{c}^\dagger$ with the "spin" $\mathbf{S}$ is represented via the auxiliary fermion $F^\dagger$ and spin $\mathbf{s}$ by $\hat{c}_\uparrow^\dagger \hat{c}_\uparrow + \hat{c}_\downarrow^\dagger \hat{c}_\downarrow = 1 - F^\dagger F$ and $\mathbf{S} = \mathbf{s}(1 - F^\dagger F)$. The t-J Hamiltonian is rather complicated

$$H_{tJ} = 2t \sum_{ij} F_i^\dagger F_j \left(\mathbf{s}_i \mathbf{s}_j + \frac{1}{4} \right)$$

$$+ J \sum_{ij} (1 - F_i^\dagger F_i)(\mathbf{s}_i \mathbf{s}_j - \frac{1}{4})(1 - F_j^\dagger F_j). \tag{155}$$

Usually this method is used for analyzing motion of single hole in the half-filled system where the antiferromagnetic order is realized.

REFERENCES

1.   J. G. Bednorz, K. A. Müller, Z. Phys. **B** 64, 189 (1986)
2.   M. L. Kulić, Phys. Reports **3**38, 1-264 (2003)
3.   C. Thomsen and M. Cardona, in Physical Properties of High Temperature Superconductors I, ed. by D. M. Ginzberg (World Scientific, Singapore, 1989), pp. 409; R. Feile, Physica **C** 159 1 (1989); C. Thomsen, in Light Scattering in Solids VI, ed. by M. Cardona and G. Güntherodt (Berlin, Heidelberg, New York, Springer, 1991), pp. 285

4. V. G. Hadjiev, X. Zhou, T. Strohm, M. Cardona, Q. M. Lin, C. W. Chu, Phys. Rev. **B** 58, 1043 (1998)
5. V. G. Hadjiev,, T. Strohm, M. Cardona, Z. L. Du, Y. Y. Xue, C. W. Chu, preprint MPI, Stuttgart, 1998
6. D. J. Scalapino, Physics Reports **2**50, 329 (1995)
7. A. P. Kampf, Physics Reports **2**49, 220 (1994)
8. V. L. Ginzburg, E, G. Maksimov, Physica **C** 235-240, 193 (1994); Superconductivity (in Russian) **5**, 1505 (1992)
9. P.B. Allen, B. Mitrović, Solid State Physics, ed. H. Ehrenreich, F. Seitz, D. Turnbull, Academic, New York, **V** 37, p. 1, (1982)
10. M. L. Cohen, P. W. Anderson, Superconductivity in d and f band metals, AIP Conference Proceedings (ed. D. H. Douglass) New York, p.17 (1972)
11. E. G. Maksimov, Uspekhi Fiz. Nauk **1**70, 1033 (2000)
12. D. A. Kirzhnits, in High Temperture Superconductivity, ed. V. L. Ginzburg and D. Kirzhnits, (Consultant Bureau New York, London 1982)
13. O. V. Dolgov, D. A. Kirzhnits, E. G. Maksimov, Rev. Mod. Phys. **5**3, 81 (1981)
14. S. I. Vedeneev, A. G. M. Jansen, A. A. Tsvetkov, P. Wyder, Phys. Rev. **B** 51, 16380 (1995)
15. H. J. Kaufmann, O. V. Dolgov, E. K. Salje, Phys. Rev. **B** 58, 9479 (1998)
16. P. Samuely, N. L Bobrov, A. G. N. Jansen, P. Wyder, S. N. Barilo, S. V. Shiryaev, Phys. Rev. **B** 48, 13904 (1993); P. Samuely, P. Szabo, A. G. N. Jansen, P. Wyder, J. Marcus, C. Escribe-Filippini, M. Afronte, Physica **B** 194-196, 1747 (1994)
17. M. L. Kulić, R. Zeyher, Phys. Rev. **B** 49, 4395 (1994); Physica **C** 199-200, 358 (1994); Physica **C** 235-240, 358 (1994)
18. R. Zeyher, M. L. Kulić, Phys. Rev. **B** 53, 2850 (1996)
19. R. Zeyher, M. L. Kulić, Phys. Rev. **B** 54, 8985 (1996)
20. M. L. Kulić and R. Zeyher, Mod. Phys. Lett. **B** 11, 333 (1997)
21. Z. B. Huang, W. Hanke, E. Arrigoni, D. J. Scalapino , cond-mat/0306131 (2003)
22. E. Cappelluti, B. Cerruti, l. Pietronero, cond-mat/0312654 (2003)
23. M. L. Kulić, in preparation
24. H. Romberg, M. Alexander, N. Nücker, P. Adelmann, J. Fink, Phys. Rev. **B**42, 8768 (1990)
25. M. S. Hybersten, M. Schlüter, N. E. Christensen, Rev. **B** 39, 9028 (1989)
26. R. Claessen, R. Manzke, H. Carsten, B. Burandt, T. Buslaps, M. Skibowski, J. Fink, Phys. Rev. **B** 39, 7316 (1989); G. Mante, R. Claessen, T. Buslaps, S. Harm, R. Manzke, M. Skibowski, J. Fink, Z. Phys **B** 80, 181 (1990)
27. S. Uchida et al., Phys. Rev. **B** 43, 7942 (1991)
28. P. Lee, N. Nagaosa, Phys. Rev. **B** 46, 5621 (1992)
29. D. Pines, preprint CNSL Newsletter, LALP-97-010, No. 138, June 1997; Physica **B** 163, 78 (1990)
30. C. C. Tsuei, J.R. Kirtley, C. C. Chi, L. S. Yu-Jahnes, A. Gupta, T. Shaw, J. Z. Sun, M. B. Ketchen, Phys. Rev. Lett., **7**3, 593 (1994)
31. C. C. Tsuei, J.R. Kirtley, M. Rupp, A. Gupta, J. Z. Sun, T. Shaw, M. B. Ketchen, C. Wang, Z. F. Ren, J. H. Wang, M. Bhushan Science **2**7, 329 (1996)
32. C. C. Tsuei, J.R. Kirtley, J. Low Temp. Phys., **1**07, 445 (1997)
33. C. C. Tsuei, J.R. Kirtley, Z. F. Ren, J. H. Wang, H. Raffy, Z. Z. Li, Nature **3**87, 481 (1998)
34. C. C. Tsuei et al., cond-mat/0402655 (2004)
35. C.C. Tsuei, J.R. Kirtley, Rev. Mod. Phys. **7**2, 969 (2000)
36. G. Hastreiter, U. Hofmann, J. Keller, K. F. Renk, Solid State Commun. **7**6, 1015 (1990); G. Hastreiter, J. Keller, M. L. Kulić, in Proceedings of the first German-Soviet bilateral Conference on High-Temperature Superconductivity, 1990
37. S. I. Vedeneev, A. G. M. Jensen, P. Samuely, V. A. Stepanov, A. A. Tsvetkov and P. Wyder, Phys. Rev. **4**9, 9823 (1994); S. I. Vedeneev, A. G. M. Jensen and P. Wyder, Physica **B** 218, 213 (1996)
38. D. Shimada, Y. Shiina, A. Mottate, Y. Ohyagi and N. Tsuda, Phys. Rev. **B 5**1, 16495 (1995); N. Miyakawa, A. Nakamura, Y. Fujino, T. Kaneko, D. Shimada, Y. Shiina and N. Tsuda, Physica **C** 282-287, 1519 (1997);
39. N. Miyakawa, Y. Shiina, T. Kaneko and N. Tsuda, J. Phys. Soc. Jpn. **6**2, 2445 (1993); N. Miyakawa, Y. Shiina, T. Kido and N. Tsuda, J. Phys. Soc. Jpn. **5**8, 383 (1989)
40. Y. Shiina, D. Shimada, A. Mottate, Y. Ohyagi and N. Tsuda, J. Phys. Soc. Jpn. **6**4, 2577 (1995); Y.

Ohyagi, D. Shimada, N. Miyakawa, A. Mottate, M. Ishinabe, K. Yamauchi and N. Tsuda, J. Phys. Soc. Jpn. **6**4, 3376 (1995)

41. R. S. Gonnelli, F. Asdente and D. Andoreone, Phys. Rev. **B** 49, 1480 (1994)
42. T. Schneider, cond-mat/0308595 (2003)
43. A. Lanzara et al., Nature **4**12, 510 (2001)
44. M. L. Kulić, O. V. Dolgov, cond-mat/0308597 (2003)
45. A. A. Kordyuk, et all, cond-mat/0402643 (2004)
46. M. L. Kulić, O. V. Dolgov, in preparation
47. T. Jarlborg, Solid State Comm., **6**7, 297 (1988); **7**1, 669 (1989)
48. S. Barišić, J. Zelenko, Solid State Comm., **7**4, 367 (1990); S. Barišić, I. Batistić, Europhys. Lett. **8**, 765 (1989)
49. S. Barišić, Intern. J. of Mod. Phys. **B** 5, 2439 (1991)
50. R. Zeyher, Z. Phys. **B** 80, 187 (1990)
51. H. Krakauer, W. E. Picket, R. E. Cohen, Phys. Rev. **B** 47, 1002 (1993)
52. C. Falter, M. Klenner, G. A. Hoffmann, Phys. Rev. **B** 55, 3308 (1997); Phys. Stat. Sol. (b) 209, 235 (1998)
53. C. Falter, M. Klenner, G. A. Hoffmann, Phys. Rev. **B** 57, 14 444 (1998)
54. P. Horsch, G. Khaliullin, V. Oudovenko, Physica C **3**41, 117 (2000)
55. O. Rösch, O. Gunnarsson, cond-mat/0308035 (2003)
56. S. Ishihara, N. Nagaosa, cond-mat/0311200 (2003)
57. M. Gurvitch, A. T. Fiory, Phys. Rev. Lett. **5**9, 1337 (1987)
58. A. T. Fiory, S. Martin, R. M. Fleming, L. F. Schneemeyer, J. V. Waczak, A. F. Hebard, S. A. Sunshina, Physica **C** 162-164, 1195 (1989)
59. A. Mackenzie, E. Marseglia, I. Marsden, G. Lonzarich, C. Chen, B. Wanklyn, Physica **C** 162-164, 1029 (1989)
60. L. F. Mattheiss, Phys. Rev. Lett. **5**8, 1028 (1987)
61. P.W. Anderson, Science **2**35, 1196 (1987)
62. A. V. Puchkov, D. N. Basov, T. Timusk, J. Phys.: Condens. Matter **8**, 10049 (1996)
63. J. Hwang, T. Timusk, G. D. Gu, Nature **4**27, 714 (2004)
64. M. Norman, Nature **4**27, 692 (2004)
65. N. Bulut, D. J. Scalapino, Phys. Rev. Lett. **6**7, 2898 (1991); Phys. Rev. Lett. **6**8, 706 (1992); Phys. Rev. **B** 47, 3528 (1994)
66. Ph. Bourges, in *The Gap Symmetry and Fluctuations in High Temperature Superconductors*, J. Bok, G. Deutscher, D. Pavuna, S. A. Wolf, Eds. (Plenum, New York, 1998), pp. 349-371; preprint cond-mat/9901333 (1999)
67. M. Mehring, Appl. Magn. Resonance **3**, 383 (1992)
68. H. -Y. Kee, S. Kivelson, G. Aeppli, Phys. Rev. Lett. **8**8, 257002 (2002)
69. M. L. Kulić, I. M. Kulić, Physica **C** 391, 42 (2003)
70. L. Pryadko, S. Kivelson, O. Zachar, cond-mat/0306342 (2003)
71. J. Rossat-Mignod et al., Physica **C** 185-189, 86 (1991)
72. H. Mook et al., Phys. Rev. Lett. **7**0, 3490 (1993)
73. E. G. Maksimov, et al., Phys. Rev. Lett. **6**3, 1870 (1989)
74. H. J. Kaufmann, Ph. D. Thesis, Uni. Cambridge, February 1999
75. A. V. Boris et al., to be published in Science, 2004
76. I. Božović, Phys. Rev. **B**42, 1969 (1990)
77. M. Tinkham, Introduction to Superconductivity(McGrow-Hill, New York, ed. 2, 1996)
78. R. Kubo, J. Phys. Soc. Japan **1**2, 570 (1957)
79. H. J. Molegraaf, C. presura, D. van der Marel, P. H. Kes, M. Li, Science **2**95, 2239 (2002)
80. J. E. Hirsch, Physica **C** 199, 305 (1992); ibid **2**01, 347 (1992)
81. M. Norman, C. Pepin, Rep. Prog. Phys. **6**6, 1541-1610 (2003)
82. A. E. Karakozov, E. G. Maksimov, O. V. Dolgov, Sol. St. Comm. **1**24, 119 (2002)
83. R. J. Radtke, S. Illah, K. Levin, M. R. Norman, Phys. Rev. **B** 46, 11975 (1992)
84. R. J. Radtke, K. Levin, H. -B. Schüttler, M. R. Norman, Phys. Rev. **B** 48, 15957 (1993)
137. H. -B. Schüttler, M. R. Norman, Phys. Rev. B **5**4, 13 295 (1996)
86. Z. Schlesinger, R. T. Collins, F. Holzberg, C. Field, V. Welp, Y. C. Chang, P. Z. Jiang, A. P. Paulikas, Phys. Rev. Lett. **6**5, 801 (1990)

87. O. V. Dolgov, E. G. Maksimov, S. V. Shulga, in Electron-Phonon Interaction in Oxide Super-conductors, World Scien., p.30 (1991)
88. S. V. Shulga, O. V. Dolgov, E. G. Maksimov, Physica **C** 178, 266 (1989)
89. H. Takagi, B. Batlogg, H. L. Kao, J. Kwo, R. J. Cava, J. J. Krajewski, W. F. Peck, Jr., Phys. Rev. Lett. **6**9, 2975 (1992)
90. S. L. Cooper, K. E. Gray, in Physical Properties of High Temperature Superconductors IV, ed. by D. M. Ginzberg (World Scientific, Singapore, 1994)
91. S. N. Rashkeev and G. Wendin, Phys. Rev. **B** 47, 11603 (1993)
92. I. Božović, J. H. Kim, J. S. Harris, Jr., C. B. Eom, J. M. Phillips, J. T. Cheung, Phys. Rev. Lett., **7**3, 1436 (1995)
93. M. Kranz, H. J. Rosen, R. M. Macfarlane and V. Y. Lee, Phys. Rev. **B** 38, 4992 (1988); C. Thomsen, M. Cardona, B. Gegenheimer, R. Liu and A. Simon, Phys. Rev. **B** 37, 9860 (1988)
94. C. Thomsen, in Light Scattering in Solids VI, ed. by M. Cardona and G. G. Güntherodt (Springer, Berlin, Heidelberg 1991)
95. W. Kress, U. Schröder, J. Prade, A. D. Kulkarni, F. W. de Wette, Phys. Rev. **B 38**, 2906 (1988)
96. R. Gajic, Thesis, Ubiversity of Belgrade (1992)
97. R. Zeyher and G. Zwicknagl, Z. Phys. **B** 78, 175 (1990)
98. C. Jiang, J. P. Carbotte, Phys. Rev. **B** 50, 9449 (1994)
99. A. Alligia, M. L. Kulić, V. Zlatić and K. H. Bennemann, Sol. State Comm. **65**, 501 (1988); Proc. Adriatico Res. Conf. on High-T$_c$-Supercond., Proceedings ICTP Trieste, p.303, World Scien. Publish., Singapore (1987)
100. T. P. Deveraux, A. Virosztek and A. Zawadovski, Phys. Rev. **B** 51, 505 (1995)
101. E. L. Wolf, Principles of Electron Tunneling Spectroscopy, Oxford University Press, 1985
102. G. D. Mahan, Many-particle Physics, Plenum Press, New York 1990, pp. 796,
103. D. Shimada, N. Tsuda, U. Paltzer and F. W. de Wette, preprint (1998)
104. Q. Huang, J. F. Zasadinski, N. Tralshawala, K. E. Gray, D. Hinks, J. L. Peng and R. L. Greene, Nature (London) **3**47, 389 (1990)
105. J. F. Franck, in Physical Properties of High Temperature Supercoductors V , ed. D. M. Ginsberg, (World Scientific, Singapore, 1994)
106. J. P.Franck, Physica **C** 282-287, 198 (1997)
107. A. Damascelli, Z. Hussain, Z. -X. Shen, Rev. Mod. Phys. **75**, 473 (2003)
108. J. C. Campuzano, M. R. Norman, M. Randeria, cond-mat/0209476 (2002)
109. T. Cuk et al., cond-mat/0403521 (2004); Z.-X. Shen, talk at the Int. Symp. "*Competing phases in novel condensed-matter systems, Würzburg*, Germany, July 9-11 (2003)
110. D. J. Scalapino, in Superconductivity ed. R. D. Parks, **V** 1, Chapter 11, Dekker, New York, 1969
111. O. V. Dolgov, E. I.Maksimov, Tr. Fiz. Inst. Akad. Nauk SSSR, **1**48 3 (1983),
112. D. Rainer, in Progress in Low-Temperature Physics (Ed. D. F. Brewer) (Amsterdam, Elsevier, 1986) p. 371
113. I. I. Mazin et al., Phys. Rev. **B** 42, 366 (1990)
114. W. Weber, Phys. Rev. Lett. **5**8, 2154 (1987)
115. W. Weber, L. F. Mattheiss, Phys. Rev. **B**37, 599 (1988)
116. S. Y. Savrasov, Phys. Rev. Lett. **6**9, 2819 (1992); S. Y. Savrasov, D. Y. Savrasov, Phys. Rev. **B** 46, 12181 (1992)
117. S. Y. Savrasov, . K. Andersen, Phys. Rev. Lett. **7**7, 4430 (1996)
118. E. I.Maksimov, D. Y. Savrasov, S. Y. Savrasov, Physics - Uspekhi **4**0, 337 (1997)
119. O. V. Danylenko, O. V. Dolgov, M. L. Kulić, V. Oudovenko, cond-mat/9710234 (1998); cond-mat/9710234 (1997); Europ. Phys. Jour. **B**9 - Cond. Matter, 201 (1999)
120. C. Grimaldi, L. Pietronero, S. Sträßler, Phys. Rev. **B** 52, 10516 (1995); ibid **B** 52, 10530 (1995)
121. J. H. Kim and Z. Tešanović, Phys. Rev. Lett. **7**1, 4218 (1993)
122. C. G. Olson, R. Liu, A. Yang, D. W. Lynch, A. J. Arko, R. S. List, B. Veal, Y. Chang, P. Jiang and A. Paulikas, Science **2**45 (1989)
123. V. J. Emery, Phys. Rev. Lett. **5**8, 2794 (1987)
124. T. Tohyama, P. Horsch and S. Maekawa, Phys. Rev. Lett. **74**, 980 (1995)
125. J. Hubbard, Proc. Roy. Soc., **A**276 238 (1963); **A**277 237 (1963); **A**281 401 (1964); **8**4 455 (1964)
126. A. Greco, R. Zeyher, Europh. Lett., **35**, 115 (1996); R. Zeyher, A. Greco, Z. Phys. **B** 104, 737 (1997)

127. M. Grilli, G. Kotliar, Phys. Rev. Lett. **6**4, 1170(1990)
128. Ju H. Kim, K. Levin, R. Wentzovitch and A. Aurbach, Phys. Rev. **B** 44, 5148 (1991)
129. M. Grilli and C. Castellani, Phys. Rev. **B** 50, 16880 (1994)
130. M. Grilli and C. Castellani, Phys. Rev. Lett. **7**4, 1488 (1995)
131. M. Mierzejewski, J. Zielinski, P. Entel, Phys. Rev. **B** 57, 590 (1998)
132. A. A. Abrikosov, Physica C **2**44, 243 (1995); J. Ruvalds et al., Phys. Rev. B **5**1, 3797 (1995); G. Santi, T. Jarlborg, M. Peter, M. Weger, J. of Supercond. **8**, 215 (1995)
133. M. Weger, B. Barbelini, M. Peter, Z. Phy. **B**94, 387 (1994); M. Weger, M. Peter, L. P. Pitaevskii, Z. Phy. **B**101, 573 (1996); M. Weger, J. of Supercond. **1**0, 435 (1997); M. Weger, M. Peter, First Euroconf. on Anomal. Complex Superc., Crete Sept. 26-Oct.3, 1998
134. G. Varelogiannis, Phys. Rev. B **5**7, 13743 (1998)
135. A. J. Millis, H. Monien, D. Pines, Phys. Rev. **B** **4**2, 167 (1990)
136. P. Monthoux and D. Pines, Phys. Rev. Lett. **6**9, 961 (1992); Phys. Rev. B **4**7, 6069 (1993); R. J. Radtke, K. Levin, H. -B. Schüttler and M. R. Norman, Phys. Rev. B **4**8, 15957 (1993)
137. H. -B. Schüttler, M. R. Norman, Phys. Rev. B **5**4, 13 295 (1996)
138. A. I. Lichtenstein, M. L. Kulić, Physica C **2**45, 186 (1995)
139. A. B. Migdal, Sov. Phys. JETP **3**4, 996 (1958); G. M. Eliashberg, Sov. Phys. JETP **1**1, 696 (1960)
140. R. Ferenbacher, Phys. Rev. Lett. **7**7, 1849 (1996); R. Ferenbacher, M. Norman, Phys. Rev. **B** 50, 3495 (1994)
141. S. K. Tolpygo et al., Phys. Rev. **B**53, 12454 (1996); ibid 12462 (1996)
142. M. L. Kulić, V. Oudovenko, Solid State Comm. **1**04, 731 (1997); M. L. Kulić, O. V. Dolgov, Phys. Rev.**B**60, 13062(1999)
143. J. R. Engelbracht, M. Randeria, C. A. R. Sa de Melo, Phys. Rev. **55**, 15 153 (1997)
144. A. Junod, A. Erb, C. Renner, Physica **C 317**, 333 (1999)
145. M. V. Sadovskii, Physics-Uspekhi **44**(5), 515 (2001)
146. A, M. Gabovich, A. I. Voitenko, M. Ausloos, Phys. Rep. **367**, 583 (2002)
147. K. Yang, S. L. Sondhi, Phys. Rev. **62**, 11 778 (2000)
148. Phys. Rev. **112**, 1900 (1957)
149. P. Monthoux, D. J. Scalapino, Phys. Rev. Lett. **72,** 1874 (1994); Chien-Hua Pao, N. E. Bickers, Phys. Rev. Lett. **72,** 1870 (1994)
150. E. Dagotto, Rev. Mod. Phys. **66**, 763 (1994)
151. D. J. Scalapino, S. R. White, S. C. Zhang, Phys. Rev. Lett. **68**, 2830 (1992)
152. F. F. Assad, W. Hanke, D. J. Scalapino, Phys. Rev. Lett. **71**, 1915 (1993)
153. Yu. A. Izyumov, Physics-Uspekhi **40**(5). pp. 445-476 (1997)
154. A. Alligia, private communication